Glaciovolcanism in the Garibaldi volcanic belt: Nine geological maps from southwestern British Columbia, Canada

Alexander M. Wilson[1, a], James K. Russell[1] and Martin A. Harris[2]

[1] Volcanology and Petrology Laboratory, Department of Earth, Ocean and Atmospheric Sciences, The University of British Columbia, 2020–2207 Main Mall, Vancouver, BC, Canada V6T 1Z4
[2] Department of Geology, University at Buffalo, Buffalo, NY, USA
[a] corresponding author: wilson.alexander08@gmail.com

Recommended citation: Wilson, A.M., Russell, J.K., and Harris, M.A., 2024. Glaciovolcanism in the Garibaldi volcanic belt: Nine geological maps from southwestern British Columbia, Canada. British Columbia Ministry of Mining and Critical Minerals, British Columbia Geological Survey Open File 2024-10, 64p.

Abstract

Glaciovolcanism involves the interaction between volcanic eruptions and ice in all its forms and produces distinct and diverse edifice morphologies and characteristic deposit lithofacies that are important proxies for local and global paleoclimates. Here, we present nine geologic maps of glaciovolcanic centers situated in the Garibaldi volcanic belt (GVB) of southwestern British Columbia, Canada. Our maps delineate lithostratigraphy, geochemistry, geochronology and petrography, and we use these data to interpret the eruption environment. The maps include (1) Monmouth Creek volcano, (2) Brohm Ridge of the Mount Garibaldi volcanic complex, (3) the Table, (4) the Black Tusk, (5) the Cinder Cone, (6) Cracked Mountain volcano, (7) Lillooet Glacier volcano, (8) the Salal Glacier volcanic field and, (9) the Bridge River volcanic field. For each map area, we use field observations to establish a glaciovolcanic versus non-glaciovolcanic origin and to constrain eruption style and the syn-eruptive paleoenvironment (i.e., paleo ice thickness and extent). These data serve to test, refine, and expand on existing paleoclimate proxies and provide a powerful terrestrial-based means to track the temporal and spatial wax and wane of the Coast Mountain sector of the Cordilleran ice sheet (CIS) beyond the last glacial stage.

Keywords: Glaciovolcanism, Volcanology, Garibaldi volcanic belt, Pleistocene volcanism, Cordilleran ice sheet

Table of Contents

1. Introduction

The Cascade volcanic arc is a chain of predominantly andesitic volcanoes extending ~1250 km from southwest British Columbia (BC) to northern California (Fig. 1.1). Quaternary magmatism is a consequence of north-easterly subduction of remnants of the Farallon Plate (Juan de Fuca, Explorer and Gorda Plates) beneath the North American plate (Rogers 1985; Green et al. 1988; Green 1990; Sherrod and Smith 1990; Hickson 1994; Hildreth 2007). The Cascade volcanic arc contains more than 2300 individual vents of which 22 form major volcanic structures (Fig. 1.1A; Hildreth 2007).

The Garibaldi volcanic belt (GVB) is the northern extension of the Cascade volcanic arc (Fig. 1.1B). The belt extends from volcanic deposits located at Watts Point to the Silverthrone and Franklin Glacier volcanic fields, located ~350 km to the northwest (Fig. 1.1A) (Green et al. 1988; Souther 1991; Green and Harry 1999). Volcanism in the southern part of the GVB (i.e., Watts Point to the Bridge River volcanic field) spans the last ~2 Ma, during which ~100 eruptive centers ranging from alkaline basalt to calc-alkaline rhyolite were produced (Wilson and Russell 2018). Volcanism in the GVB has occurred in conjunction with a protracted history of advancing and retreating Cordilleran Ice Sheets (CIS) (Fulton 1991; Ryder et al. 1991; Clague and Ward 2011). At its last maximum extent (locally referred to as the Fraser glaciation, ~17 ka), the CIS reached up to 3 km in thickness and stretched well into southern Washington (Booth et al. 2003).

A large number of GVB volcanoes show evidence of eruption under, or adjacent to, glacial ice (Mathews 1958; Wilson and Russell 2018). The physical properties of these glaciovolcanoes (e.g., their shape, location, form, and lithofacies architecture) directly reflect their eruption environment, which results in confinement or impoundment by ice, as well as accelerated cooling by contact with ice, snow, and/or meltwater (Russell et al. 2014; Smellie and Edwards 2016; Smellie 2018; Wilson and Russell 2018). In the GVB, many glaciovolcanoes are identified by indicators of accelerated lava cooling/quenching, and/or subaqueous deposition (Kelman et al. 2002a; Wilson and Russell 2018). These indicators commonly occur in physiographic areas that would otherwise be unable to support standing bodies of water (e.g., mountain ridges). Given the age of the volcanic deposits in southwestern BC (i.e., typically <1 Ma), and the tendency towards well-preserved deposits that conform to the current topography, erosion and modification of the local topography cannot be used to explain the paleo-presence of syn-eruptive water. For this reason, glacial ice is often the only plausible explanation. Common lithofacies indicators used to identify glaciovolcanic deposits in these maps include:

i) Pervasive palagonitisation of deposits (e.g., Stroncik and Schmincke 2002; Harder and Russell 2006).

Wilson, A.M., Russell, J.K., and Harris, M.A., 2024. Glaciovolcanism in the Garibaldi volcanic belt: Nine geological maps from southwestern British Columbia, Canada. British Columbia Ministry of Mining and Critical Minerals, British Columbia Geological Survey Open File 2024-10, 64p

ii) Indicators of subaqueous deposition including pillow lava, pillow lava breccias and diagnostic sorting, grading, and bedding within volcaniclastic deposits.
iii) Accidental inclusion of glacial xenoliths within the deposits (e.g., incorporation of till or xenoliths melted from overlying ice).
iv) Erratic and/or radial, slender columnar joint orientations (e.g., Lescinsky and Sisson 1998; Wilson et al. 2019).
v) Glassy lava textures and hackly jointing (e.g., Lodge and Lescinsky 2009).
vi) Overthickened lava accumulations (e.g., Mathews 1952b).

Glaciovolcanic lithofacies can preserve highly detailed information about the local environment and climate at the time of the eruption. Coupled with high-resolution geochronology, these volcanoes can be used to independently test, refine, and expand on existing local and global paleoclimate proxies (e.g., the Marine Isotope Stages (MIS) record; Lisiecki and Raymo 2005). For example, the presence of young pillow lava overlying a mountain ridge indicates that the local area was covered by a glacier with a surface elevation that was at least as high as the highest mapped elevation of glaciovolcanic lithofacies (e.g., Wilson et al. 2019a). Similarly, the occurrence of glaciovolcanic passage zones may be used to reconstruct the depth and extent of paleo-englacial lakes (Russell et al. 2013, 2014; Smellie 2018; Wilson and Russell 2018), thereby providing an independent measurement of minimum local paleo-ice thickness. These data, when combined with accurate geochronology, are powerful, empirical, terrestrial evidence that may be used to inform or test models of paleo-glacier distributions and extents (Smellie et al. 2008; Smellie 2018; Wilson et al. 2020).

1.1. Objectives and organisation

Here, we provide nine new geologic maps of areas in southwestern British Columbia that host glaciovolcanic deposits, including (1) Monmouth Creek volcano, (2) Brohm Ridge Area (part of the Mount Garibaldi volcanic complex), (3) the Table, (4) the Black Tusk, (5) the Cinder Cone, (6) Cracked Mountain volcano, (7) the Lillooet Glacier volcano, (8) the Salal Glacier volcanic field and, (9) the Bridge River volcanic field. The map areas include several recently recognized glaciovolcanic deposits (e.g., Cracked Mountain volcano) and several areas that have limited mapping or lithofacies descriptions (e.g., The Bridge River volcanic field). The map areas target volcanic deposits with limited prior geological investigation and were selected to fill knowledge gaps concerning Pleistocene GVB volcanism (e.g., Mathews 1958; Read 1977; Souther 1980; Roddick and Souther 1987; Kelman 2005). The maps include common lithofacies designations, petrological descriptions, new geochronological and geochemical data and interpretive geological cross-sections. The work complements recently published studies, including: Wilson, 2019, Wilson et al. 2016, 2019; Wilson and Russell 2017, 2018; and Harris et al. 2022.

This report is organized into map-based chapters including an introduction and supporting information. Each map is accompanied by tables that provide petrographic lithofacies descriptions, figures providing geochemical and geochronological information, and original field photographs.

1.2. Regional geology and geomorphology

The Coast Mountains of British Columbia are constructed of voluminous, Jurassic to Miocene plutonic rocks (the Coastal Plutonic Complex) and subordinate metamorphic assemblages (Monger and Journeay 1994; Bustin et al. 2013). These basement rocks were accreted to the margin of western North America and form a 100 to 200 km-wide belt that extends for ~1700 km from Vancouver, Canada to Alaska, United States (Monger and Journeay 1994). The Quaternary volcanic GVB is situated within the southern Coast Mountains, primarily straddling the suture between the Wrangell and the Cadwallader terranes. In the Monmouth Creek volcano map area, the basement rocks comprise leucogranite of the Middle Cretaceous Squamish Batholith (Cui and Russell 1995). Further north in the Brohm Ridge, Table, Black Tusk, and Cinder Cone map areas, the basement rocks are Upper Jurassic Cloudburst Formation granodiorite with a thin veneer of Late Cretaceous Gambier Group greenschist, slate, conglomerate, and metavolcanic assemblages (Mathews 1958; Lynch 1992; Cui and Russell 1995). At Cracked Mountain volcano and Lillooet Glacier volcano the basement rocks include Late Cretaceous Coastal Plutonic Complex granodiorite and Early Cretaceous Gambier and Cadwallader Group metamorphic assemblages (Read 1977; Monger and Journeay 1994; Reyes and Clague 2004). The Salal Glacier volcanic field map area has basement rocks that include Late Miocene quartz monzonite (the Salal Pluton), one of the youngest plutonic bodies exposed in the Coastal Mountain range (Roddick and Woodsworth 1975). The basement rocks in the Bridge River volcanic field comprise Late Cretaceous, Coastal Plutonic Complex granodiorite (Roddick and Woodsworth 1975; Roddick and Souther 1987; Cui and Russell 1995).

The topography in southwestern BC is rugged and remote. Alpine areas are typically unvegetated and covered by loose glacial debris, felsenmeer and permanent snow and ice. Lower-elevation areas host dense forests of western hemlock, fir, cedar, and spruce.

1.3. Field and laboratory methods

Geologic outcrop mapping was conducted at a 1:5,000 scale during the 2015 and 2016 summer field seasons. The map areas were accessed through a combination of vehicle, foot, canoe, floatplane, and helicopter charter. In the southern GVB, access utilized existing hiking trails and the extensive network of backcountry forest service roads. The deposits further north used a combination of floatplane and helicopter. Field mapping used a 1:20,000 scale base map with the TRIM (Terrain Resource Information Management) DEM (Digital Elevation Model) and GPS (Global Positioning System; Garmin GPSMAP 60CSx) for outcrop and sample location accuracy. All geological contacts were made in the field and were revised following chemical and petrographic sample analysis. The maps and cross sections were digitized and compiled using both ESRI ArcGIS and QGIS, with final editorial adjustments in Adobe Illustrator CC.

Major and trace element geochemistry was collected using X-Ray Fluorescence (XRF) and Inductively Coupled Plasma-Mass

Wilson, A.M., Russell, J.K., and Harris, M.A., 2024. Glaciovolcanism in the Garibaldi volcanic belt: Nine geological maps from southwestern British Columbia, Canada. British Columbia Ministry of Mining and Critical Minerals, British Columbia Geological Survey Open File 2024-10, 64p

Spectrometry (ICP-MS) at the Peter Hooper GeoAnalytical Laboratory in Washington, US, and at ALS Laboratories, in North Vancouver, BC, respectively. The analytical methods for these analyses followed the procedures outlined in Johnson et al., (1999) and method published on the ALS Global website (www.alsglobal.com/myals/downloads, accessed, June 1, 2020). The results of all geochemical analyses are included in Appendix Table A1. Petrographic thin sections were prepared by Vancouver Petrographics in Langley, BC, and were analysed using a binocular petrographic microscope at the University of British Columbia.

1.4. Geochronology methodology

At several localities, the timing of volcanism is investigated using $^{40}Ar/^{39}Ar$ geochronology. We selected field samples that were holocrystalline and as fresh as possible. The samples were sent to two laboratories for preparation and analysis at various stages throughout the project: The Geochronology Facility at the University of Alaska–Fairbanks, US, and the WiscAr Geochronology Laboratory at the University of Wisconsin-Madison, US. All results are reported alongside an estimate of 1σ analytical uncertainty.

Samples sent to the Geochronology Laboratory, University of Alaska-Fairbanks for analysis were crushed and a bulk separate was sieved, washed in acetone, and hand-picked for phenocryst-free whole-rock groundmass chips. The monitor mineral TCR–2 with an age of 28.619 Ma (Kuiper et al. 2008) was used to monitor neutron flux and calculate the irradiation parameter (*J*).

The samples and standards were wrapped in aluminum foil and loaded into aluminum cans of 2.5 cm in diameter and 6 cm in height. The samples were irradiated in the research reactor of McMaster University in Hamilton, Ontario, Canada for 20 megawatt-hours. Upon return, the samples were step-heated and analyzed using a 6-watt argon-ion laser following the technique described in York and others (1981), Layer and others (1987), and Benowitz and others (2014) using a VG–3600 mass spectrometer at the Geophysical Institute, University of Alaska Fairbanks.

Samples analyzed at the WiscAr Laboratory, University of Wisconsin-Madison, US were crushed and sieved to 180-250 μm. A bulk separate containing groundmass and feldspar crystals was isolated from the samples using magnetic sorting, and density separation using methylene iodide. The separates were then ultrasonically leached in a 10–25% HCl, rinsed ultrasonically with deionized water, and then hand-picked under a binocular microscope to remove any altered domains or phenocrysts. Feldspar separates were also leached in 5% HF and rinsed ultrasonically with deionized water. The purified separates were wrapped in aluminum foil, placed in 2.5 cm aluminum disks, and irradiated along with the 1.1864 Ma Alder Creek sanidine standard (Jicha et al. 2016) at the Oregon State University TRIGA reactor in the Cadmium-Lined In-Core Irradiation Tube facility for 5 hours. Approximately 10 to 15 mg of groundmass was placed in a 5 mm copper well and incrementally heated with a 60 W CO_2 laser. Gas was analyzed using a Noblesse multi-collector mass spectrometer following the procedures in Jicha et al. (2016). Reported ages are calculated using the decay constants of Min et al. (2000). The atmospheric argon value used is that of Lee et al. (2006).

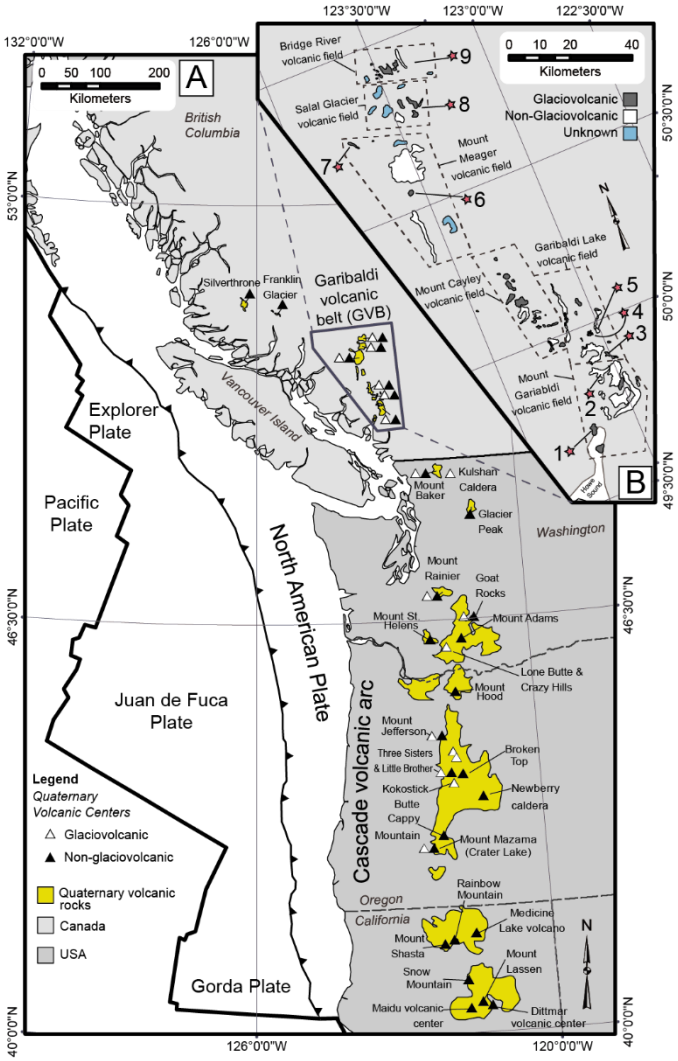

Fig. 1.1. Location and tectonic setting of the Cascade volcanic arc and Garibaldi volcanic belt (GVB; modified from Wilson and Russell 2018). (A) Tectonic setting of the GVB showing the distribution of Quaternary volcanic rocks and major volcanic centers. The outlined area is enlarged in B. (B) Distribution of Quaternary volcanic rocks in the GVB. The extent of the major volcanic fields is outlined using dashed boxes. Individual map areas included in this publication are indicated using red stars: Monmouth Creek volcano (1), Brohm Ridge (2), the Table (3), the Black Tusk (4), the Cinder Cone (5), Cracked Mountain volcano (6), Lillooet Glacier volcano (7), the Salal Glacier volcanic area (8), the Bridge River volcanic area (9).

This report adds 5 successful age determinations, 2 successful age determinations with unresolved relative stratigraphic implications and 5 unsuccessful (failed) age estimations (Table 1.1). Aborted and failed geochronology measurements were caused by either excess atmospheric ^{36}Ar (due to rock micro-vesicularity) or limited radiogenic ^{40}Ar (due to the young age of the rocks or saturation by atmospheric ^{36}Ar. Two of the failed experiments (samples AW-15-007 and AW-15-065) returned an inferred "zero age" due to limited radiogenic ^{40}Ar and appropriate levels of atmospheric ^{36}Ar. For these samples, we

Volcanic phase/Volcano	Sample ID	Map unit	Latitude	Longitude	Source*	Age (ka)	+/- 1s	Status	Comment
Monmouth Creek volcano	AW-15-007	CaAd	49.69374013	-123.1966635	1	NA	NA	Failed	Plateau and isochron age estimates are within error of zero age.
Microwave Bluff (Black Tusk)	AW-16-100	MsDl	49.98544402	-123.0503030	2	160.6	2.8	Success	Plateau age estimate.
West Bluff (Black Tusk)	AW-16-118	WBcAl	49.97119722	-123.0622376	2	1090.6	26.24	Success	Plateau age estimate.
The Cinder Cone	AB-22-43	CCcBl	49.98321900	-123.0167240	2	16.7	4.7	Success	Plateau age estimate.
Lillooet Glacier volcano	AW-15-065	LpBl	50.74214724	-123.7251255	2	NA	NA	Failed	Plateau and isochron age estimates are within error of zero age.
Salal Mountain (Salal Glacier volcanic field)	AW-16-253	SMcAl	50.76171001	-123.4176167	2	831.55	11.43	Success	Plateau age estimate.
Ochre Mountain (Salal Glacier volcanic field)	AW-16-259	OsBl	50.78909872	-123.3606024	2	408.68	6.70	Success	Plateau age estimate.
Logan Ridge (Salal Glacier volcanic field)	AW-16-241	LRpBl	50.81108445	-123.4086874	2	NA	NA	Failed	High atmospheric Ar.
NW volcanic remnant (Salal Glacier volcanic field)	AW-16-273	NpBd	50.81240050	-123.4518570	2	NA	NA	Failed	High atmospheric Ar.
Sham Plateau lava (Bridge River volcanic field)	AW-16-182	SPsBl	50.91424766	-123.4942963	2	746.9	7.67	Unresolved	Plateau age estimate. *Note*: Sample is from a unit stratigraphically above rocks dated at 598 ± 15 ka (K-Ar; Roddick and Souther, 1987).
Glacier View lavas (Bridge River volcanic field)	AW-16-122	GVcMl	50.92157202	-123.3995261	2	806.91	8.50	Unresolved	Plateau age estimate. *Note*: Sample is from a unit stratigraphically above rocks dated at 598 ± 15 ka (K-Ar; Roddick and Souther, 1987).
Thunder Creek volcano (Bridge River volcanic field)	AW-16-201	TCsMl	50.90784171	-123.4111272	2	NA	NA	Failed	High atmospheric Ar.

***Sources include: 1: Univ. Fairbanks, Alaska; 2: WiscAr, Univ. Wisconsin-Madison.**

Table 1.1 Summary of $^{40}Ar/^{39}Ar$ geochronology results based on analysis of groundmass material.

Prefix (phase)		Texture		Composition		Lithofacies		Non-volcanic lithofacies**	
Volcanic (undivided)	**V**	Aphyric	**a**	Basalt	**B**	Lava	**l**	Undivided till	**ut**
Castle	**C**	Porphyritic	**p**	Basaltic andesite	**BA**	Dikes & sills	**d**	Undivided alluvium	**ua**
Box Canyon	**BC**	Glassy	**g**	Andesite	**A**	Hyaloclastite	**h**	Undivided colluvium	**uc**
Warren Glacier	**W**	Coursely jointed	**c**	Basaltic trachyandesite	**BT**	Pillow lava	**p**	Undivided basement	**ub**
Cheekye	**CH**	Slender jointed	**s**	Dacite	**D**	Tephra	**t**	Silt (glaciolacustrine)	**sgl**
Atwell Peak	**A**	Flaggy jointed	**f**	Hawaiite	**H**	Tuff	**tu**	Ablation till	**at**
Table Meadows	**TM**	Hackly jointed	**k**	Mugearite	**M**	Tuff breccia	**tx**	Basal till	**bt**
Table East	**TE**	Bedded	**b**			Lapilli tuff	**lt**	Moraine till	**mt**
Table	**T**	Massive	**m**			Breccia	**bx**	Paraglacial sediments	**pg**
East Bluff	**E**	Aggultinated	**ag**			Conglomerate	**c**		
West Bluff	**WB**	Palagonitised	**pg**			Pillow breccia	**px**		
Back Tusk	**B**	Intrusive	**i**			Peperite	**pp**		
Microwave Bluff	**M**	Peperitic	**pe**			Intrusion	**i**		
Helm Creek	**H**	Oxidised	**o**						
Cinder Cone	**CC**								
Cracked Mountain	**CM**								
Lillooet Glacier	**L**								
Salal Center	**SC**								
Salal Tinder	**ST**								
Logan Ridge	**LR**								
Northwest volcanic remnant	**N**								
Ochre Mountain	**O**								
Salal Mountain	**SM**								
Mud Lake	**ML**								
Sham Hill	**SH**								
Bridge Glacier	**BG**								
Tuber Hill	**TH**								
Glacier View	**GV**								
Sham Plateau	**SP**								
Nichols Valley	**NV**								
Arrowhead Glacier	**AG**								
Sham Ridge	**SR**								
Thunder Creek	**TC**								

**** Used for non-volcanic lithofacies and without other designations.**

Table 1.2. Unit naming conventions and map codes

interpret a young (i.e., < 20 ka) volcanic event. Two of the successful age determinations (samples AW-16-122 and AW-16-182) returned acceptable age estimates, however, these estimates contradict the relative stratigraphic age inferred through field observations and a previously published geochronology study that used the K-Ar method). All geochronology implications and interpretations are discussed at relevant locations in this text.

1.5. Map organisation, lithofacies codes and unit colors

The lithofacies are discussed in relative chronological order (i.e., oldest to youngest). We have organised the mapped volcanic lithofacies into three groups: 1) "volcanic fields", 2) "volcanoes" and 3) "volcanic areas". The broadest group, "volcanic field", is used to collect the numerous volcanic occurrences in the geographically large Salal Glacier and Bridge River map areas. The "volcano" grouping is used when the volcanic edifice boundaries are well defined, the vent location is known or closely inferred, and the eruption events are interpreted to have occurred within a discrete period. The more generalised term "volcanic area" is used to describe geographically restricted volcanic occurrences that show multiple eruptive episodes, have unconstrained vent locations and/or have an unconstrained geologic history.

At each volcano, or volcanic area, the lithofacies are subdivided into "phases". Each phase defines a period of volcanic activity recognised though lithofacies exhibiting similar petrographic, geochemical, and mineralogical characteristics. Each phase is assumed to have been erupted and deposited within a restricted chronostratigraphic timeframe. The volcanic phases are named using local geographic features (e.g., the "Castle" phase) or using names previously established in literature. Each volcanic phase may comprise one or more "map units".

We have designed a lithofacies naming convention that is specifically tailored to this series of Quaternary volcanology-specific maps. Map unit names and map codes are constructed from the named volcanic phases along with the physical characteristics that define the deposit, including deposit-scale

features (e.g., bedding), petrographic texture (e.g., porphyritic), rock composition (e.g., andesite) and lithofacies association (e.g., pillow lava). A further numeric subunit designation (i.e., 1-4) is used only in the Lillooet Glacier volcano map to denote relative stratigraphic ages of layered, onlapping basaltic pillow lava horizons.

The volcanic map unit names and codes comprise four parts:

i) An uppercase volcanic phase prefix (e.g., the "Castle" phase – "C").
ii) A lowercase physical deposit characteristic descriptor (e.g., "massive" – "m").
iii) An uppercase description of the rock composition (e.g., "Basalt" – "B").
iv) A lowercase volcanic facies descriptor (e.g., "pillow lava" – "p").

Unit names and codes for non-volcanic rocks use two lowercase letters that identify the lithofacies (e.g., "Basal till) – "bt". A full list of all codes used in all maps is provided in Table 1.2. Where possible, closely related rock units that exist within a single volcanic phase are grouped in the supporting text to avoid unnecessary repetition. Because all volcanic rocks erupted in the Quaternary, the traditional "Q" prefix is not used.

Numerous maps exhibit multiple lithofacies sharing similar characteristics. As an example, the Black Tusk map has eight distinct map units that are all coherent andesite lava. Consequently, the selection of colors for these map units aims to enhance the contrast between units within each volcano or volcanic region, rather than strictly adhering to a color convention. Mafic rocks are typically depicted in varying shades of red, brown, and orange, intermediate rocks in shades of green, and felsic rocks in blue and yellow. To ensure consistency across all maps, rocks that appear on multiple maps, such as undivided basement (pink) and undivided till (yellow), maintain standardized colors.

2. Monmouth Creek volcano (1:10,000)

Monmouth Creek volcano is a small, eroded intermediate composition volcano exposed on the wall of Howe Sound in the southern Garibaldi volcanic belt (Mathews 1958; Green 1994; Kelman et al. 2002a). The Monmouth Creek volcanic rocks unconformably overlie glacially-scoured phaneritic leucogranite of the Cretaceous Squamish pluton (Bostock 1963; Cui and Russell 1995). Although extensively eroded, the volcanic deposits form a broad pile that is at least 200 m thick and cover an elevation range of ~10 to 800 m asl (Fig. 2.1A). The volcanic lithofacies include andesitic lava flows, domes, lobes, dikes, and hyaloclastite breccia in addition to dacitic dikes and a dacite lava dome. Numerous dikes crosscut the volcanic stratigraphy, and their erosional remnants crop out as steep-sided, pinnacles and spires. The "Castle", a prominent volcanic feature within the map area, is the eroded remains of several intersecting, subvertical andesite dikes (Fig. 2.1B). The volcanic rocks at Monmouth Creek at locally unconformably overlain by alluvial and colluvial deposits.

Volcanic phase	Map unit	Map unit code	Texture	Groundmass	Components
Castle (C) phase	Aphyric andesite lava	CaAl	Aphyric, aphanitic	Glassy, sometimes partially devitrified (5-30 %); flow-aligned trachytic plagioclase (50-60 % , <0.1 mm) and blocky Fe-Ti oxide (10-20 % , 0.1 mm)	Microphenocrysts: euhedral orthopyroxene (<10% , <0.1 mm); rare embayed olivine crystals (<0.5 mm diameter) surrounded by rims of recrystallized augite; rare subhedral augite (<1 % , <0.1 mm)
	Glassy andesite lava	CgAl	Aphyric, glassy		
	Massive andesite hyaloclastite	CmAh	Aphyric, glassy		
	Aphyric andesite dikes	CaAd	Aphyric, hypocrystalline		
Box Canyon (BC) phase	Porphyritic dacite lava	BCpDl	Porphyritic, glassy	Glass (~5-30 %), fine microlites of trachytic plagioclase, sometimes flow-aligned (~30-60 % , 0.1 mm) and blocky Fe-Ti oxides (5-10 % , 0.1 mm).	Phenocrysts: augite (~5% , 0.1–1 mm) and orthopyroxene (~5% , 0.1–1 mm) are subhedral and display subtle resorbed margins. Plagioclase phenocrysts (~10 %, 0.5–1 mm) are euhedral and show intense oscillatory zoning. Acicular hornblende phenocrysts (<2 mm length, ~ 1%)
	Porphyritic dacite dikes	BCpDd	Porphyritic, aphanitic		

Table 2.1 Petrographic characteristics of rocks from Monmouth Creek volcano.

The volcanic lithofacies at Monmouth Creek are divided into two phases of volcanic activity based on their petrographic characteristics. The older Castle (C) phase is made up of aphyric to sparsely orthopyroxene phyric andesite and minor basaltic andesite (Table 2.1). The younger Box Canyon (BC) phase rocks are augite, orthopyroxene, and hornblende phyric dacite (Table 2.1). Castle phase rocks have whole-rock compositions ranging from basaltic andesite to andesite and Box Canyon phase

Wilson, A.M., Russell, J.K., and Harris, M.A., 2024. Glaciovolcanism in the Garibaldi volcanic belt: Nine geological maps from southwestern British Columbia, Canada. British Columbia Ministry of Mining and Critical Minerals, British Columbia Geological Survey Open File 2024-10, 64p

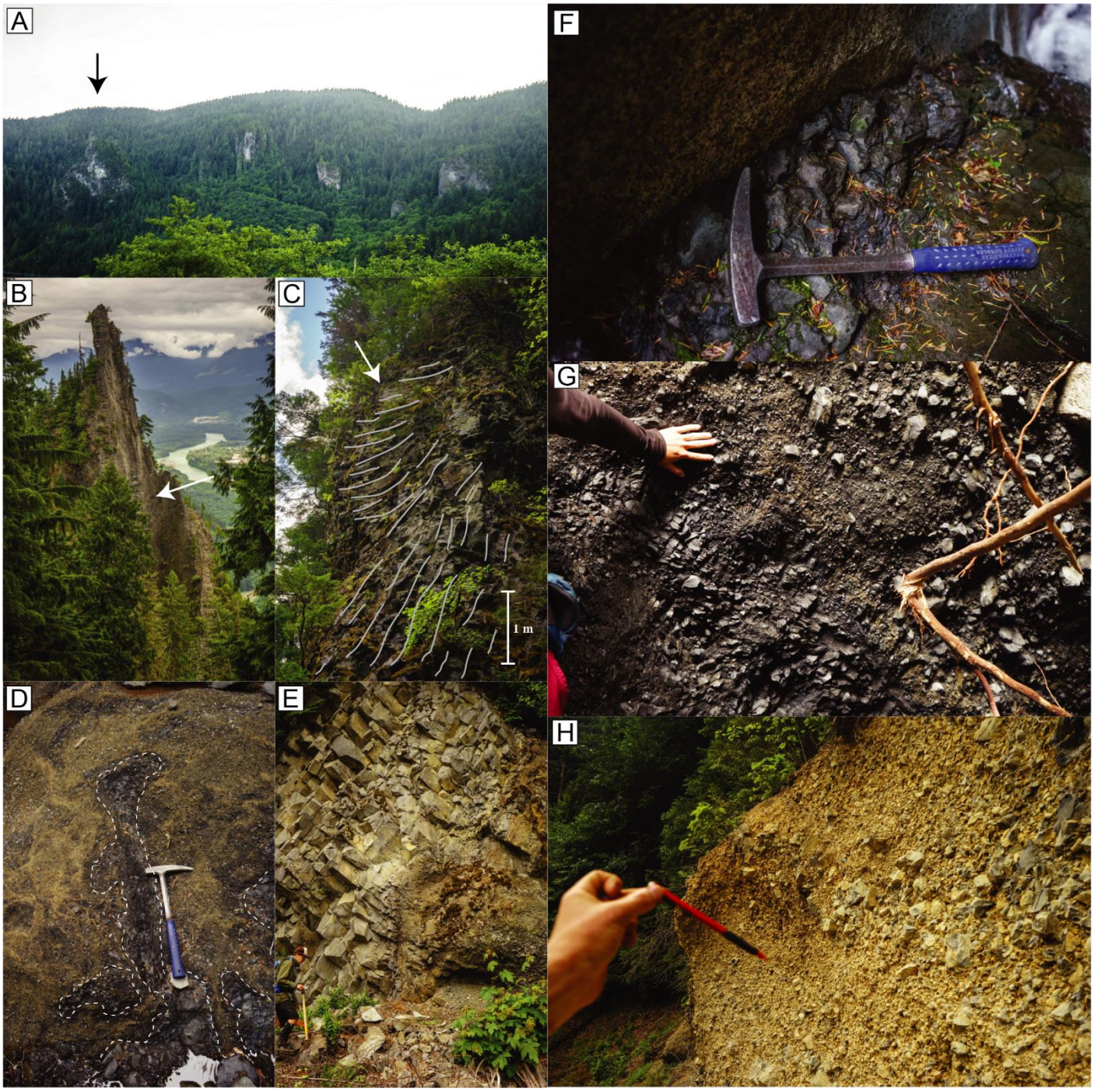

Fig. 2.1. Field photographs showing lithofacies of Monmouth Creek volcano. (A) Photograph looking west at the central portion of Monmouth Creek volcano. The Castle is indicated with an arrow. (B) The Castle, a prominent spire viewed from the south. (C) Coarse, subvertical basal colonnade and radiating lower margin surface of ~100 m thick, Castle phase aphyric andesite lava (unit CaAl) in the northern map area. Slender outer columns (white arrow) change orientation abruptly to ~45º. (D) Glassy, coherent irregularly shaped andesite lava lobes (unit CaAl) intruding and sourcing an accumulation of cogenetic hyaloclastite (unit CmAh). (E) Photograph showing Box Canyon phase porphyritic dike (unit BCpDd) cross cutting Castle phase andesite hyaloclastite (unit CmAh). (F) Photograph showing Monmouth Creek volcano lithofacies resting of smooth, glacially scoured leucogranite bedrock. (G) Photograph showing Castle phase massive andesite hyaloclastite (unit CmAh) exposed in Box Canyon creek. (H) Photograph looking south showing westerly dipping beds of crudely bedded Castle phase andesite hyaloclastite (unit CmAh).

rocks range from andesite to dacite (Fig. 2.2A). All Monmouth Creek volcanic lithofacies have subduction-related calc-alkaline trace element profiles (Fig. 2.2B). The Castle phase rocks are volumetrically predominant and form a 100–200 m-thick sequence of radially jointed andesite lavas (northern map area; Fig. 2.1C), lava lobes, and lava domes with irregular columnar jointing, and a glassy to sub-glassy groundmass (Fig. 2.1D). The coherent Castle phase rocks are typically encased in carapaces of

cogenetic hyaloclastite (Fig. 2.1D) (Wilson et al. 2016). The Box Canyon phase deposits mark the end of volcanism and comprise a series of en-echelon dacite dikes distributed throughout the map area (Fig. 2.1E).

The lithofacies at Monmouth Creek preserve a record of glaciovolcanism. Elongate lavas in the northern map area display slender, radially oriented columnar joint sets indicative of rapid cooling and physical confinement within the ice. The abundance of hyaloclastite deposits provides further evidence of rapid lava quenching. There are no indicators of explosive volcanism at Monmouth Creek. All volcaniclastic lithofacies were derived either by quench fragmentation by effusive eruption into the water and/or ice or by the syn-eruptive gravity-driven collapse of the volcanic pile. The volcaniclastic rocks are poorly sorted and lack indicators for significant sediment transport or deposit reworking. These strong glaciovolcanic indicators suggest that

the Monmouth Creek volcano erupted during a time that Howe Sound was filled with a glacier that had an upper surface elevation of at least 800 m asl (Wilson et al. 2016).

Preservation of delicate volcanic lithofacies at Monmouth Creek (e.g. unconsolidated hyaloclastite and the "Castle" pinnacle) and their distribution in an area of steep bedrock topography (i.e., they would rapidly erode), suggests that the deposits likely erupted during the waning stages of the MIS (MIS) 2 (Fraser) glaciation (ca. 17 to 13 ka; Clague and Ward 2011). This is consistent with the results from an unsuccessful whole-rock $^{40}Ar/^{39}Ar$ age estimate for a sample of the Castle phase rock (AW-15-007, Table 1.1). The rock contained limited radiogenic ^{40}Ar and did not have appropriate levels of atmospheric ^{36}Ar. For this sample, we interpret a young (i.e., < 20 ka) volcanic event. (pers. comm. Jeff Benowitz, 2016).

2.1. Basement geology

Undivided basement rocks (ub)

Pink–white, medium-grained (2–5 mm) leucogranite of the Squamish pluton (Bostock 1963; Cui and Russell 1995) are the basement rocks in the map area. The Squamish pluton leucogranite forms an irregular topography of glacially rounded peaks and steep-sided valleys. Where observed, rocks of Monmouth Creek volcano rest directly on a smooth, glacially scoured surface (Fig. 2.1F).

2.2. Geology of Monmouth Creek volcano

2.2.1. The Castle (C) phase (Glaciovolcanic)

Aphyric andesite lava (CaAl)

Dark grey, poorly vesicular (<15 %), aphyric, aphanitic andesite lavas form three northeast-trending, steep-sided, elongate ridges that have high width-to-thickness ratios in the northern part of the map area. As exposed in a canyon near Monmouth Creek, the andesite lavas are >100 m thick (Fig. 2.1C). Here, the rocks directly overlie glacially scoured leucogranite basement (ub). In Box Canyon, the andesite lavas are underlain by minor accumulations of cogenetic beds of andesite hyaloclastite (CmAh) (Fig. 2.1G). Irregular, slender (<10 cm-diameter) columnar jointing is pervasive and typically oriented in radial, fanning structures (Fig. 2.1C). The rocks are sparsely orthopyroxene phyric and have a groundmass of partially devitrified glass, flow-aligned trachytic plagioclase, and blocky Fe-Ti oxide (Fig. 2.3A and Table 2.1). The low width-to-thickness aspect ratio of these lavas and their radially jointed, glassy margins suggest physical confinement and emplacement in an ice-marginal environment (Wilson et al. 2016).

Glassy andesite lava (CgAl)

Dark grey, poorly vesicular (<10 % vol.) glassy, hackly and radially jointed (sensu, Lescinsky and Fink 2000) lavas and lava lobes form small (<20 m-diameter) coherent rock masses in the southern part of the map area (e.g., Fig. 2.1D). Lobes (i.e., those with sub-equal width and thickness) display hackly jointed margins that grade laterally into associated (i.e., cogenetic) massive, andesite hyaloclastite (CmAh). Lavas (i.e., those with a width/thickness ratio >2) display stout, sub-vertical columnar jointing, and brecciated and hackly jointed fronts. Several volumetrically large flows occur in the northern map area. These lavas are elongate, have high aspect ratio profiles, and show slender, radially oriented marginal columnar joint sets. The rocks have a glassy groundmass containing fine trachytic plagioclase and Fe-Ti oxide (Table 2.1). We interpret that a significant portion of the southern map area likely comprises sheets and lobes of lava that are surrounded by carapaces of quenched hyaloclastite breccia (e.g., Fig. 2.1D). The radially jointed lobe morphologies are consistent with enhanced cooling and emplacement into an ice and/or meltwater-rich environment. The elongate, northeast-trending orientation of the lavas in the northern map area suggests propagation and confinement within pre-existing subglacial cavities (i.e., crevasses).

Aphyric andesite dikes (CaAd)

Light to medium grey, poorly vesicular (<10% vol.), aphyric, hypocrystalline, columnar jointed dikes (2–10 m diameter) form several deeply eroded spires and pinnacles throughout the map area. The "Castle" comprises at least three northeast-southwest oriented, sub-vertical dikes that are closely spaced, each 5 to 10 m wide. The Castle (Fig. 2.1B) has a steep eastern face that is ~180 m high that exposes the U-shaped intersection of two branching dikes. Horizontal columnar joints are pervasive, with the long axes of the columns radiating around the inner part of the structure (Wilson et al. 2016). The dikes have a fine, holocrystalline groundmass of minor glass, flow-aligned (trachytic) plagioclase and blocky Fe-Ti oxide (Table 2.1). The glass is commonly concentrated within thin (0.5 mm), elongate bands that parallel the dike walls. Vesicles are sub-rounded, elongate, and concentrated in glassy bands. The Aphyric andesite dikes are observed to crosscut massive, andesite hyaloclastite (unit CmAh) in several places, including, at the base of the "Castle".

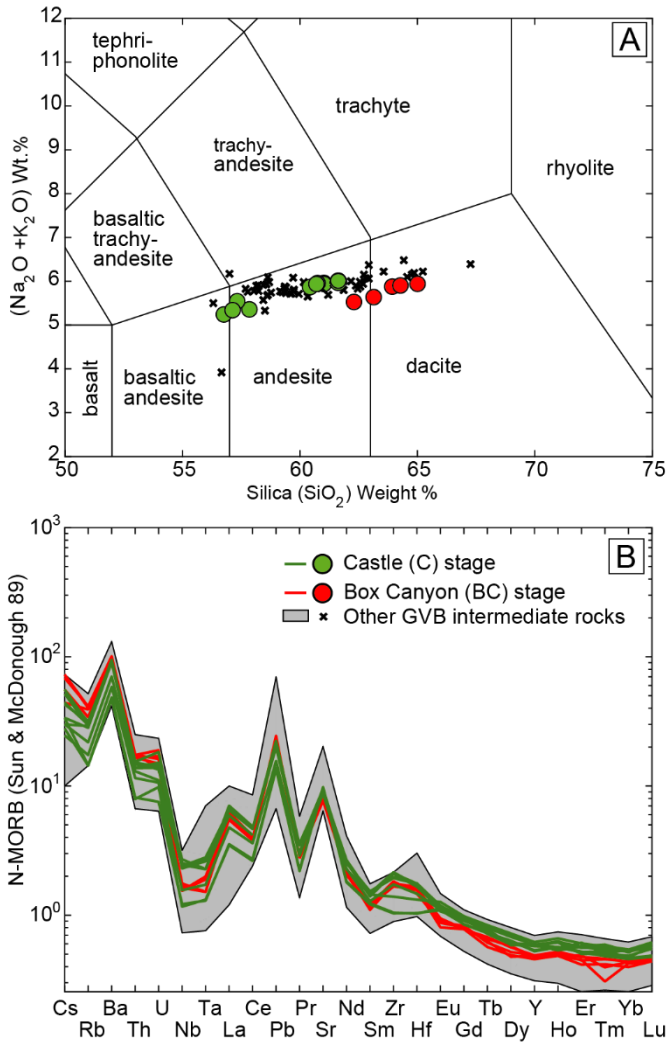

Fig. 2.2. Geochemical characteristics of Monmouth Creek volcano rocks. (A) Total alkali-silica plot showing Castle phase andesite (and minor basaltic andesite) and Box Canyon phase dacite. Data are plotted against other intermediate volcanic rocks from the GVB for comparison (sourced from Bye et al. 2000; Kelman 2005; Fillmore and Coulson 2013; and other maps in this publication). (B) Trace element compositions normalized to N-MORB (Sun and McDonough 1989) of Monmouth Creek volcanic rocks displaying Nb-Ta depletion consistent with a subduction-related calc-alkaline origin.

Massive andesite hyaloclastite (CmAh)

Poorly consolidated, massive to crudely bedded, monolithic, poorly sorted, clast supported andesite breccias are variably exposed throughout the map area. The clasts are angular and have a jigsaw fit texture. Clast sizes range from fine ash to blocks. The clasts are fine-grained, aphyric, and glassy (similar to the associated aphyric and glassy andesite units (CaAl, CgAl). The matrix contains blocky, ash to lapilli-sized fragments of palagonitized glass, giving the breccia an orange-yellow colour. Sensu stricto, these breccias are considered hyaloclastites (e.g., Smellie and Edwards 2016). These breccias are recessive and have a subdued topography expression. This topography is present in numerous places that lack outcrop suggesting that these rocks may form a major volumetric constituent of the map area. In several places, the rocks are observed to rest directly on glacially scoured bedrock (Fig. 2.1F). In Box Canyon, they form thin accumulations underling aphyric andesite lavas (unit CaAl) (Fig. 2.1G) and massive to crudely bedded carapaces surrounding nearby (associated) lava lobes (Fig. 2.1D). The deposits change gradationally from massive to crudely bedded with distance from the central lava lobe source (Fig. 2.1D) and are commonly observed to dip westward at a shallow angle into the hillside (Fig. 2.1H). The rocks show no evidence of significant clast transport (i.e., clast rounding) or deposit reworking (e.g., crossbedding). We interpret that these rocks were produced by hydroclastic fragmentation of the adjacent aphyric and glassy andesite lavas (units CgAl and CaAl) in response to contact with ice and/or meltwater. Westerly dipping beds are consistent with accumulation against a valley glacier in Howe Sound.

2.2.2. Box Canyon (BC) phase (Glaciovolcanic)

Porphyritic dacite lava (BCpDl)

Light grey, poorly vesicular (<10%), hackly (sensu Lescinsky and Fink 2000) and radially columnar jointed, sub-glassy dacite lavas form a wide dome-shaped structure in the western map area. These rocks have phenocrysts of augite, orthopyroxene, plagioclase, and hornblende. The groundmass is glassy and contains fine microlites of trachytic plagioclase and blocky Fe-Ti oxide (Table 2.1). At the margins of the dome, the rocks display hackly jointing (sensu Lescinsky and Fink 2000). Towards the dome center, they show slender columnar jointing. Contacts with the surrounding Castle phase andesite hyaloclastite (CmAh) are also not well exposed, however, the presence of ex-situ fragments of massive hyaloclastite with aphyric clasts (i.e., CmAh) nearby suggests a younger, intrusive relationship. The geometry, pervasive slender columnar jointing, and glassy nature of these rocks support emplacement involving accelerated cooling (i.e., subaqueous or subglacial). Because the extreme local topography would facilitate efficient surface water drainage, these lithofacies are consistent with emplacement under and/or against glacial ice.

Porphyritic dacite dikes (BCpDd)

Light to medium grey, poorly vesicular (<5%), columnar jointed dikes (column diameter 1–2 m) crosscut all other lithologies at Monmouth Creek volcano. The erosional remnants of these dikes form several steep-sided, elongate (<400 m long), pinnacles and spires rising >50 m above the surrounding hillside (Fig. 2.1A). The rocks are holocrystalline and have phenocrysts of augite, orthopyroxene, plagioclase, and acicular hornblende (Fig. 2.3B and Table 2.1). Acicular hornblende phenocrysts are typically aligned parallel to the direction of the dike wall. The groundmass is medium-grained and comprises flow-aligned trachytic plagioclase and blocky Fe-Ti oxides. We interpret these dikes probably fed the porphyritic, glassy dacite lava dome (BCpDl) exposed in the western map area. There is no other surface expression of these dikes (i.e., erupted material such as hyaloclastite or lava with a porphyritic texture), suggesting that the Monmouth Creek volcano has probably undergone extensive

erosion since emplacement. Porphyritic dacite dikes are observed to crosscut Castle phase hyaloclastite breccia near the "Castle" in the southern map area (Fig. 2.1E), and directly crosscut plutonic bedrock in the northern map area.

2.3. Quaternary sediments

Undivided alluvium (ua)

Undivided, unconsolidated, poorly sorted polymictic gravel, sand, and silt with a wide range of clast types and deposit structures. This unit forms a broad alluvial fan at the mouth of the Squamish River and is observed to unconformably overlie the Monmouth Creek volcanic rocks in several places.

Undivided colluvium (uc)

Undivided, unconsolidated, poorly to well-sorted, massive to crudely bedded breccia, sand, and gravel with a dark orange matrix are exposed in thin sequences (<5 m-thick) in the southern and eastern map area. The unit is matrix-supported and contains mainly dense, sub-angular to sub-rounded andesitic volcanic clasts and liberated plagioclase crystals. Larger volcanic clasts (up to 20 cm diameter) are sub-angular and columnar-jointed. Rare, sub-rounded plutonic cobbles and boulders occur in some places. The unit is observed to unconformably overlie Castle phase massive, andesite hyaloclastite (unit CmAh), and bedrock (unit ub). It is crudely bedded to massive and shows minor crossbedding in several places. X-ray diffraction and binocular and granulometry analysis indicate that the components are mostly locally derived, aphyric volcanic material, supporting a local colluvial origin.

2.4. Summary

Wilson et al. (2016) use field relationships and the distribution of the volcanic lithofacies to establish a glaciovolcanic origin for the Monmouth Creek volcano (termed Monmouth Creek volcanic complex by these authors). They suggested that the deposits accumulated along the valley wall of Howe Sound while it was occupied by >800 m of ice. This map provides additional detailed physical volcanological, petrographic, and geochemical lithofacies descriptions that support the glaciovolcanic hypothesis.

The sequence of eruptive events at Monmouth Creek is as follows. Effusive volcanism began in the southern map area where a series of aphyric lava domes and dikes erupted along the western wall of Howe Sound (the Castle phase). At this time, Howe Sound was filled with glacial ice to a depth of at least 800 m asl. Rapid cooling and quenching of the lavas in contact with the ice and/or meltwater produced large accumulations of cogenetic hyaloclastite. These volcaniclastic lithofacies were deposited locally and eventually constructed a volcanic pile that was physically constrained by ice along the eastern margin. The steep local relief facilitated rapid meltwater drainage and prohibited the buildup of an englacial meltwater lake. As the eruption progressed several large, aphyric lavas were emplaced on the northern edifice slope. These lavas propagated towards the north, probably taking advantage of pre-existing cracks (crevasses) in the adjacent valley glacier. A second,

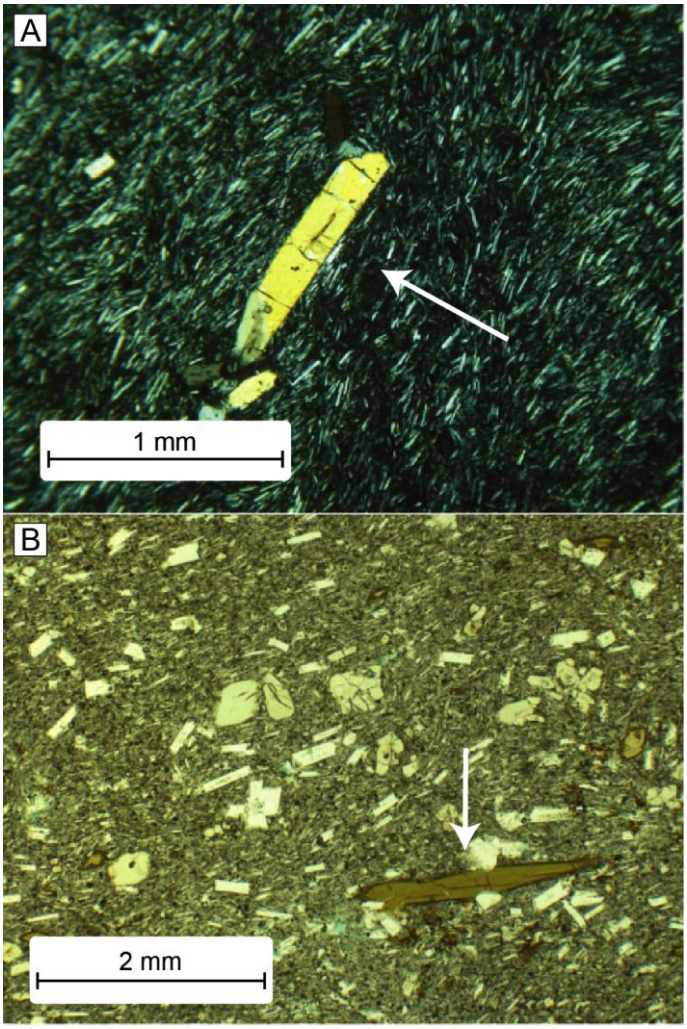

Fig. 2.3. Petrographic characteristics of the Monmouth Creek volcano rocks. (A) Photomicrograph showing orthopyroxene phenocryst in a groundmass of trachytic plagioclase and Fe-Ti oxides in a Castle phase, aphyric andesite lava (unit CaAl). (B) Photomicrograph showing Box Canyon phase porphyritic dacite dike (unit BCpDd) with large phenocrysts of plagioclase, orthopyroxene, augite, and hornblende. White arrow indicates a large, flow-aligned hornblende phenocryst.

geographically isolated Castle phase lava was also emplaced on the slope north of the main volcanic pile. Like other Castle phase lithofacies, this deposit shows evidence of glacial confinement and rapid marginal quenching. The Box Canyon phase of volcanism involved the intrusion of several dispersed porphyritic dikes and a large subglacial lava dome in the western map area. It is unclear if there was a significant time involved between the Castle phase eruptions and these intrusive events, however, their evolved geochemical and petrographic character suggests some degree of magmatic differentiation. The glassy nature of the Box Canyon phase lava dome indicates that this phase of activity also took place at a time when the local area was also glaciated. Following the eruption, deglaciation facilitated rapid erosion of the loosely consolidated volcanic breccia pile, exposing the coherent (i.e., resistant) dike lithofacies.

3. Brohm Ridge area (1:10,000)

Mount Garibaldi is a stratovolcano located approximately 60 km north of Vancouver in southwestern British Columbia, Canada (Fig. 1.1). (Mathews 1952a, 1958; Hickson 1994; Kelman et al. 2002a; Hildreth 2007). Mount Garibaldi has been intermittently active since the Middle Pleistocene, however, the majority of the preserved volcanic structure is interpreted to be <50 ka (Mathews 1952a). Mathews (1952) suggested that Late Pleistocene volcanism at Garibaldi occurred supraglacially (i.e., erupted through and deposited on top of glacial ice), with deposited pyroclastic material residing on the top of a receding glacier located in the adjacent Cheekye River valley. As the ice melted, the western flank of the edifice collapsed, producing large debris flows and rock avalanches that inundated the Cheekye River and constructed the Cheekye Fan (Mathews 1952a; Friele and Clague 2002; Clague et al. 2003). Through a study of the preserved volcanic and glacial sediments in the Cheekye valley, Friele and Clague (2009) estimate that the summit of Mount Garibaldi probably formed shortly before 13.5 ka.

Brohm Ridge is a prominent ridge extending westward from Mount Garibaldi. Based on relative stratigraphic age and previous K-Ar geochronology measurements, we subdivide the deposits of Brohm Ridge into three phases of activity. The older, Warren Glacier (W) phase comprises a ~50 m-thick sequence of bedded basaltic tuff breccia and hyaloclastite and columnar-jointed basaltic lava that is unconformably overlain by a thick deposit of polymictic diamicton (glacial basal till) (Table 3.1 and Fig. 3.1A). We infer that this till also overlies the Cheekye (CH) phase rocks, which consist of hornblende and orthopyroxene phyric andesite lava and autobreccia (Table 3.1 and Figs. 3.1B). The Cheekye phase lavas form at least six, shallow southeasterly-dipping stacked flows exposed along the crest of Brohm Ridge. Green et al. (1988) reports a K-Ar age estimate for these lavas of 460 ± 20 ka. In several places, the Cheekye phase andesite lavas are overlain by poorly sorted lahar and debris flow deposits (Fig 3.1C). The clasts in these deposits suggest a close association with the coherent Cheekye phase rocks.

The youngest volcanism in the area is represented by the Atwell Peak (A) phase. These rocks include porphyritic dacite lava and pyroclastic block and ash deposits that unconformably overlie all other volcanic lithologies (Table 3.1 and Fig. 3.1E). At higher elevations (>1700 m asl) the unconsolidated surface exposures of these rocks are free from overlying glacial debris (e.g., ablation till). Their stratigraphic position and unconsolidated nature suggest that the Atwell Peak phase rocks were laid down during one of the most recent phases of volcanic activity at Mount Garibaldi and have an interpreted young age (i.e., ~13.5 ka; Friele and Clague, 2009). Supporting this interpretation, the Atwell Peak phase pyroclastic rocks are also texturally, mineralogically and chemically similar in situ, block-and-ash deposits that are located ~16 km southwest of the main summit in a quarry near the town of Squamish (cf., AW-15-001, AW-15-103, AW-15-104; Table A1). A wood fragment entrained in this deposit yielded a radiocarbon age of 11.7 ± 0.48 ka (Median of reported age: 12,130 – 11,280 yr. B.P. from Friele and Clague, 2009, as reported by Wilson and Russell, 2018).

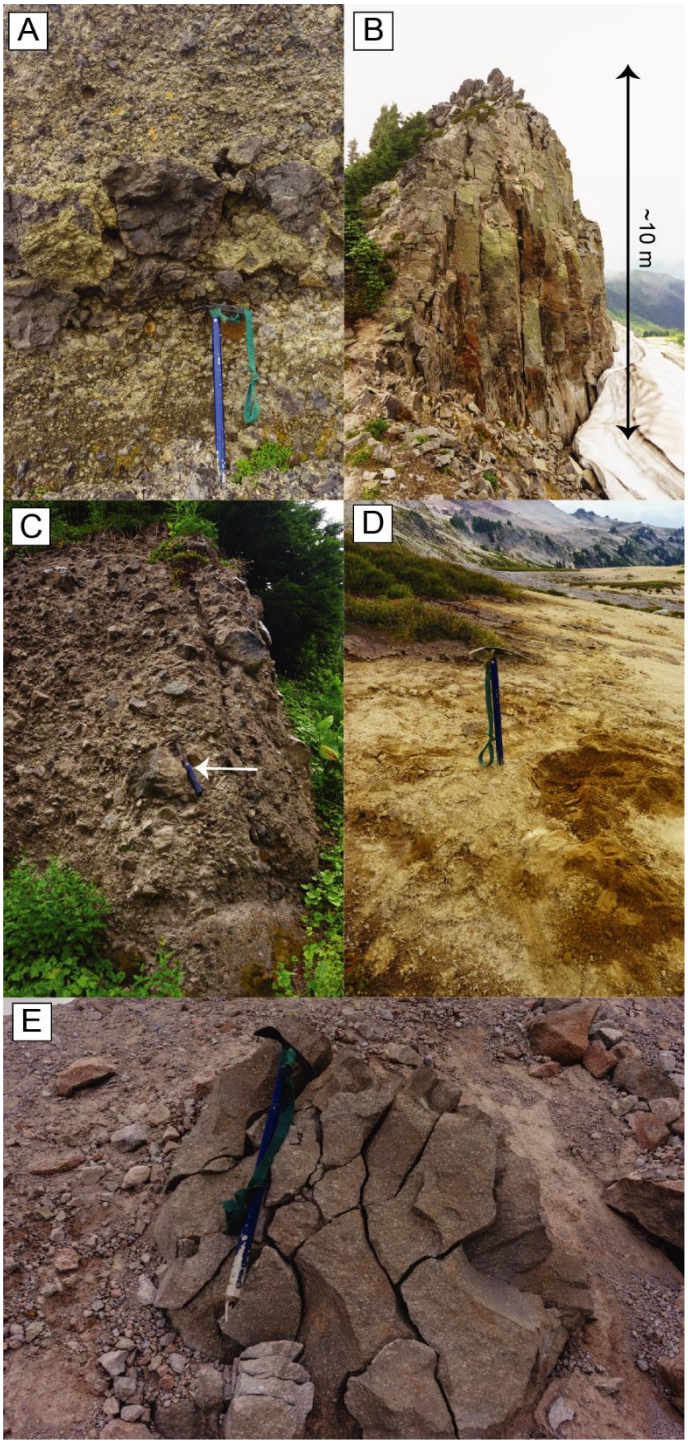

Fig. 3.1. Field photographs of the Brohm Ridge lithofacies. (A) Warren Glacier phase basaltic tuff breccia exposed in the eastern map area (unit WbBtx). (B) Porphyritic andesite lava exposed along the crest of Brohm Ridge (unit CHpAl). (C) Poorly sorted andesite lahar/debris flow deposits exposed in the western map area (unit CHmAc). (D) Orange brown glaciolacustrine sediments (unit sgl) along the northern edge of Brohm Ridge. (E) Poorly sorted, monolithologic dacite block and ash deposits of the Atwell Peak phase (unit AmDtx).

This apparent correlation suggests that active volcanism of the Atwell Peak phase may have continued until this time.

All Quaternary volcanic rocks in the map area are observed to unconformably overlie weakly-foliated quartz diorite and well-foliated greenschist of the Cloudburst Formation (Cretaceous) (Mathews 1958). Several Late Pleistocene glacial deposits also occur; in the western map area, glacial ablation till (not mapped) covers the ridge to an elevation of ~1700 m asl. On the northern side of the ridge, glaciolacustrine sediments are observed to unconformably overlie the Cheekye phase rocks. These sediments form a 2 to 5 m-thick veneer along the northern margin of Brohm Ridge (Fig. 3.1D), elucidating the presence of a glacially dammed lake occupying the upper reaches of the southern branch of the Culliton Creek valley during the waning stages of the last glaciation during MIS 2 (i.e., Fraser).

3.1. Basement geology

Undivided basement rocks (ub)

Grey to green, medium to fine-grained, weakly foliated quartz diorite and well-foliated greenschist are exposed along the northern side of Brohm Ridge and at lower elevations in the Cheekeye valley. Mathews (1958) maps this unit as Cretaceous Cloudburst Formation.

3.2. Geology of the Brohm Ridge area

3.2.1. Warren Glacier (W) phase (Glaciovolcanic)

Bedded, basaltic tuff breccia and hyaloclastite (WbBtx)

Moderately consolidated, poorly sorted, matrix supported, bedded basaltic tuff breccia and hyaloclastite forms a <50 m-thick accumulation in the eastern map area (Fig. 3.1A). The deposits contain angular to sub-angular, moderately vesicular, porphyritic basalt blocks and cauliflower bombs that are up to 50 cm in diameter (Table 3.1). Bedding is crude and varies over a range of 10 to 30 cm. Individual beds are defined by variations in average clast size. Accessory quartz diorite and greenschist lithics (up to 20 cm) comprise ~20 % of the unit. The rocks rest directly on the underlying basement rocks. Glassy clasts and a deep orange brown palagonitised matrix support an emplacement into a wet environment (i.e., glaciovolcanic). Chemically, the Warren Glacier phase rocks show Nb-Ta depletion, consistent with a calc-alkaline volcanic arc origin (i.e., they do not appear to be related to alkaline basaltic volcanism in the northern GVB (Fig. 3.2) (Mullen and Weis 2015).

Porphyritic basaltic lava (WpBl)

Dark grey, moderately vesicular, columnar jointed, porphyritic basalt forms a ~15 m-thick lava overlying bedded basaltic tuff (unit WbBtx) in the eastern map area. Columnar jointing near the core of the flow is coarse (~30 cm-diameter) and subvertical. Near the margins, the columns are irregular, fine scale and form lobe-like pseudo-pillow structures. The rocks contain phenocrysts of plagioclase, olivine, and augite and a groundmass of microlitic plagioclase, minor augite, and Fe-Ti oxide (Table 3.1). The lava is underlain by a 0.5 to 1 m-thick zone of poorly sorted autobreccia (not mapped), which grades into underlying bedded tuff and hyaloclastite (unit WbBtx).

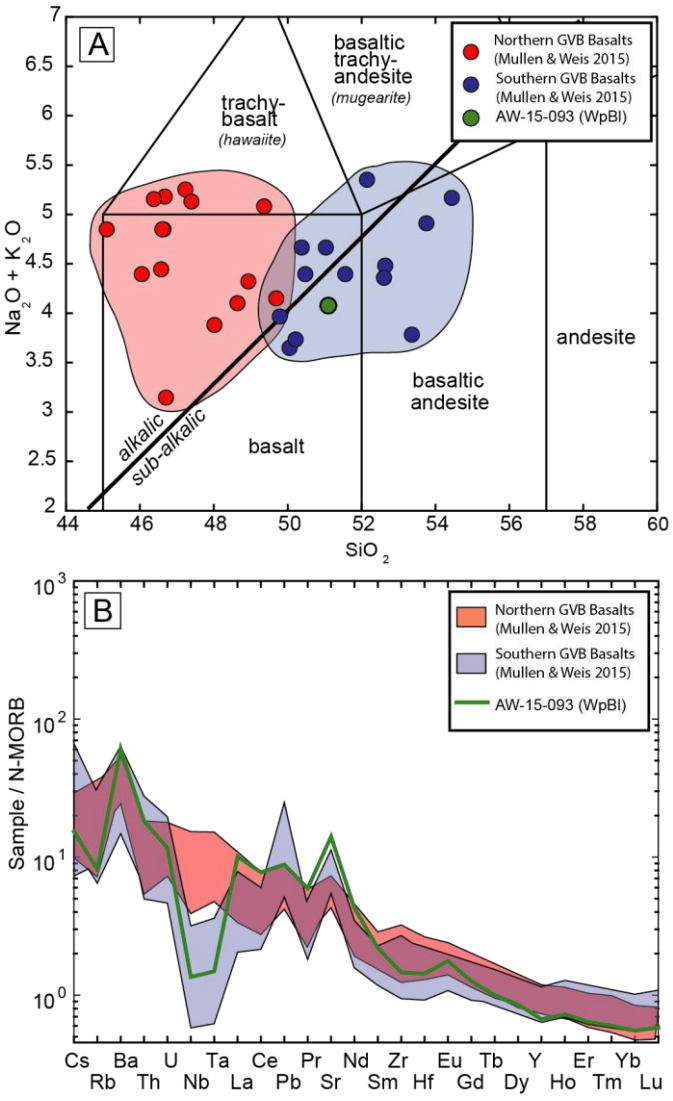

Fig. 3.2. Geochemical characteristics of the Warren Glacier phase basalts compared with other basalts in the GVB (data are from Mullen and Weis 2015) (A) Total Alkali-Silica plot (after Le Bas et al. 1986) and, (B) Trace element profile, showing sub-alkaline, basaltic affinity of unit Warren Glacier phase rocks (sample AW-15-093). The trace elements are normalised to N-MORB (Sun and McDonough, 1989).

3.2.2. Cheekye (CH) phase (Non-glaciovolcanic)

Porphyritic andesite lava and massive andesite breccia (CHpAl and CHmAbx)

Medium grey, poorly vesicular andesitic lava forms at least six, shallow southeasterly dipping stacked flows exposed along the crest of Brohm Ridge. Individual lavas range in thickness from ~20 to ~50 m (Fig. 3.1B). The lavas are porphyritic and contain phenocrysts of plagioclase, hornblende, and orthopyroxene. They have a fine groundmass of trachytic plagioclase and Fe-Ti oxide (Table 3.1). In several places, these rocks are underlain by 1 to 5 m-thick accumulations of massive, clast supported, poorly sorted, autobreccia (mapped as unit

CHmAbx). Exposures near the base of the sequence contain ~5 % cumulate-textured cognate inclusions. The inclusions are sub-rounded, ~5 to ~10 cm-diameter, and are characterised by a coarse groundmass of interlocking plagioclase and acicular hornblende. Green et al. (1988) report a K-Ar age for the lavas of 460 ± 20 ka, indicating an approximate age of Cheekye phase activity.

Massive andesite conglomerate (CHmAc)

Moderately consolidated, clast supported, massive to very crudely bedded conglomerate forms several accumulations overlying porphyritic andesite lavas (CHpAl) in the western map area (Fig. 3.1C). The true thickness is not observed however the deposits are interpreted to be up to 50 m thick. The clasts comprise angular to subrounded, porphyritic andesite cobbles, boulders and gravel, and minor rounded granodiorite and greenschist pebbles. The matrix consists of fine silt and sand. A distinct lack of clast striations and deposit matrix support suggests that these rocks are not glacial in origin. We interpret these rocks as debris flow and lahar deposits associated with Cheekye phase volcanism.

3.2.3. Atwell Peak (A) phase (Non-glaciovolcanic)

Porphyritic dacite lava (ApDl)

Light grey to dark red, poorly vesicular, coarsely columnar jointed porphyritic dacite lava forms several ~10 to 15 m-thick accumulations in the western and eastern map areas. The rocks are variably oxidised and contain phenocrysts of plagioclase, magnetite-pseudomorphed-hornblende and orthopyroxene. Although the rocks do not contain visible quartz, they are classified as dacite due to a total SiO_2 content of >63 % (Table A1). They have a hypocrystalline groundmass of plagioclase, glass, and Fe-Ti oxide (Table 3.1). In the eastern map area, the lavas conformably underlie, mineralogically and texturally similar, massive dacite tuff breccia (unit AmDtx) (block and ash deposits). In the western map area, a single, 15 m-thick, westward-dipping lava is encased in cogenetic massive dacite tuff breccia (unit AmDtx).

Massive dacite tuff breccia (AmDtx)

Unconsolidated, light grey to dark red, massive, poorly sorted, monolithologic, matrix-supported, dacite tuff breccia occurs in several places in the eastern and western map areas. The deposits contain radially jointed, sub-rounded, bread crust textured dacite clasts that are up to 2 m in diameter (Fig. 3.1E). The clasts are supported by a matrix of loose ash and lapilli. The mapped accumulations are <10 m thick. The clasts are mineralogically and texturally like associated porphyritic dacite lavas (unit ApDl) suggesting a shared eruptive origin. Poor sorting, monolithology, and presence of abundant radially-jointed clasts (e.g. Stewart et al. 2003) suggest that these rocks were emplaced as high-temperature block and ash rock avalanches likely in response to the collapse of a dome/lava flows during the eruptions. These rocks are also potentially associated with further accumulations of dacite pyroclastic rocks located in the

Volcanic phase	Map unit	Map unit code	Texture	Groundmass	Components
Warren Glacier (W) phase	Bedded basalt tuff breccia and hyaloclastite	WbBtx	Porphyritic	Fine, chaotically-oriented plagioclase microlites (0.01 to 0.05 mm; 35 %), augite (0.01 mm; ~5 %) and equant Fe-Ti oxides (0.01; ~10 %).	Phenocrysts: euhedral, equant plagioclase (0.01–0.5 mm; 30 %), subhedral olivine (~0.3 mm; ~10 %); pale green, subhedral, augite (0.2 mm; ~ 10 %)
	Porphyritic basalt lava	WpBl			
Cheekye (CH) phase	Porphyritic andesitic lava	CHpAl	Porphyritic, trachytic	Fine trachytic plagioclase (0.01 to 0.1 mm; 80 %) and small, equant Fe-Ti oxides (0.01-0.1 mm; ~20%)	Phenocrysts: euhedral, unzoned, equant to elongate plagioclase (~0.1-0.5 mm, 10 %), small, elongate, dark brown, hornblende with ragged, magnetite pseudomorphed margins (0.1-0.5 mm in length, ~5 %) and small, equant, stubby, sub-hedral orthopyroxene (0.1-0.3 mm; ~1 %). Xenocrysts: minor embayed quartz
	Massive andesite breccia	CHmAbx			
	Massive andesite conglomerate	CHmAc			
Atwell Peak (A) phase	Porphyritic dacite lava	ApDl	Porphyritic	Fine microlitic plagioclase (0.01-0.1 mm; 65 %), and fine, 0.1 mm Fe-Ti oxides (~15%).	Phenocrysts: fine, euhedral plagioclase (0.1-0.5 mm, 15 %), elongate (0.5-1 mm length), ragged and magnetite-pseudomorphed-hornblende (~8 %), and minor fine, equant, subhedral orthopyroxene (~2 %).
	Massive dacite tuff breccia	AmDtx			

Table 3.1. Petrographic descriptions of coherent rocks from Brohm Ridge

surrounding valleys. One instance includes in situ, block-and-ash deposits that are located ~16 km southwest of the main Mount Garibaldi summit, in a quarry near the town of Squamish (sample AW-15-001; Table A1). A fragment of wood from these deposits yielded an age of 11,7 ± 0.48 ka (Median of reported age: 12,130 – 11, 280 yr. B.P. from Friele and Clague, 2009, as reported by Wilson and Russell, 2018).

3.3. Glacial sediments

Basal till (bt)

Poorly sorted diamicton forms a ~15 m-thick deposit in the eastern map area, situated between rocks of the Warren Glacier phase (units WbBtx and WpBl) and rocks of the Atwell Peak phase (unit AmDtx). The clasts are sub-rounded and striated porphyritic andesite (~80 %), granodiorite (~15 %), and greenschist (~5 %). The clasts are up to 20 cm in diameter and are supported by a fine matrix of fine sand and silt matrix. We interpret these rocks as a glacial basal till. Clear contact relationships with overlying Atwell Peak phase rocks are observed in several places, however, the lack of an exposed contact between this till and the nearby Cheekye phase lavas (CHpAl) prohibits delineating the relative age of the rocks. We have interpreted this till to have an age that is younger than Cheekye phase volcanism (i.e., <460 ± 20 ka) and older than Atwell Peak phase deposits (i.e., > 13.5 ka).

Glaciolacustrine silt (sgl)

Unconsolidated, massive, well-sorted, fine-grained silt forms flat-lying accumulations up to 5 m thick is exposed in the northern map area. Fragments comprise ~90 % sub-rounded, fine plagioclase, trace amounts of hornblende, biotite and quartz and indistinguishable, subrounded orange silt (~10 %). Visible clasts lack vesicularity, shard-like clast shapes or any other definitive primary volcanic componentry. The unit distribution is topographically controlled, forming several sub-horizontal benches along the northern flank of Brohm Ridge between 1580 m and 1660 m above sea level. Unlike all other deposits in the area at similar elevation, these sediments are not overlain by scattered, unconsolidated ablation till (unit at), suggesting a late to post-glacial age (Fig. 3.1D). Their distribution and sedimentological character suggest a local source and probable glaciolacustrine origin. The deposits may imply the presence of an ephemeral glacially dammed lake occupying the upper reaches of the Culliton Creek valley during the waning stages of the last (Fraser; MIS 2) glaciation.

3.4. Summary

The volcanic lithologies exposed on Brohm Ridge are subdivided into three phases of activity: i) the older Warren Glacier (W) phase, comprising a small, partially dissected pyroclastic basalt tephra cone, ii) the Cheekye (CH) phase, consisting of a thick package of shallow-dipping lavas, debris flow and lahar deposits distributed along the crest of Brohm Ridge, and iii) the younger Atwell Peak (A) phase, comprising a series of dacite lavas and pyroclastic block and ash rock avalanche deposits.

The Warren Glacier phase deposits are the only rocks at Brohm Ridge that record a potential glaciovolcanic interaction. These rocks show palagonitized hyaloclastite tuff breccias alongside coherent lavas forming lobate, pseudo pillow structures that are suggestive of a water-rich emplacement environment. The topographic position of these rocks (i.e., hyaloclastite and pillow lava situated on an alpine ridge), suggest that this water was derived from a glacier, however, further studies of the age and detailed lithostratigraphy are required to confirm the paleoenvironmental implications of event.

The sequence of eruptive events that constructed the deposits on Brohm Ridge is as follows: Early to Middle Pleistocene volcanism emplaced a small, calc-alkaline basaltic tuff cone in the eastern map area (Warren Glacier phase). The cone likely erupted within an ice-confined environment (either an alpine glacier or larger ice sheet). Following basaltic Warren Glacier phase activity, the Cheekye phase andesitic rocks were emplaced as a series of lavas, debris flows, and lahars that were probably confined to a paleo-valley that ran westward along the axis of Brohm Ridge (Mathews 1958). A period of erosion followed this phase of activity, resulting in significant topographic reconfiguration and the development of the modern Cheekye and Culliton creek valleys. Atwell Peak phase volcanism probably began during the waning stages of the Fraser glaciation during effusive dome emplacement and collapse (Mathews 1952a; Green et al. 1988). These collapse events sourced hot block and ash rock avalanches that traveled westward from Mount Garibaldi to be deposited along the eastern part of Brohm Ridge. Atwell Peak volcanism probably occurred while the adjacent Cheekye River valley was filled with waning glacial ice. Mathews (1952) interprets that a portion of the Atwell Peak phase pyroclastic rocks was deposited on top of this ice. As the ice retreated, the western flank of Mount Garibaldi collapsed, producing large debris flow and rock avalanche events that inundated the Cheekye River valley. At a similar time, melting ice in the Culliton Creek valley caused an ephemeral, glacially dammed lake to form. Sediment derived from the local area was deposited in a glaciolacustrine setting on the northern side of Brohm Ridge.

4. The Table (1:7,500)

The Table is a steep-sided, flat-topped pile of porphyritic andesite lava located in Garibaldi Provincial Park (Fig. 4.1). The Table was one of the first recognized examples of intermediate-composition (andesite) glaciovolcanism (Mathews 1951) and is now regarded as the type-example of a lava-dominated tuya, namely, a flat-topped glaciovolcanic edifice that is constructed entirely by the effusive eruption of lava (Kelman et al. 2002b; Smellie 2013; Andrews et al. 2014; Smellie and Edwards 2016; Wilson et al. 2019). On this map, we subdivide the volcanic rocks into four phases of eruption activity. All volcanic rock units unconformably overly undivided quartz diorite basement rock of the Cloudburst Formation (Cretaceous) (Mathews 1958).

The oldest volcanic lithologies are mapped as undivided volcanic (V) rocks. These deposits comprise epiclastic lithic breccias that form a bedded, ~50 m-thick layer that is well exposed on the northern side of the Table massif along with a small (~15 m-thick), massive accumulation in a ravine in the

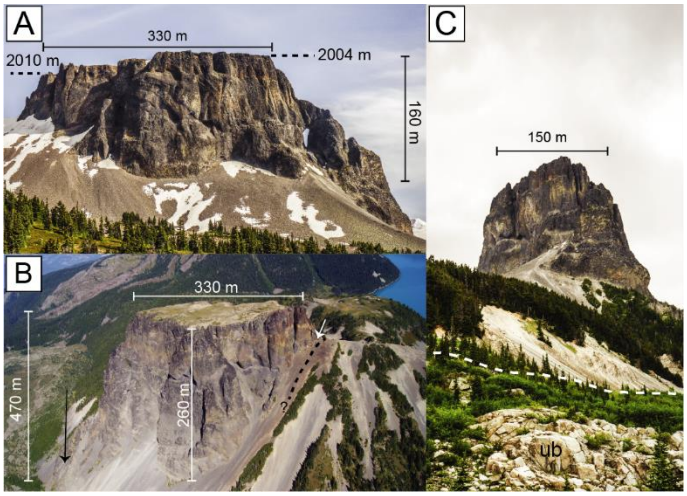

Fig. 4.1. Field photographs showing geomorphology of the Table (after Wilson et al. 2019). Views of the Table (A) looking south, (B) looking northwest, (C) looking east.

southwestern map area (Figs. 4.2A and 4.2B). The breccias are unrelated to any other volcanic deposits in the area. The Table Meadows (TM) and Table East (TE) phase rocks comprise two

lavas that are up to ~100 m thick each. These two eruption phases are distinguished mineralogically; the Table Meadows phase rocks are plagioclase and orthopyroxene phyric, while the Table East phase rocks are plagioclase, orthopyroxene, and hornblende phyric. Although the rocks are highly eroded, both deposits show evidence of a glaciovolcanic emplacement (e.g., relic slender, horizontally oriented marginal columnar jointing). The Table East and Table Meadows phase rocks show an unconformable overlying contact relationship with the older undivided volcanic breccias (interpreted to be unconformable), however, they do not show clear contact relationships with one another. Their relative ages are therefore unknown.

The youngest, Table (T) phase rocks form the iconic, flat-topped Table massif in the centre of the map area. These rocks include plagioclase and hornblende phyric andesite lava that is subdivided into four units (Fig. 4.3, Table 4.1). The andesite is typically glassy and slender columnar and hackly jointed (sensu Lodge and Lescinsky 2009) (Figs. 4.2C, D, and E). These rock textures, along with the steep-walled edifice morphology, indicate ice confinement during the Table phase eruptions (Wilson et al. 2019). The upper 30 m of the Table is oxidised, a feature that indicates ice breaching and a subaerial eruption of the upper part of the volcano (Wilson et al. 2019). The massif is also intruded by a network of medium-grained, porphyritic andesite dikes and sills. These intrusive rocks form thin sheets (2 to 5 m thick) that crosscut the edifice at a high angle (Fig. 4.2F). The contacts with surrounding glassy andesite lava are gradational and lack breccia and chill margins, implying late-to-synchronous injections of magma into a partially molten massif. An $^{40}Ar/^{39}Ar$ geochronology measurement on a sample obtained from an andesite sill yielded an age of 100 ± 12 ka, providing a representative age for the Table phase event (Wilson et al. 2019).

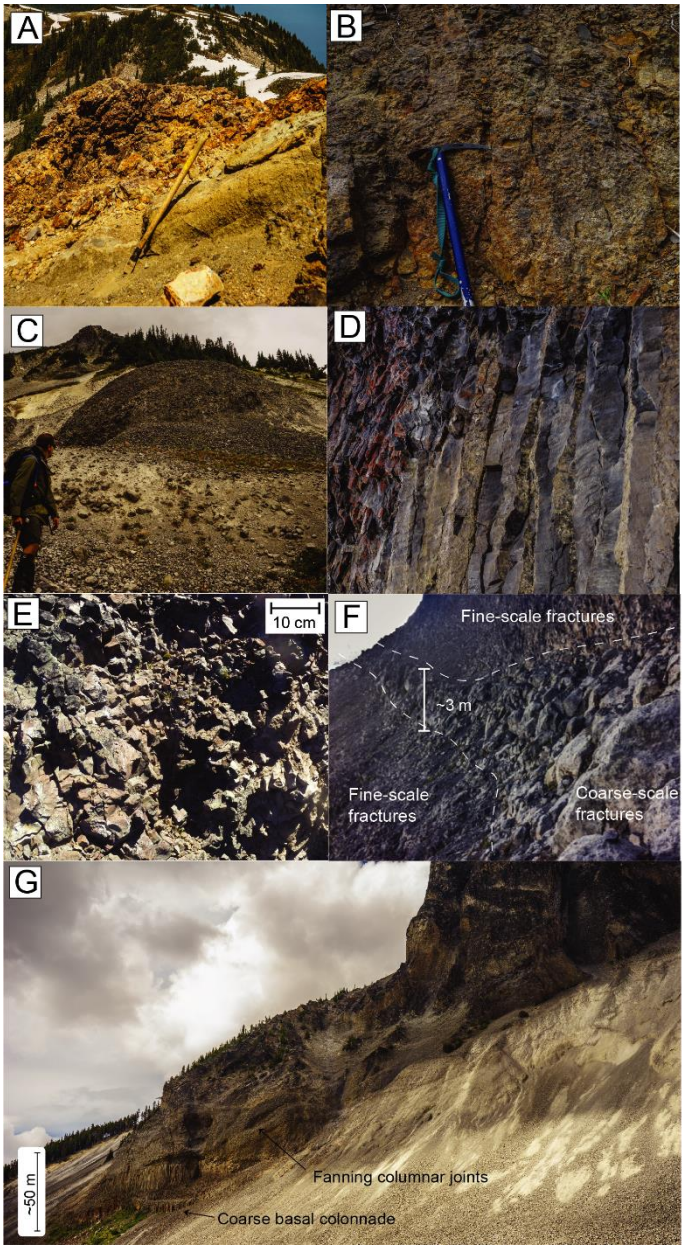

Fig. 4.2. Field photographs showing lithofacies and jointing within Table volcanic complex rocks. (A) Crudely bedded lithic breccia exposed along the northern base of the Table (unit Vbx). (B) Clast-supported lithic breccia exposed in narrow ravine within the southern map area (unit Vbx). (C) Hackly-jointed lobe of porphyritic andesite exposed along the southern margin of the Table East deposit (unit TEpAl). (D) Photograph showing slender columnar joints (~20 cm diameter) developed in Table phase glassy andesite lava (unit TgAl). (E) Close-up image showing hackly-fractured, oxidised lava of the Table phase (unit ToAl). (F) Photograph looking east showing intrusive contact relationships between coarse, columnar jointed holocrystalline, sub-horizontal sill (unit TpAd) and glassy andesite lava host rock (unit TgAl). (G) Photograph of vertical and fanning columnar jointed lobe of andesite draped over the edge of Warren valley (unit TpAl).

The last volcanism is illustrated by a ~50 m-thick, radially jointed lobe of porphyritic andesite lava that is draped across the northern wall of Warren valley (Fig. 4.2G). Clear contact relationships between this lava and the other Table phase rocks are not well exposed, however, the deposit morphology and lava

jointing (slender and radially-oriented columnar joints) suggest emplacement within a late-stage subglacial meltwater drainage channel (Wilson et al. 2019). The Table East and Table Meadows rocks are overlain by unconsolidated glacial till. No evidence for post-eruptive glacial overriding was found on the upper surface of the Table.

4.1. Basement geology

Undivided basement rocks (ub)

White to pink, medium grained (2 to 5 mm) diorite forms steep, glacially scoured bluffs in the southern map area. These basement rocks unconformably underlie all other rocks. Mathews (1958) interpreted the diorite as part of the Cloudburst Formation (Cretaceous).

4.2. Older volcanic rocks

4.2.1. Undivided volcanic (V) rocks (Non-glaciovolcanic)

Volcanic breccia (Vbx)

Bedded to massive, orange brown, polymictic epiclastic volcanic breccia forms an ~50 m-thick, bedded accumulation on the northern side of the Table and a ~15 m-thick massive exposure in a narrow ravine southeast of the Table. The rocks are observed to unconformably underly porphyritic andesite lava of the Table Meadows phase (unit TMpAl) and porphyritic andesite of the Table East phase (unit TEpAl). The contact with Table phase rocks is interpreted, but locally obscured by talus. Clasts show a wide range of sizes (1 to 20 cm-diameter) and consist of a mixture of angular to rounded, sparsely vesicular, porphyritic andesite (~85 %), well rounded, dark grey porphyritic andesite (~5 %), and subrounded quartz-biotite granodiorite (~10 %). The clasts are texturally dissimilar to all other volcanic lithologies in the map area. Clast rounding and deposit bedding support an epiclastic origin. We suggest that these rocks were probably produced during erosion of one or more nearby (older) volcanic exposures (e.g., Glacier Pikes, Brohm Ridge, and/or Mount Price).

4.3. Geology of the Table area

4.3.1. Table Meadows (TM) phase (Glaciovolcanic)

Porphyritic andesite lava (TMpAl)

Light grey, sparsely vesicular, porphyritic andesite lava forms a ~30 to 50 m thick lava plateau in the northern map area. At the center of the plateau, columnar jointing is coarse (1 to 2 m-diameter) and oriented subvertically. Near the margins of the deposit, however, the joints are slender (~20 cm-diameter) and typically orientated subhorizontally. The upper surface of the Table Meadows plateau is glacially scoured and covered in scattered glacial till. The rocks contain phenocrysts of plagioclase and orthopyroxene and have a fine groundmass of plagioclase, minor augite, Fe-Ti oxide, and pale-brown glass (Table 4.1). Although substantially eroded, the presence of slender, horizontally oriented columnar joints suggests lateral ice buttressing and a possible glaciovolcanic eruption.

Volcanic phase	Map unit	Map unit code	Texture	Groundmass	Components
Table Meadows (TM) phase	Porphyritic andesite lava	TMpAl	Porphyritic	Fine plagioclase (55 %, 0.01–0.5 mm); Fe-Ti oxide (10 %, 0.1 mm); minor glass (<1%).	Phenocrysts: ~0.1 to 1 mm, euhedral, non-zoned, equant to elongate plagioclase (~30 %), 0.1 to 0.5 mm, equant orthopyroxene (5 %). Microphenocrysts: fine (< 0.01 mm), equant, subhedral microphenocrysts of augite (<1 %).
Table East (TE) phase	Porphyritic andesite lava	TEpAl	Porphyritic	Fine plagioclase (20 %, 0.01 to 0.1 mm) and fine, equant Fe-Ti oxide grains (5 %, 0.1 mm).	Phenocrysts: euhedral, unzoned, equant plagioclase, (50 %, 0.1–0.5 mm); acicular hornblende (20 %, 0.1 to 2 mm); fine, equant orthopyroxene surrounded by dusty opaque material (5%, 0.1 mm).
Table (T) phase	Porphyritic, glassy andesite lava	TgAl	Porphyritic, glassy	Fine, trachytic plagioclase (50%, 0.01–0.5 mm); Glass (20%); Fe-Ti (10%, 0.1 mm).	Phenocrysts: euhedral, unzoned, equant plagioclase phenocrysts (~20 %, ~0.1 to 0.5 mm); minor, equant, subhedral microphenocrysts of augite (~1 %, 0.1 mm). All Table phase rocks contain minor xenocrysts of quartz (<1%, embayed). Xenocrysts: the Warren lobe (TpAl) contains minor xenocrystic olivine (<1 %, 0.1 mm).
	Porphyritic, oxidised andesite lava	ToAl	Porphyritic, oxidised	Fine, trachytic plagioclase (50%, 0.01–0.5 mm); fine oxidised material (20%); Fe-Ti (10%, 0.1 mm).	
	Porphyritic, andesite dikes and sills	TpAd	Porphyritic, holocrystalline	Fine, trachytic plagioclase (60%, 0.01–0.5 mm); Fe-Ti (20%, 0.1 mm).	
	Porphyritic, andesite lava	TpAl	Porphyritic, holocrystalline		

Table 4.1. Petrographic descriptions of coherent rocks from the Table map area

4.3.2. Table East (TE) phase (Glaciovolcanic)

Porphyritic andesite lava (TEpAl)

Light grey, flow banded, dense, columnar jointed andesite lava forms a ~40 m-thick dome-shaped mass in the eastern map area. The rocks are coarsely columnar jointed (1 to 2 m-diameter) and have a glacially scoured upper surface that is covered by scattered glacial debris. At the southern margin of the deposit the joints are slender and hackly (e.g., Lodge and Lescinsky 2009) (Fig. 4.2C). The rocks contain phenocrysts plagioclase, hornblende, and minor orthopyroxene. The groundmass is fine, containing plagioclase, Fe-Ti oxide, and pyroxene (Table 4.1). These rocks are distinguished mineralogically from Table Meadows phase rocks based on the presence of hornblende phenocrysts. They show surface jointing that is consistent with ice interaction during an eruption, however, further geochronological analysis and mapping are required to fully investigate the timing and nature of this glaciovolcanic event.

4.3.3. The Table (T) phase (Glaciovolcanic)

Glassy andesite lava (TgAl)

Dark grey, sparsely vesicular (<5 %), slender to hackly-jointed, glassy andesite lava forms the main component of the Table edifice (Fig. 4.2D). The rocks are aphanitic to glassy and contain phenocrysts of plagioclase and minor hornblende (pseudomorphed to magnetite). They have a trachytic groundmass of plagioclase, Fe-Ti oxide, minor augite, and light-brown glass (Table 4.1). The rocks display slender columnar and hackly jointing, with joint axes typically oriented perpendicular to the edifice surface. The surface texture (i.e., jointing) and glassy lava character suggest accelerated cooling and quenching against a subvertical cooling surface, consistent with ice confinement during the eruption (Wilson et al. 2019). Clear contact relationships between these rocks and surrounding Table Meadows and Table East phase rocks are not observed, however, the Table phase rocks appear to overlie these other lithologies. A recent $^{40}Ar/^{39}Ar$ geochronology analysis indicates the age of Table phase volcanism to be 100 ± 12 ka (Wilson et al. 2019).

Oxidised andesite lava (ToAl)

Dark red to grey, jointed andesite and minor autobreccia form the upper ~30 m of the Table (Fig. 4.2E). These rocks have similar mineralogy to other Table phase lava; however, the groundmass is incipiently oxidised (Table 4.1). The contact with underlying glassy andesite lavas (unit TgAl) is gradational and occurs over several meters. Incipient oxidation suggests that these rocks were exposed to the atmosphere during emplacement, supporting the notion that the enclosing ice was breached and the upper lithofacies were erupted subaerially (Wilson et al. 2019). The porphyritic, oxidised andesite lavas exposed on the upper surface of the Table lack any indication of post-eruption glacial overriding (e.g., erratic boulders, striated surfaces).

Porphyritic andesite dikes and sills (TpAd)

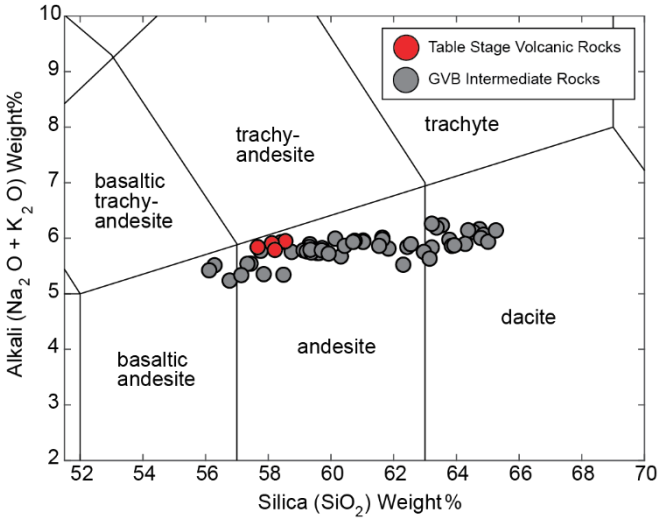

Fig. 4.3. Total alkali-silica plot showing geochemical character of the Table phase volcanic rocks (red circles). Data are plotted against a selection of other intermediate volcanic rocks from the GVB (sourced from Bye et al. 2000; Kelman 2005; Fillmore and Coulson 2013; and other maps in this publication).

Light grey, sparsely vesicular (<5 %), fine to medium-grained, holocrystalline, coarse columnar jointed andesite dikes and sills form a network of thin sheets (2 to 5 m thick) that crosscut the Table at a high angle (Fig. 4.2F). The rocks have identical mineralogy to the other Table phase rocks; however, they have a holocrystalline groundmass (Table 4.1). This intrusive lithology shows gradational upper and lower contacts against enclosing porphyritic, glassy andesite lava (TgAl). The contacts lack glass or breccia. This contact relationship, along with their holocrystalline texture, suggests that the dikes and sills were emplaced as late-to-synchronous injections of magma into a partially-molten, growing Table massif (Wilson et al. 2019).

Porphyritic andesite lava (TpAl)

Light grey, sparsely vesicular (<5 %), coarse and slender columnar jointed andesite lava forms a ~50 m thick, radially jointed lobe that is draped across the northern wall of Warren valley (Fig. 4.2G). The lobe has a 2 to 5 m-thick coarsely jointed lower colonnade that is overlain by a 10 to 15 m-thick zone of fanning entablature. The rocks have similar mineralogy to other Table phase rocks; however, they also contain rare, fine xenocrysts of olivine (Table 4.1). The superposition of this lava unit is unclear as contact relationships with surrounding Table phase rocks are not well exposed. The rocks appear to overlie (i.e., are younger than) all other Table phase lithologies. The geometry of this lava (that is, draped over the wall of Warren valley) suggest that it flowed downhill. Rapidly changing (fanning), slender columnar jointing indicates rapid cooling. Combined, these features suggest a late-stage eruption of lava, emplaced in a hemispherical cooling cavity or downstream subglacial meltwater drainage channel.

4.4. Glacial sediments

Undivided till (ut)

Polymictic, unconsolidated pebbles, gravel, boulders and cobbles form a loosely consolidated, clast-supported deposit in Warren valley. The clasts are variably rounded, striated volcanic rocks, granodiorite and foliated greenschist that range in diameter from <1 cm to >30 cm. We interpret this unit as a glacial till that was deposited during the early Holocene retreat of the Warren Glacier.

4.5. Summary

The Table was first described by Mathews (1951), who noticed the striking superficial resemblance to the flat-topped basaltic tuyas in northern BC. Mathews (1951) used this similarity to suggest that the Table erupted beneath glacial ice. Wilson et al., (2019) provide a detailed study of the lithofacies and geomorphology of the Table. Their analysis corroborates Mathews (1951), the Table is glaciovolcanic in origin, however, they offer a new conceptual model for the eruption involving eruption as dikes injected directly into ice and endogenous inflation of the growing edifice within a tightly confined subglacial cavity. Recent $^{40}Ar/^{39}Ar$ geochronology (100 ± 12 ka; Wilson et al. 2019) indicates that the Table is considerably older than previously interpreted (c.f., Mathews 1951). This new age indicates eruption during the MIS 5d–5b glacial stage (Wilson and Russell 2018). Given the abundance of features suggesting glaciovolcanism at the Table, we interpret that, at the time of eruption, the Coast Mountain portion of the past CIS upper surface resided at an elevation of at least 2010 m above sea level (i.e., coinciding with the elevation of the upper, oxidised surface of the edifice). The age of the older volcanic lithologies exposed in the map area is uncertain, although the Table Meadows and Table East lavas probably erupted in the Late Pleistocene.

Here, we outline the sequence of eruption events at the Table and the surrounding area. Volcanism began during the Middle Pleistocene (i.e., before 100 ± 12 ka) when two effusive porphyritic andesitic lavas (the Table Meadows phase and the Table East phase) erupted beneath glacial ice. The relative timing of these two eruptions is unclear. During the Table Meadows eruption, glacial ice covered the local area to an elevation of at least 1900 m asl. During the Table East phase event, glacial ice covered the area to an elevation of at least 1880 m asl. Late Pleistocene (100 ± 12 ka) volcanism began at the Table (Table phase) with the injection of northeast to southwest trending dike into an overlying ice mass that was ~250 m thick (coinciding with an ice surface elevation of ~2010 m asl). Ice melting and lava quenching along the margins of the dike produced a carapace of unconsolidated, permeable breccia (not preserved in the field or represented on this map) that thermally insulated the dike and permitted efficient meltwater drainage from the eruption site (see, Wilson et al. 2019). Accelerated marginal cooling caused lava quenching and the development of hackly and slender columnar joints. Continued injection of lava facilitated endogenous dike inflation, expanding the subvertical edifice walls outward and forming an elongate, pipe-shaped massif. Oxidised surface lithofacies (i.e., unit ToAl) indicate that the inflating edifice breached the surrounding ice, and the upper surface was exposed to the atmosphere. Near the end of the eruption, a tight network of dikes and sills (unit TpAd) was injected into the cooling, partially molten massif and a large lobe of andesite lava (TpAl) flowed southward, probably exploiting a subglacial drainage channel situated on the edge of Warren valley.

5. The Black Tusk (1:10,000)

The Black Tusk is an iconic, steep-sided pile of andesite lava located in Garibaldi Provincial Park, southwestern British Columbia. (Fig. 5.1A). The Black Tusk forms the central part of a small group of andesite lava domes and flows that erupted during the Pleistocene. These volcanic rocks unconformably overlie slate, meta-conglomerate and greenschist of the Cretaceous Gambier group (Mathews 1948; Lynch 1992; Monger and Journeay 1994). Mathews (1948, 1958) identified that the lithofacies present at the Black Tusk signify glaciovolcanism and suggested that the formation of this volcanic feature shares a comparable origin with the Table, a lava-dominated tuya, situated approximately 9 km towards the southeast (Wilson and Russell 2018; Wilson et al. 2019). Following this however, the Black Tusk was reinterpreted (with no additional or new field observations) as an eroded volcanic neck (i.e., the core of a large stratovolcano) (Green 1977, 1981). In this map, we report lithofacies, lava jointing textures and an edifice morphology that demonstrate a clear glaciovolcanic origin for the Black Tusk. Indicators for glaciovolcanism (emplacement and accelerated cooling in an ice-confined environment) include glassy, hackly (e.g., Lescinsky and Fink 2000) and slender columnar jointed lavas, pseudo-pillow fracture systems (e.g., Forbes et al. 2014), and a steep-walled, elongate edifice morphology (Fig. 5.2).

We divide the lithofacies in the Black Tusk map area into four phases of volcanic activity. The phases are distinguished by their mineralogical and geochemical character and geographic distribution (Table 5.1 and Fig 5.3). The oldest, East Bluff (E) phase rocks form a mound of coarsely jointed plagioclase and clinopyroxene phyric andesite lava in the southern part of the map. Overlying these rocks, the West Bluff (WB) phase rocks form two small, aphyric andesite lava domes. The domes exhibit slender radial columnar and hackly surface jointing textures. The Black Tusk (B) phase lavas occur in the central part of the map area. The Black Tusk rocks are glassy and plagioclase and orthopyroxene phyric. The margins of the edifice show slender columnar, hackly, and pseudo-pillow jointing. Finally, in the eastern map area, the Microwave Bluff (M) phase rocks comprise plagioclase and hornblende phyric andesite lavas that are arranged in a circular, ~1 km-wide dome. The dome has slender radial columnar and hackly jointed margins.

Unconformable contact relationships are observed between the older, East Bluff phase deposits and the younger West Bluff and Black Tusk phase rocks. A single K-Ar age determination on the East Bluff phase deposit of 1300 ± 100 ka indicates that these rocks erupted during the Early Pleistocene (Green et al. 1988). A new $^{40}Ar/^{39}Ar$ analysis (1090.6 ± 52.48 ka) was obtained on a sample collected from the West Bluff edifice (Figure 5.4). Clear stratigraphic contact relationships between the Black Tusk phase rocks and the older West Bluff and East Bluff phase rocks are not observed.

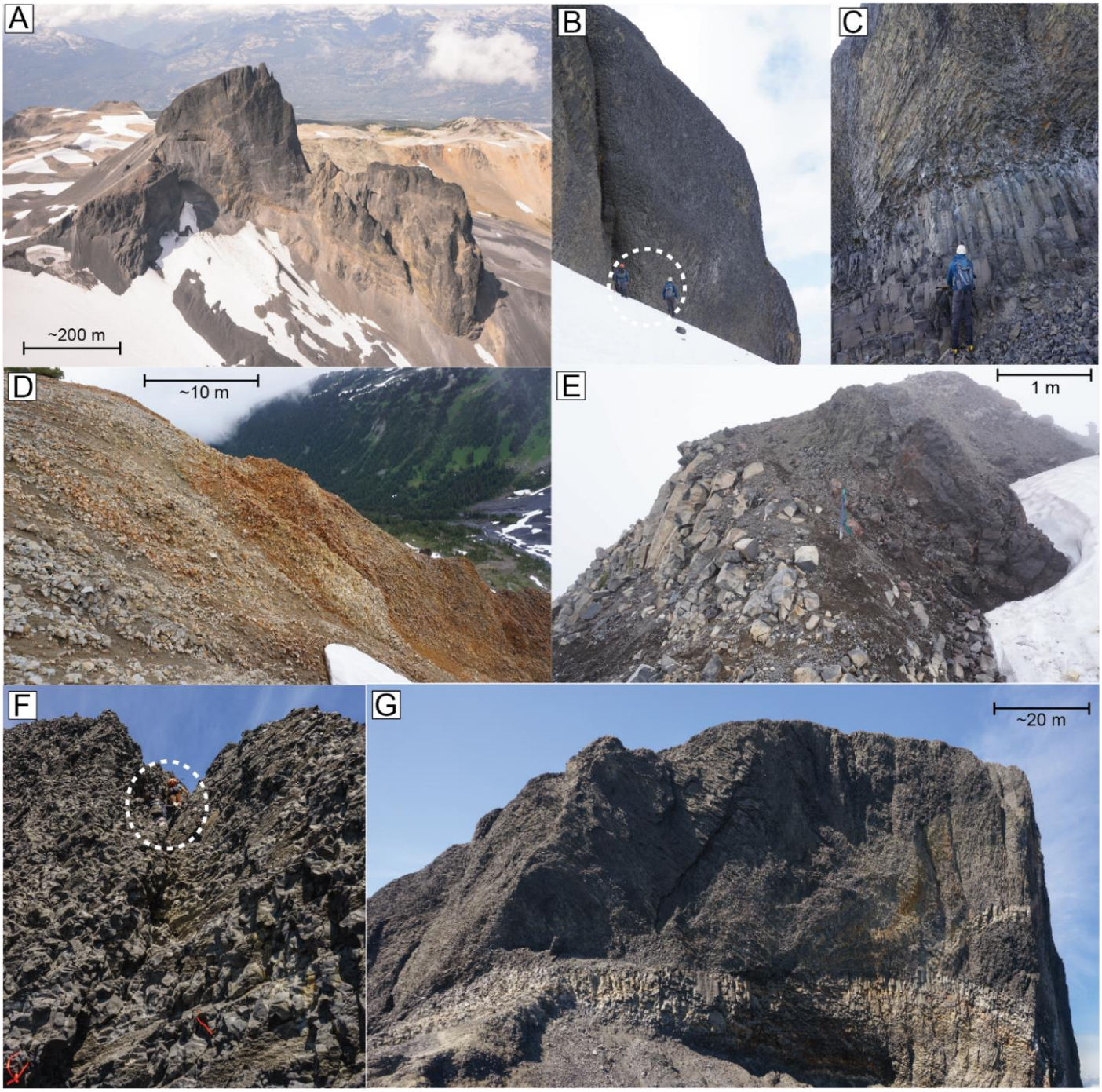

Fig. 5.1. Field photographs showing lithofacies in the Black Tusk map area. (A) Photograph of the Black Tusk looking west. (B) Image looking south showing West Bluff phase lava dome. (C) Image looking north, showing contact between coarse, columnar jointed lower colonnade at West Bluff and the overlying slender and hackly-jointed andesite lava (entablature). (D) Image looking west showing hydrothermally altered portion of hackly jointed dacite at Microwave Bluff. (E) Image looking south showing Black Tusk phase oxidised porphyritic andesite lava and autobreccia on the eastern ridge of the edifice. (F) Image looking north at Black Tusk phase hackly jointed porphyritic andesite lava exposed on the southern edifice margin. Two climbers are circled for scale. (G) Image looking west showing Black Tusk phase slender columnar jointed lavas intruded by coarsely jointed porphyritic andesite dike.

Their relative stratigraphic relationship is inferred by a geochronology measurement (177 ± 16 ka; as reported by Wilson and Russell 2018) that suggests that the Black Tusk phase rocks erupted during the Middle Pleistocene. The Microwave Bluff phase rocks rest directly on glacially scoured bedrock and are not connected physically with any other volcanic rocks in the map area. A new $^{40}Ar/^{39}Ar$ determination for Microwave Bluff phase volcanism indicates eruption at 160.6 ± 2.8 ka (Figure 5.5, Table 1.1). There are no direct stratigraphic relationships exposed between the West Bluff and Black Tusk or Microwave Bluff deposits.

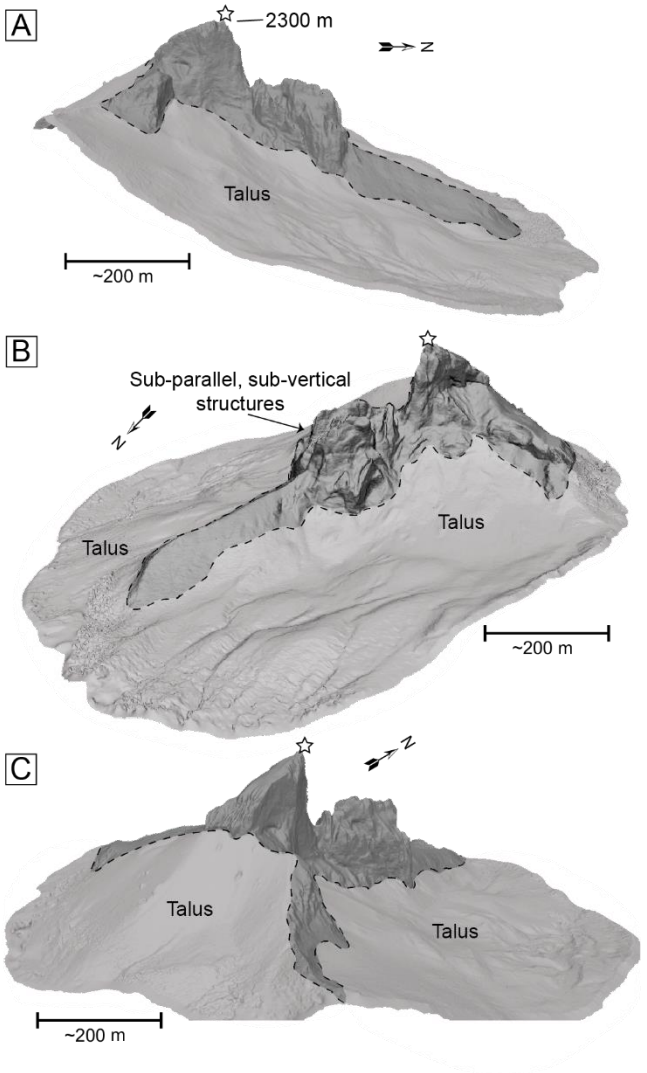

Fig. 5.2. 3D photogrammetry model of the Black Tusk showing elongate profile and steep-walled edifice morphology. Portions of exposed, in situ rock are indicated in dark grey. All models show a white star at a shared point of reference. North orientation is indicated with an arrow.

The West Bluff phase, Black Tusk, and Microwave Bluff phase deposits demonstrate lithofacies that are consistent with glaciovolcanic emplacement (e.g., hackly, slender radial columnar jointing preserved in an area of rugged, alpine topography with abundant water drainage). These volcanoes also preserve edifice morphologies that indicate physical restriction during emplacement. For example, the Black Tusk is strongly elongate in a north to south orientation (Fig. 5.2) and has steep, minimally eroded outer surfaces that are covered in glassy, hackly joints. These features suggest that the Black Tusk was physically constrained by the surrounding ice during the eruption and may therefore have been constructed through a similar mechanism to the Table (i.e., as a dike injected into the ice, and endogenously inflation of the lava mound; see chapter 4 and Wilson et al. 2019).

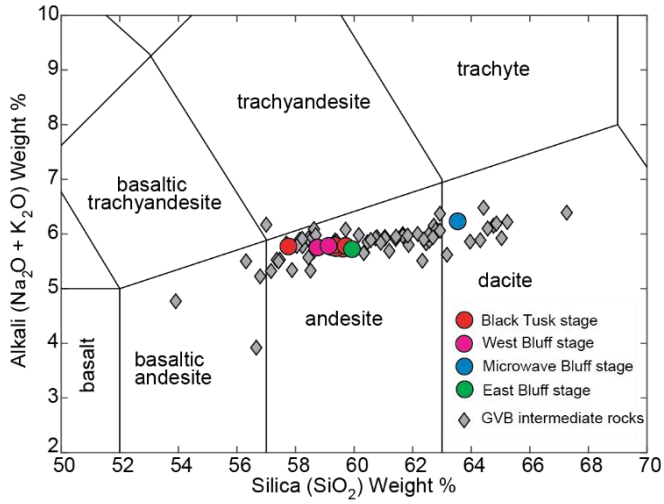

Fig. 5.3. Total alkali-silica plot (after Le Bas et al. 1986) showing geochemical character of the Black Tusk lavas (circles) in comparison to other intermediate volcanic rocks from the Garibaldi volcanic belt (grey diamonds). Data are sourced from Bye et al. (2000); Fillmore and Coulson (2013); Wilson et al. (2016) and other field localities within this study (i.e. the Table, Brohm Ridge and Monmouth Creek). Whole rock major and trace element geochemical analyses are reported in Appendix A1.

5.1. Basement geology

Undivided basement rocks (ub)

Foliated metavolcanic and metasedimentary slate, conglomerate, and greenschist of the Gambier group (Cretaceous) form the basement rocks in the map area (Mathews 1948; Lynch 1992; Monger and Journeay 1994). These rocks are mapped as part of the Helm and Emptrum Formations (Mathews 1958).

5.2. Geology of the Black Tusk area

5.2.1. East Bluff (E) phase (Non-glaciovolcanic)

Coarsely jointed and flaggy jointed andesite lava (EcAl and EfAl)

Light grey, sparsely vesicular (<5 %), porphyritic, holocrystalline andesite lava forms a 100 m-thick, broad dome in the eastern map area (Table 5.1). The rocks show evidence for significant glacial dissection (striated surfaces, glacially rounded bluffs, etc.). A K-Ar age determination indicates that these rocks erupted 1300 ± 100 ka (Early Pleistocene, Green et al. 1988). The rocks show no evidence for glaciovolcanic interactions. The East Bluff phase lithofacies are subdivided according to their jointing character. The base of the sequence consists of coarse, columnar jointed lava (unit EcAl). Near the top of the dome, the jointing becomes flaggy and rocks are incipiently oxidised (unit EfAl). The contact between these two map units is gradational.

5.2.2. West Bluff (WB) phase (Glaciovolcanic)

Coarsely jointed, slender jointed and hackly jointed andesite lava (WBcAl, WBsAl, WBhAl)

Dark grey, sparsely vesicular (10 to 15 %), aphyric andesite lava forms two, partially coalesced lava domes in the southwestern map area (Table 5.1). Both domes are ~200 m wide, ~50 m high and are well preserved. They show intense radial (i.e., fanning) slender columnar joints (unit WBsAl) and have bulbous, hackly fractured surfaces (unit WBhAl) (Fig. 5.1B). The base of the domes comprises a 2 to 10 m-thick basal colonnade with coarse (1 to 2 m-diameter) columnar joints (unit WBcAl) (Fig. 5.1C). The West Bluff phase rocks stratigraphically overlie East Bluff phase rocks in several places, although the contact is obscured by scree and vegetation cover. The contact is interpreted to be unconformable. The West Bluff lavas show evidence for minor glacial dissection (i.e., several glacially scoured surfaces and glacial erratic material on the upper surface), however, overall, the deposit is well preserved. The surface jointing (i.e., fine radial columnar and hackly jointing) and restricted edifice shape (i.e., a steep-sided dome) suggest enhanced cooling and quenching in a physically-restricted subglacial eruption environment (Lescinsky and Fink 2000; Kelman et al. 2002a; Wilson and Russell 2018). A holocrystalline sample collected from the base of the southern West Bluff dome (unit WBcAl) was analysed using $^{40}Ar/^{39}Ar$ at the WiscAr laboratory at the University of Wisconsin-Madison. The sample returned an age of 1090.6 ± 12.12 ka (Table 1.1, Figure 5.4). Given the lack of extensive deposit erosion (c.f., the similar age East Bluff rocks; Green et al., 1988), we suggest that further geochronological analysis should be used to verify the age of the West Bluff phase.

5.2.3. The Black Tusk (B) phase (Glaciovolcanic)

Slender jointed and hackly jointed andesite lava (BsAl and BhAl)

Dark grey, dense to sparsely vesicular (<10 %), slender columnar and hackly jointed porphyritic andesite lavas form the enigmatic Black Tusk edifice in the center of the map area (Figs. 5.1A and 5.1F and Table 5.1). Towards the southern part of the deposit, the columnar joint dimeters are slender and fan towards a horizontal long axis orientation (unit BsAl). The north, western and southern sides of the Black Tusk show glassy, hackly jointing (unit BhAl). The glassy texture of these rocks and the presence of closely spaced irregular joints indicate accelerated cooling and quenching. Hackly jointing preserved on the subvertical southern wall of the edifice suggest only minor post-eruptive erosion of this part of the Black Tusk. The steep-walled overall edifice shape and the abundance of lava quench indicators suggest that the lava erupted beneath and possibly within glacial ice (i.e., using a similar emplacement mechanism to the Table; Wilson et al., 2019). Lithofacies indicators for glaciovolcanism are preserved up to the summit of the edifice (~2300 m asl) indicating that, at the time of the eruption, the Coast Mountain sector of the CIS had an upper surface elevation of at least 2300 m asl.

Volcanic phase	Map unit	Map unit code	Texture	Groundmass	Components
East Bluff (E) phase	Porphyritic, coarsely jointed andesite lava	EcAl	Porphyritic, holocrystalline	Fine plagioclase (50%, 0.01–0.1 mm), Augite (~10%, 0.1 mm) and Fe-Ti oxides (~5 %, 0.1 mm).	Phenocrysts: euhedral, unzoned, plagioclase (~25 %, 0.1–0.5 mm) and augite (~10 %, 0.1 mm).
	Porphyritic, flaggy jointed andesite lava	EfAl			
Black Tusk (B) phase	Porphyritic, slender jointed andesite lava	BsAl	Porphyritic, hypocrystalline	Glass (50%); Plagioclase (25%); Orthopyroxene (1%); Fe-Ti oxide (10%)	Phenocrysts: phenocrysts of plagioclase (~10 %) and orthopyroxene (~2 %)
	Porphyritic, hackly jointed andesite lava	BhAl			
	Oxidised andesite autobreccia	BoAbx			
	Porphyritic, coarsely jointed andesite dikes and sills	BcAd			
Microwave Bluff (M) phase	Porphyritic, slender jointed dacite lava	MsDl	Porphyritic, hypocrystalline	Fine plagioclase (~60 %), Fe-Ti oxide (~5 %) and glass	Phenocrysts: elongate plagioclase (15 %; 0.5 to 1 mm), acicular hornblende (10 %; 0.5–1 mm).
	Porphyritic, hackly jointed dacite lava	MhDl			
West Bluff (WB) phase	Aphyric, coarsely jointed andesite lava	WBcAl	Aphyric	Very fine plagioclase (20%, 0.01 mm) and fine, equant Fe-Ti oxide grains (5 %, 0.1 mm)	Microphenocrysts: orthopyroxene (<0.1%, 0.1 mm)
	Aphyric, slender jointed andesite lava	WBsAl			
	Aphyric, hackly jointed andesite lava	WBhAl			

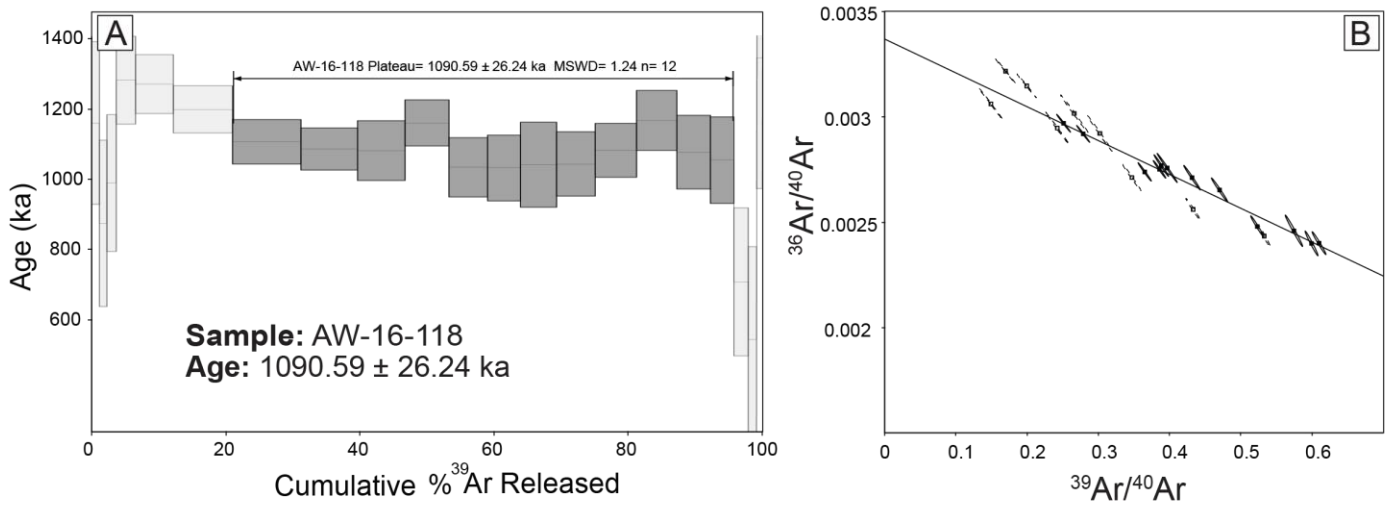

Fig. 5.4. Summary of $^{40}Ar/^{39}Ar$ geochronology results for sample AW-16-118 (unit WBcAl). (A) Plateau diagram showing fraction of ^{39}Ar versus age for the sample. (B) Inverse isochron plot. Ellipses denote 1 analytical uncertainty.

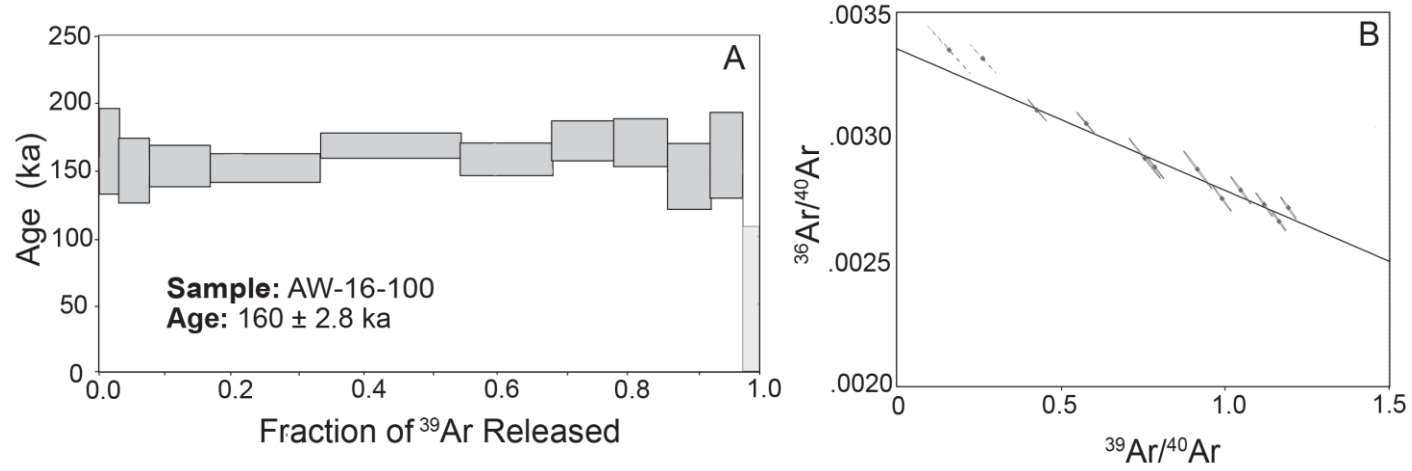

Fig. 5.5. Summary of $^{40}Ar/^{39}Ar$ geochronology results for sample AW-16-100 (unit MsAL). (A) Plateau diagram showing fraction of ^{39}Ar versus age for the sample. (B) Inverse isochron plot. Ellipses denote 1 analytical uncertainty.

There have been several previous geochronological estimations for the age of Black Tusk phase, including K-Ar measurements of 90 ± 80 ka, 210 ± 40 ka, and 170 ± 40 ka (Green et al. 1988), and a recent, unpublished $^{40}Ar/^{39}Ar$ determination of 177 ± 16 ka (as reported by Wilson and Russell, 2018). The age of the edifice is unresolved, however, we take the most recent estimate to be the most likely representation at this time (177 ± 16 ka, as reported by Wilson and Russell, 2018).

Oxidised andesite breccia (BoAbx)

Dark red to grey, moderately vesicular (~30 %), oxidised, clast supported, poorly sorted scoriaceous andesite breccia forms a thin carapace along the eastern ridge of the Black Tusk. The deposit consists of 0.5 to 1 m-diameter andesite lava pods that are encased in thick accumulations of cogenetic, monolithologic autobreccia (Fig. 5.1E). The deposit has a maximum thickness of ~5 m. The rocks are mineralogically like other Black Tusk phase lithologies (Table 5.1). They are observed to overlie Black Tusk phase slender jointed andesite lava (unit BsAl) via a sharp, sub-horizontal contact that shows no indication for glacial modification. Oxidation of these rocks suggests exposure to the atmosphere during eruption and cooling. We interpret that they were emplaced as ‘a‘ā lavas into an open subglacial channel extending eastward from the main edifice.

Coarsely jointed andesite dikes and sills (BcAd)

Light grey, sparsely vesicular (<5 %), porphyritic, holocrystalline, coarse columnar jointed andesite dikes and sills (10 to 15 m-thick) crosscut the Black Tusk massif at a high angle (Fig. 5.1G). The rocks are well exposed along the eastern and western walls. The rocks are mineralogically identical to all other Black Tusk phase lithofacies, however, they show a holocrystalline, fine to medium-grained groundmass. The contacts with surrounding porphyritic Black Tusk phase rocks

are gradational and lack glass (chill margins) or breccia. We interpret these rocks to be a network of dikes and sills that were injected into the growing massif during the later stages of the eruption (e.g., Wilson et al. 2019). The relative stratigraphic age of the dikes and sills concerning the oxidised andesite autobreccia on the eastern ridge (unit BoAbx) is undetermined.

5.2.4. Microwave Bluff (M) phase (Glaciovolcanic)

Slender jointed and hackly jointed dacite lava (MsDl and MhDl)

Light grey, sparsely vesicular (<10 %) dacite lava forms a broad, ~750 m-wide, ~50 m-thick dome in the western map area. Along the southern margin and upper surface of Microwave Bluff the rocks are holocrystalline and slender columnar jointed (unit MsAl). All other surfaces show glassy lava that is hackly jointed (unit MsDl). The Microwave Bluff phase rocks are porphyritic and distinguished from other Black Tusk area lithologies by a population of acicular hornblende phenocrysts (Table 5.1). The deposits are locally hydrothermally altered (Fig. 5.1D). Microwave Bluff is covered in scattered glacial debris and other indicators for post-eruptive glacial overriding (i.e., striated surfaces). The hackly joints and glassy rock textures indicate enhanced cooling and quenching in a subglacial environment, suggesting that the Microwave Bluff phase rocks erupted beneath a CIS (Wilson and Russell 2018). We report a new $^{40}Ar/^{39}Ar$ determination for the Microwave Bluff phase event of 160.6 ± 2.8 ka (Figure 5.5). This age suggests an eruption during the MIS 6 (Illinoian) glaciation and insinuates that at this time, the southern Coast Mountains were covered by ice with a minimum surface elevation of ~1960 m asl (i.e., the upper elevation of these glaciovolcanic lithofacies).

5.3. Glacial sediments

Undivided till (ut)

Unconsolidated, poorly sorted, clast-supported polymictic glacial till with a matrix of fine sand and silt occurs in the northern map area forming a sharply crested lateral moraine deposit that is observed to unconformably overlies the volcanic lithofacies at several places. Accumulations >1 m-thick are mapped as a discrete unit.

5.4. Summary

The Black Tusk is a prominent volcanic feature in southwestern British Columbia, representing multiple phases of Pleistocene volcanic activity. This map highlights four eruption phases, which together provide a record of the Coast Mountain sector's glacial history.

Volcanism began in the Early Pleistocene (1300 ± 100 ka) with the East Bluff phase (E), characterized by an effusive lava dome of coarse, columnar jointed, and incipiently oxidized lava, indicating an ice-free, subaerial environment.

The West Bluff (WB) phase erupted slightly later (1090.6 ± 12.12 ka), showing clear evidence of glacial influence during the eruption. It consists of two slender, hackly-jointed lava domes that overlie East Bluff deposits. The preservation of these glaciovolcanic features suggests that the age determination may require further verification.

The Black Tusk (B) phase, potentially dating to the Mid Pleistocene (177 ± 16 ka), began with an andesite dike injected into a glacier. This phase produced a steep-walled structure of slender, hackly-jointed andesite, along with late ʻaʻā lava flows and co-magmatic dikes. The eruption suggests the Coast Mountain sector had an upper surface of ~2300 m, likely a nunatak above surrounding ice since the eruption (Mathews 1958; Green et al. 1988).

The Microwave Bluff (M) phase, also Mid Pleistocene (160.6 ± 2.8 ka), formed a broad dome of hackly andesite erupted beneath a glacier, indicating that the southern Cordillera was covered by ice with an elevation of at least 1960 m asl during the MIS 6 glaciation.

6. The Cinder Cone (1:20,000)

The Cinder Cone is a Late Pleistocene basaltic scoria cone in Garibaldi Provincial Park, situated near to the current terminus of Helm glacier. The deposits comprise a pair of partially overlapping basalt and basaltic trachyandesite volcaniclastic cones and associated lavas in the nearby Helm Creek valley (Mathews 1958; Green 1977; Green et al. 1988; Wilson and Russell 2018) (Fig. 6.1A). All volcanic lithologies in the Cinder Cone area unconformably overlie Gambier group rocks (Cretaceous), comprising slate, argillite, greenschist, quartzite, and granodiorite (Mathews 1958; Monger and Journeay 1994).

We divide the Cinder Cone deposits into two eruption phases based on their inferred stratigraphic position and petrographic and geochemical character. The older, Helm Creek (H) phase rocks comprise a ~300 m-thick stack of plagioclase, olivine and augite phyric basaltic trachyandesite lavas that form flows, tubes and lobes that are well exposed at the northern end of Helm Creek valley. Above ~800 m asl, the lavas show coarse, subvertical columnar jointing. Below ~800 m asl, the lavas display slender, radial and horizontally oriented columnar joints.

The Helm Creek phase lavas terminate in the northern part of Helm Creek valley in a 2 km-wide apron featuring steep, 30 to 50 m-high bluffs along the northern margin. These lavas appear to have erupted at the Cinder Cone (Mathews 1958; Green et al. 1988; Wilson and Russell 2018) and flowed downhill to fill Helm Creek valley producing the present-day, flat topographic profile. Helm Creek phase rocks are also exposed in the lower part of the Cinder Cone where they form a broad mound of indurated, partially-palagonitised pyroclastic surge beds, bedded proximal pyroclastic fall out and coarsely jointed basaltic trachyandesite lava lobes. The Helm Creek phase rocks at the Cinder Cone are linked with the lavas exposed in northern Helm Creek based on their petrographic and geochemical similarity (Fig. 6.2).

The younger Cinder Cone (CC) phase comprises oxidised, plagioclase, olivine ± augite phyric basaltic scoria cone and associated basaltic lava distributed in the upper Helm Creek valley. The scoria cone is constructed of unconsolidated, crudely bedded ash, lapilli, pyroclastic spindle bombs, and agglutinated lava. Although clear contact relationships between the older Helm Creek phase and younger Cinder Cone phase deposits are closely inferred, the contact is not directly exposed (i.e.,

evidence for a significant time gap between the two phases such as an unconformable, reworked surface was not observed).

The timing of volcanism at the Cinder Cone is constrained by two K-Ar age determinations (Green et al. 1988) and a recent $^{40}Ar/^{39}Ar$ measurement. The older Helm Creek phase may date to 110 ± 30 ka (Green et al. 1988). The transition from coarse to slender columnar joint morphologies in Helm Creek valley suggests the lavas were emplaced in an ice-free environment above ~800 m asl but were later impounded by a glacier in the lower Cheakamus valley. The Helm Creek volcaniclastic rocks show minor water interaction (e.g., palagonitized clasts, surge bedding) but no conclusive evidence of glaciovolcanism, suggesting limited water, such as from snow or a thin alpine glacier. The age of the Cinder Cone phase is constrained by a K-Ar age of 40 ± 40 ka (Green et al. 1988) and a $^{40}Ar/^{39}Ar$ measurement of 16.7 ± 4.7 ka (A. Borch, personal communication, 2024). While the eruption occurred in an ice-free environment (inferred from oxidized scoria and basaltic lava in the upper Helm Creek valley), evidence of glacial overriding (glacial striae and debris) suggests the eruption happened shortly after the last glaciation (i.e., > 17 ka, MIS 2, Fraser glaciation), but before a local alpine ice re-advance, such as the Younger Dryas (Friele and Clague 2002).

6.1. Basement geology

Undivided basement rocks (ub)

Foliated slate, argillite, meta-conglomerate, greenschist, and granodiorite of the Gambier Group (Cretaceous) (Mathews 1948; Lynch 1992; Monger and Journeay 1994). The basement rocks in the map area comprise parts of the Helm and Cheakamus Formations as mapped by Mathews (1958).

6.2. Geology of the Cinder Cone area

6.2.1. Helm Creek (H) phase (Glaciovolcanic)

Coarsely jointed and slender jointed basaltic trachyandesite lava (HcBTl and HsBTl)

Dark grey, dense to sparsely vesicular (<10 %), porphyritic basaltic trachyandesite lava (Table 6.1) is divided into two map units (HcBTl and HsBTl) that are distinguished by their columnar jointing (i.e., coarse or slender). Near the base of Helm Creek valley, the rocks form a sheer, ~2 km-wide, fan-shaped mass of lava tubes and lava lobes that are slender columnar jointed. Along the northern edge of the deposit, the columns are oriented horizontally and point directly outward into the open air above the upper Cheakamus River valley (Fig. 6.1B). Above ~800 m asl, the columnar jointing transitions from slender to coarse and subvertical. The lower contact with undivided basement rocks is not exposed. Helm Creek phase basaltic trachyandesite lava also occurs at the northern base of the Cinder Cone, where the lavas form several 10 to 20 m-wide, 1 to 2-m high, slender, radially jointed lobes. Although these rocks are not physically connected with those occupying the lower Helm Creek valley, geochemical and petrographic similarities strongly suggest that the Cinder Cone was the vent for these rocks

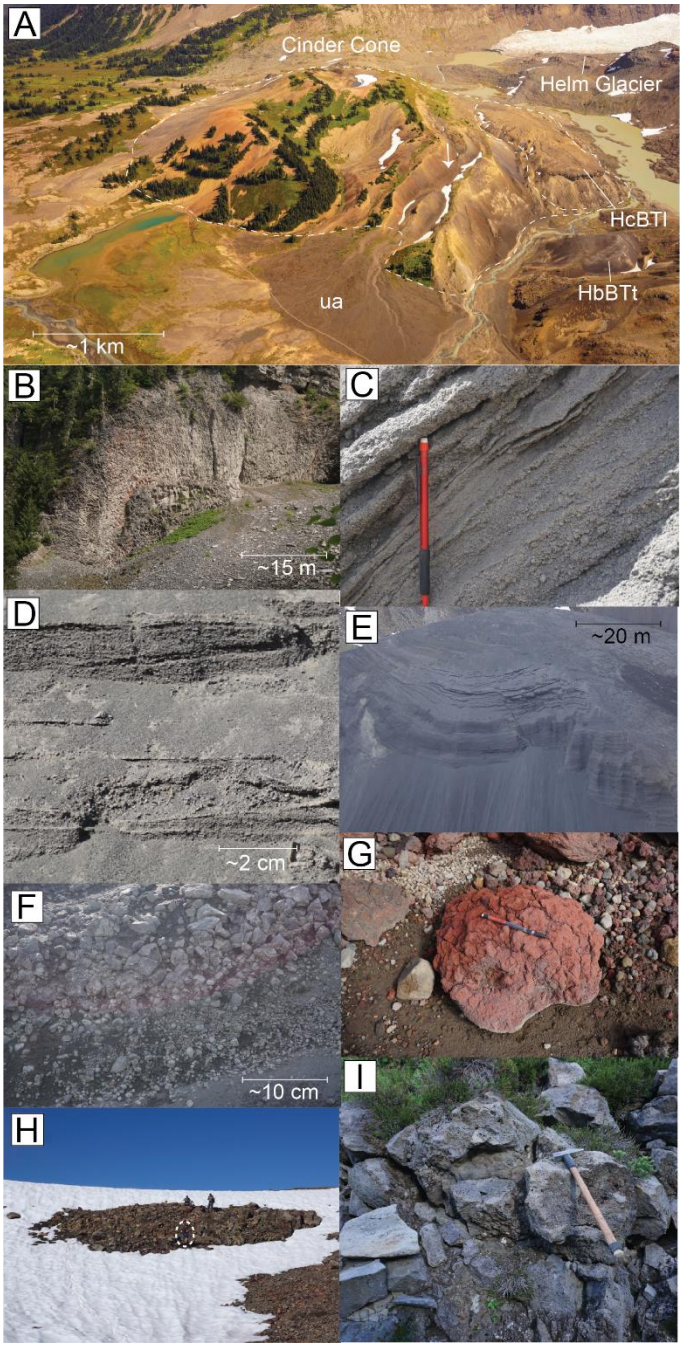

Fig. 6.1. Field photographs showing the lithofacies at the Cinder Cone. (A) Aerial image of the Cinder Cone looking northeast. The large alluvial deposit (ua) is located in the lower middle of the image. (B) Photograph looking west showing slender jointed, radially jointed lobe exposed at the northern end of Helm Creek valley (unit HsBTl). The top of the photo is located at ~800 m in elevation. (C) Image looking west showing indurated, palagonitised surge beds (unit HbBTtu) on the southern flank of the Cinder Cone. (D) Close up image showing laminated, cross stratified pyroclastic surge deposits (unit HbBTtu) located on the northern flank of the Cinder Cone. (E) Photograph looking south showing bedded, surge deposits (unit HbBTtu) located directly south of the Cinder Cone. (F) Photograph showing well sorted, clast supported proximal pyroclastic fallout (unit HbBTt) on the northern side of the Cinder Cone. (G) Photograph showing bread crusted, oxidised pyroclastic spindle bomb (unit CCmBt) located in the upper crater of the Cinder Cone. (H) Photo looking south showing Cinder Cone phase coarsely jointed clastogenic basalt (unit CCagBl) exposed in the southern wall of the Cinder Cone crater. Person circled for scale. (I) Photograph showing vesicular, blocky basaltic lava (unit CCcBl) exposed in the upper part of the Helm valley.

(Mathews 1958; Green et al. 1988; Wilson and Russell 2018). A K-Ar geochronometric determination yielded an age of 110 ± 30 ka (Green et al. 1988) indicating eruption during Late Pleistocene. The Helm Creek phase lavas provide compelling evidence for glaciovolcanism. Steep, over thickened (i.e., ~300 m-thick) bluffs and slender, horizontally oriented columnar jointing in the lower Helm Creek valley suggest that the lavas may have cooled rapidly against a subvertical cooling surface. Wilson and Russell (2018) suggest that these rocks were impounded against ice and record the paleo-presence of a valley glacier in the upper Cheakamus valley during the MIS 5d (locally known as the Sangamonian interglacial interval).

Bedded basaltic trachyandesite tuff (HbBTtu)

Dark grey, bedded, matrix-supported, moderately sorted basaltic trachyandesite tuff form a broad, 15 to 30 m-thick pile at the base of the Cinder Cone and an isolated 10 to 15 m-thick accumulation located south of the main Cinder Cone deposit. The rocks are weakly palagonitised and moderately indurated (Fig. 6.1C). The matrix comprises fine, angular ash and lapilli. Larger clasts include vesicular blocks and scattered cauliflower bombs (~5 %, 1 to 10 cm-diameter). The deposits lack accessory bedrock lithics. The bedding dips away from the center of the Cinder Cone at a shallow angle. Bedding in the isolated southern exposure dips shallowly northward. Beds are defined by fine to moderate laminations (1 to 5 cm-thick) that are commonly graded and cross-stratified (Fig. 6.1D). The southern exposures show beds that are intersected by numerous, discontinuous, syn-depositional growth faults (Fig. 6.1E). The basal contact with Cretaceous bedrock is observed in several places. The contact is sharp and unconformable. The fine ash-sized matrix, laminated bedding structures and weak palagonitisation suggest emplacement as pyroclastic surges accompanying phreatomagmatic eruptions. The lack of accessory bedrock lithic clasts possibly suggests magma fragmentation near the surface (i.e., not within the bedrock). This may imply that the water causing these phreatomagmatic eruptions were probably sourced from a surface reservoir such as an alpine lake, snowpack, or a thin glacier (i.e., rather than groundwater).

Bedded basaltic trachyandesite tephra (HbBTt)

Dark grey to black, coarse to finely bedded, well sorted, unconsolidated tephra forms a 60 to 80 m-thick mound overlying bedded basaltic trachyandesite tuff at the Cinder Cone. The deposits are well bedded and show both reverse and normally graded beds that range in thickness from several centimeters to several meters. The deposit is clast supported and very well sorted (Fig. 6.1F). Clasts comprise highly vesicular basaltic trachyandesite lapilli and blocks. These rocks are best exposed on the northern side of the Cinder Cone where they form broad, outward-dipping beds that overlie (via down-lapping beds) bedded basaltic trachyandesite tuff (pyroclastic surge deposits; unit HbBTtu). The contact is conformable with no erosion or reworking. Clast support, the high degree of sorting, and reverse and normal grading suggest that these rocks were deposited as

Volcanic phase	Map unit	Map unit code	Texture	Groundmass	Phenocrysts
Helm Creek (H) phase	Coarsely jointed porphyritic basaltic trachyandesite lava	HcBTl	Porphyritic, hypocrystalline, trachytic	Trachytic plagioclase (~10 %; 0.01–0.1 mm), equant Fe-Ti oxide (~10 %; 0.1 mm), fine augite (~10 %; 0.2 mm), olivine (<1 %; 0.01 mm) and glass (~10 %).	Phenocrysts: plagioclase (~30 %; 0.1–0.5 mm), olivine (~15 %; 0.2 mm) and augite (~10 %).
	Slender jointed porphyritic basaltic trachyandesite lava	HsBTl			
	Bedded basaltic trachyandesite tuff	HbBTtu			
	Bedded basaltic trachyandesite tephra	HbBTt			
Cinder Cone (CC) phase	Massive basaltic tephra	CCmBt	Porphyritic, holocrystalline	Plagioclase (~30 %; 0.01–0.1 mm), Ti-augite (~15 %; 0.01–0.1 mm) and equant Fe-Ti oxides (~10 %; 0.01 mm).	Phenocrysts: plagioclase (~20 %; 0.5–1 mm), olivine (~20 %; 0.2–1 mm) ± augite (~1 %).
	Agglutinated porphyritic basaltic lava	CCagBl			
	Coarsely jointed porphyritic basaltic lava	CCcBl			

Table 6.1 Petrographic characteristics of volcanic rocks in the Cinder Cone map area.

Wilson, A.M., Russell, J.K., and Harris, M.A., 2024. Glaciovolcanism in the Garibaldi volcanic belt: Nine geological maps from southwestern British Columbia, Canada. British Columbia Ministry of Mining and Critical Minerals, British Columbia Geological Survey Open File 2024-10, 64p

proximal pyroclastic fallout. The rocks lack fine bedding laminations and palagonitisation and have a low ash component, suggesting magmatic versus phreatomagmatic fragmentation. These deposits were probably formed in response to drying out of the eruption column and a transition from wet, pyroclastic surges to Hawaiian style basaltic fountaining. The reverse and normally graded beds were produced by local variations in plume height and position in response to fluctuating eruption intensity and changing wind direction.

6.2.2. Cinder Cone (CC) phase (Non-glaciovolcanic)

Massive basaltic tephra (CCmBt)

Dark red, oxidised, poorly sorted, massive tephra forms the upper part of the Cinder Cone sequence. The deposits comprise unconsolidated ash, lapilli, spatter, and agglutinated spindle bombs (Fig. 6.1G). They are plagioclase, olivine ± augite phyric, and are distinguishable from Helm Creek phase rocks based on their relatively low augite phenocryst component (i.e., ~1 % versus ~10 %) and the presence of groundmass Ti-augite (Table 6.1). These rocks are massive to very crudely bedded (arranged in shallow, outward-dipping beds) and form a ~400 m-wide scoria cone with a ~100 m-wide central eruption crater. The deposit is covered in scattered glacial debris, indicating that the rocks have been glacially overridden since the eruption. Pervasive deposit oxidation and the presence of pyroclastic spindle bombs suggest a subaerial eruption environment. The basal contact with the underlying Helm Creek phase rocks is not well exposed, however it is closely constrained in many places. It is interpreted to be unconformable, primary due to the apparent geochronometric age disparity between the Helm Creek and Cinder Cone volcanic phases. Clear indicators for a significant period of time separating the two phases are not observed.

Agglutinated basaltic lava (CCagBl)

Dark red to grey, oxidised, moderately vesicular (~10 to 30 %), agglutinated porphyritic basaltic lava forms a 5 to 10 m-thick, 30 m-wide lobes of lava that is situated in the southern crater wall of the Cinder Cone (Fig. 6.1H). The lava is agglutinated and shows fluidal, lensoidal shaped, welded clasts of variable vesicularity and size (~1 to 30 cm). The rocks are geochemically and petrographically identical to the coarsely columnar jointed basaltic lavas (unit CCcBl) occupying the upper part of Helm Creek valley (Fig. 6.1I) suggesting that they are co-magmatic. The agglutinated texture of these lavas records a clastogenic origin, likely formed due to subaerial strombolian basaltic spatter accumulation and deposit mobilisation.

Coarsely jointed basaltic lava (CCcBl)

Dark grey to black, moderately vesicular (~20 %), porphyritic basaltic lava forms a ~10 m-thick lava field covering the upper part of the Helm Creek valley. The surface of the lava is extensively glacially scoured and covered by undivided glacial till (unit ut). These rocks are best exposed in the bed of Helm Creek where they form continuous exposure for ~2 km towards the northeast. The lavas show coarse, subvertical columnar

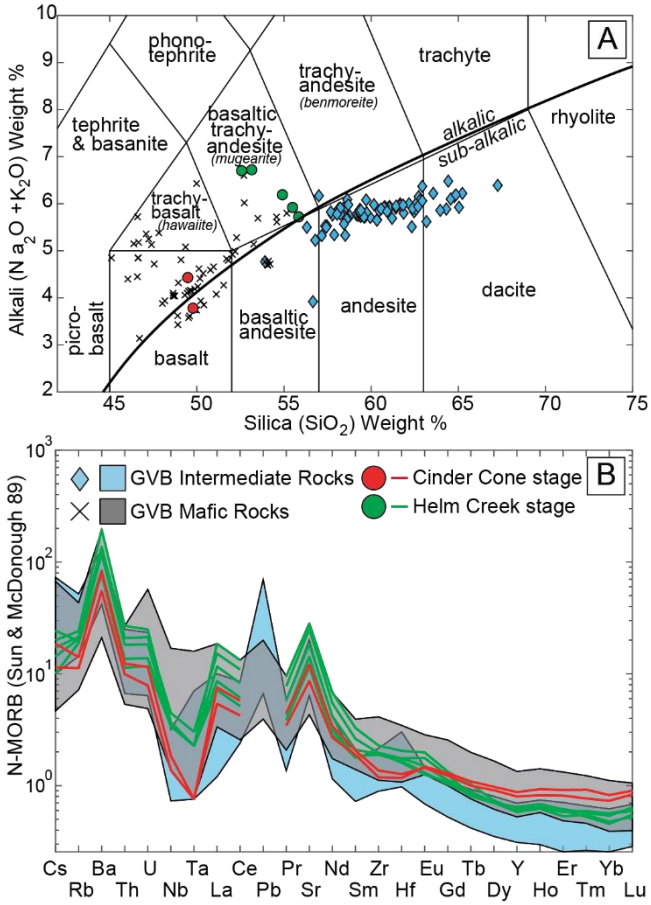

Fig. 6.2. Geochemical characteristics of rocks in the Cinder Cone map area. (A) Total alkali-silica plot defines the two chemically distinct phases of activity: The Helm Creek (H) phase basaltic trachyandesite, and the Cinder Cone (CC) phase alkaline to sub-alkaline basalts. Additional analyses of GVB basaltic rocks are from Mullen and Weis (2015) and Wilson and Russell (2017). Additional analyses of GVB intermediate rocks are from Bye et al. (2000); Fillmore and Coulson (2013); Wilson et al. (2016) and other map areas from this study (see appendix A1). (B) Trace element compositions of the Cinder Cone rocks normalized to N-MORB (Sun and McDonough 1989). Mineralogically, the rocks are alkaline (they show Ti-augite in the groundmass) however they are alkalic to sub-alkalic and show Nb–Ta depletion.

jointing and have both ropey pahoehoe and rubbly ‘a‘ā textured upper surfaces (Fig. 6.1I). The petrographic and geochemical similarity suggests a close affiliation with other Cinder Cone phase volcaniclastic and clastogenic rocks (units CCmBt and CCagBl). Despite alkaline mineralogy (i.e., the rocks contain groundmass Ti-augite; Table 6.1), the rocks show a strong Nb–Ta depletion, suggesting a volcanic arc affinity (Fig. 6.2). These trace element compositions may have been caused by the assimilation of crustal material during magma storage and ascent. Like other Cinder Cone phase deposits, the rocks record a subaerial eruption environment. We report a new $^{40}Ar/^{39}Ar$ determination for the Cinder Cone phase event of 16.7 ± 4.7 ka (Figure 6.3; Table 1.1; A. Borch, personal communication, 2024), suggesting eruption after the last glaciation, but prior to a local alpine ice re-advance.

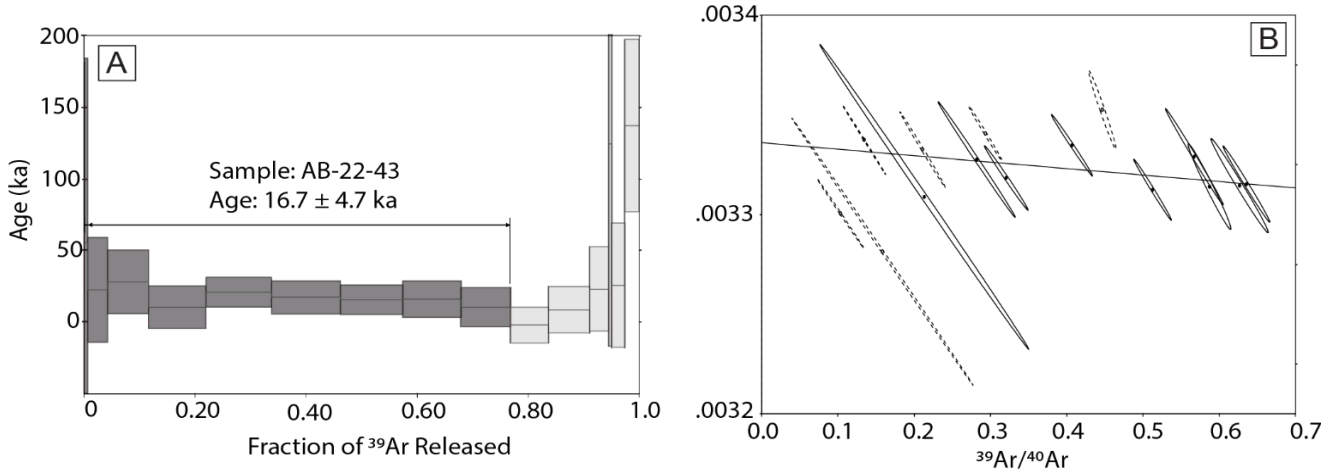

Fig. 6.3. Summary of $^{40}Ar/^{39}Ar$ geochronology results from the Cinder Cone sample AB-22-43 (unit CCcBl). (A) Plateau diagram showing fraction of ^{39}Ar versus age. 9 out of 15 fractions released 77 % ^{39}Ar, and the mean squared weighted deviation is equal to 0.47. The sample shows a plateau at 16.7 ka with a calculated 1 uncertainty of 4.7 ka. (B) Inverse isochron plot showing 15 heating steps. Ellipses denote 1 analytical uncertainty.

6.3. Glacial sediments

Undivided till (ut)

Poorly sorted, unconsolidated polymictic silt and gravel form a thin scattered glacial deposit around the terminus of Helm Glacier and at the base of Helm Creek valley. Accumulations >1 m-thick are mapped as a discrete geologic unit. Clast lithologies are diverse, comprising variably rounded, striated plutonic, and metamorphic rocks as well as rare volcanic clasts.

6.4. Quaternary sediments

Undivided alluvium (ua)

Undivided, poorly sorted, unconsolidated alluvial sediments comprising clasts of locally sourced Cinder Cone tephra, plutonic rocks, and metamorphic rocks form a ~400 m-wide outwash fan on the eastern side of Helm Lake. The observed deposit thickness is ~3 m, and unconformably overlies Cretaceous bedrock as well as Cinder Cone phase basaltic lava.

6.5. Summary

The Cinder Cone is a Late Pleistocene basaltic scoria cone in Garibaldi Provincial Park, with two eruption phases. The older Helm Creek (H) phase consists of trachyandesite lava flows, tubes, and lobes filling the Helm Creek valley. Older K-Ar geochronology suggests that this eruption occurred around 110 ± 30 ka (coinciding with the MIS 5d interglacial period). At the valley's northern end, the lava exhibits steep, thickened profiles and joint morphologies indicating ice confinement. We interpret that these lavas flowed northward, encountering a glacier in the Cheakamus River valley and were impounded by an ice dam at ~800 m asl. The Helm Creek phase rocks also form the lower part of the Cinder Cone, with phreatomagmatic and later dry pyroclastic deposits. The Helm Creek phase rocks provide important local paleoenvironmental constraints; at the time of the eruption the lower Cheakamus River valley was occupied by a glacier of substantial thickness, while the upper alpine areas around the Cinder Cone were relatively ice free.

The younger Cinder Cone (CC) phase comprises a porphyritic basaltic scoria cone and lava field in the upper Helm Creek valley. These eruptions were subaerial; initially Strombolian style, followed by an effusive basaltic pahoehoe eruption that covered the upper valley. While the rocks show evidence for post eruption glacial overriding, the original deposit morphologies are well preserved. The age of the Cinder Cone phase eruption is constrained by a new $^{40}Ar/^{39}Ar$ analysis of 16 ± 4.7 ka. We propose that the Cinder Cone eruption occurred shortly after the end of the last glaciation (i.e., > 17 ka, during the MIS 2, Fraser glaciation), but prior to the re-advance of local alpine glaciers, such as those associated with the Younger Dryas (Friele and Clague 2002).

7. Cracked Mountain volcano (1:5,000)

Cracked Mountain volcano is part of the Mount Meager volcanic complex in the northern GVB (Read 1977; Stasiuk and Russell 1990; Wilson and Russell 2018; Harris et al. 2022). The edifice is one of several small, isolated occurrences of Pleistocene alkaline basalt that are distributed around the periphery of the Mount Meager stratovolcano (Read 1977, 1979, 1990; Green et al. 1988; Stasiuk and Russell 1989; Wilson and Russell 2017). These volcanic rocks unconformably overlie Coastal plutonic complex (Cretaceous) bedrock consisting of biotite-quartz monzonite, hornblende diorite, biotite-muscovite schist and gneiss (Read 1979).

The oldest volcanic rocks in the area are mapped as undivided volcanic (V) andesite lava that crops out in an isolated mound ~100 m east of Cracked Mountain. These rocks are probably associated with the Early Pleistocene Pylon assemblage of the Mount Meager volcanic complex. Clear contact relationships with the surrounding rocks are not exposed.

The Cracked Mountain (CM) phase lithofacies form a broad, ~200 m-thick, circular pile of basaltic palagonitised lapilli tuff, intrusive dikes, dike-fed peperites, pillow lava, and tuff breccia (Fig. 7.1). The Cracked Mountain phase lithofacies are seen to unconformably overlie undivided basement rocks at several

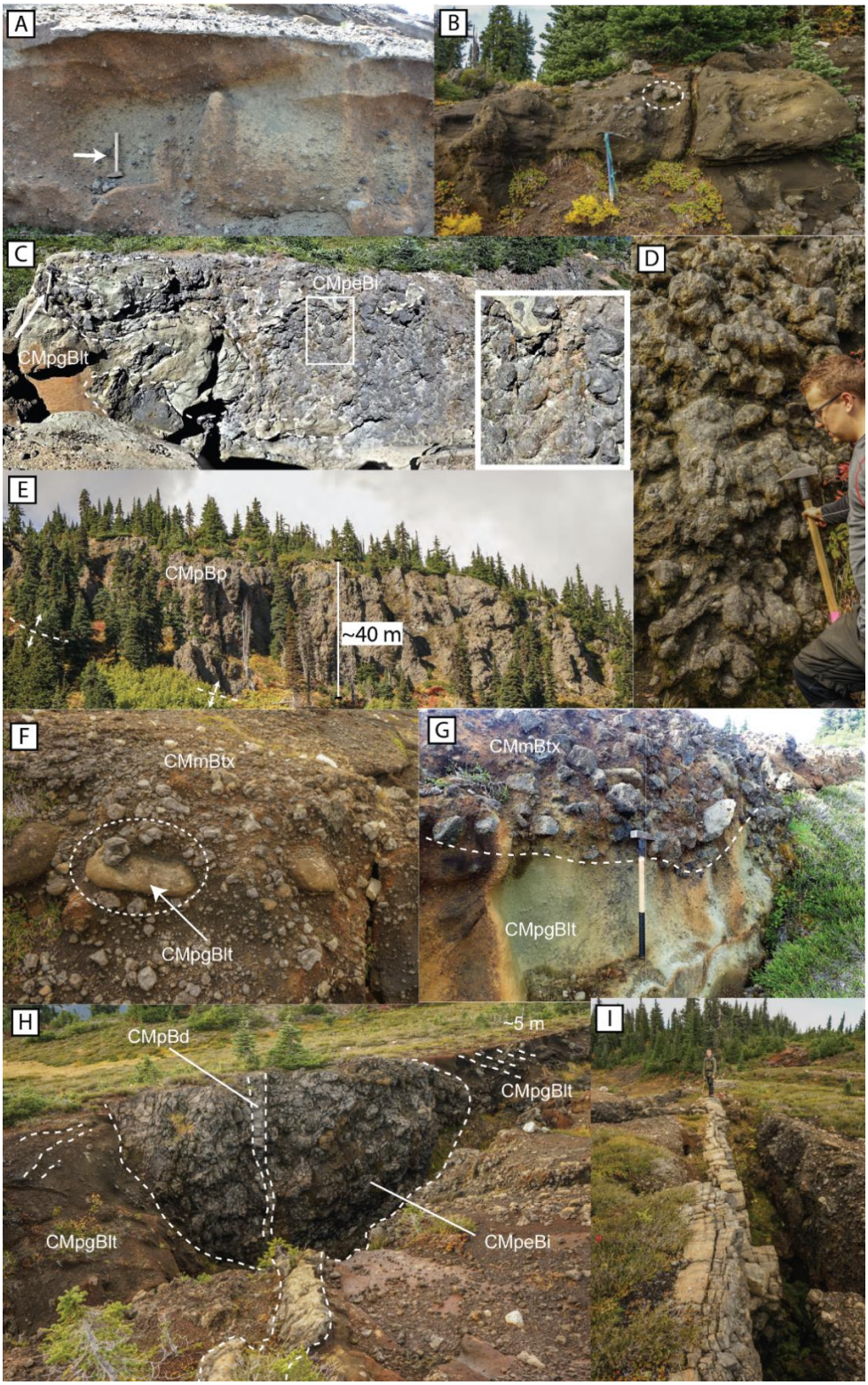

Fig. 7.1. Field photographs showing the volcanic lithofacies at Cracked Mountain. (A) Field photo showing ~2 m thick exposure of massive, moderately sorted ash and lapilli tuff (CMpgBlt) underlying poorly sorted tuff breccia (CMmBtx). (B) Crudely stratified, matrix-supported, palagonitised lapilli tuff (unit CMpgBlt). Arrow indicates a collection of vesicular bombs. (C) Photomosaic of ~30 m wide by~ 4 m thick exposure of peperitic intrusions (CMpeBi) mingled with massive lapilli tuff (CMpgBlt). Inset (white box) shows pillowed lobes with a lens of lapilli tuff. One metre hammer (white arrow) for scale. (D) Densely packed, porphyritic basaltic pillow lava near the outer eastern margin of the edifice (unit CMpBp). (E) A stacked sequence of pillow lavas (CMpBp) (view looking NW at SE base of CM), ~150 m wide and ~40 m thick. White arrows mark approximate edifice basement contact at 1500 m a.s.l. (F) Rounded accessory lithic of incipiently palagonitised lapilli tuff (unit CMpgBlt) entrained within massive tuff breccia (unit CMmBtx). (G) Massive, ~1.5 m thick, tuff breccia (CMmBtx) dominated by subrounded to blocky lava, overlying massive lapilli tuff (CMpgBlt). Hammer (1 m) for scale. (H) Semi-circular pod of dike-fed pillowed lava (CMpeBi) intruding bedded basaltic lapilli tuff (CMpgBlt). Extensional crack offsets dike. (I) 0.5 m-thick, subvertical porphyritic basaltic dike (unit CMpBd), parallel to the extensional crack. Person for scale.

places around the periphery of the edifice. Cracked Mountain is intersected by more than 50 subvertical, subparallel basaltic dikes (Fig. 7.1I). These dikes are ~1 to 3 m-thick and mostly strike northeast-southwest. Cracked Mountain is ~1.5 km long, ~1 km wide, and has a rounded, semi-flat upper surface. The volcanic lithofacies cover an elevation range of ~300 m to a maximum upper elevation of ~1600 m asl. The surface of Cracked Mountain is covered by scattered glacial debris (ablation till) and other indicators for post-emplacement glacial overriding (e.g., rounded bluffs and striated surfaces). The edifice is dissected by a network of active extensional fault scarps (e.g., Figs. 7.1H and I). These "cracks" are aligned subparallel to the margins of the edifice and form deep (>20 m), steeply dipping incisions that provide excellent lithofacies exposure. Fault displacements are greatest near the margins of the volcanic pile, where horizontal and vertical offsets typically exceed 20 m. Near the center of the edifice the faults are more subdued (1 to 2 m-wide, ~5 to 10 m-deep cracks with little to no vertical offset).

The Cracked Mountain phase lithofacies show moderate petrographic and geochemical variation. They are sub-alkalic (Fig. 7.2A) and have primitive trace element compositions that are similar to other northern GVB basaltic rocks (Fig. 7.2B) (Lawrence et al. 1984; Roddick and Souther 1987; Green et al. 1988; Stasiuk and Russell 1989; Mullen and Weis 2015; Wilson and Russell 2017). Most Cracked Mountain phase rocks are plagioclase and olivine phyric and have a glassy to fine-grained groundmass of microcrystalline plagioclase, olivine, Ti-augite, and Fe-Ti oxide (Figs. 7.3A, B, and E, Table 7.1). Some samples contain minor phenocrysts of augite (Fig. 7.3F). These slight differences in phenocryst content indicate polymagmatic crustal storage preceding the eruption. However, the overall trace element signatures for all samples are similar, suggesting a single mantle source for the Cracked Mountain eruption (Harris and Russell 2022).

The Cracked Mountain phase deposits show complex and chaotic within-phase stratigraphic relations. Our map provides a representation of the predominant unit distribution. In the field, however, the lithofacies distribution is disorganized. Harris et al., (2022) provide a detailed account of the best representative stratigraphic exposures and relationships.

Lapilli tuff is the stratigraphically oldest identified Cracked Mountain phase deposit (unit CMpgBlt). These rocks are incipiently palagonitised and show high vesicularity with blocky and cuspate clast shapes. These textures indicate that the Cracked Mountain eruption commenced explosively (probably both phreatomagmatic and magmatic). A relatively continuous eruption pile, with no significant mappable eruption hiatuses, unconformable lithofacies boundaries or indicators of eruption environment change (e.g., passage zones) suggests that the eruption occurred over a single, continuous phase of activity. This indication of short-lived, monogenetic activity is corroborated by paleomagnetic studies, which show that all Cracked Mountain volcanic lithofacies overlap within a single magnetic moment (Harris and Russell 2022; Harris et al. 2022). The timing this activity is constrained by a single $^{40}Ar/^{39}Ar$ geochronology determination of 401 ± 38 ka (Harris et al. 2022).

Volcanic phase	Map unit	Map unit code	Texture	Groundmass	Components
Cracked Mountain (CM) phase	Palagonitised basaltic lapilli tuff	CMpgBlt	Vitric, palagonitised	Moderately to poorly sorted, yellow-grey, ash to lapilli; ~ 25 - 40% cuspate and highly vesicular juveniles, ~60% dense and blocky juveniles	Monolithic, ash to block sized, moderately to highly vesicular, plagioclase (5-10%) olivine (5%) microlitic vitric juveniles (5-30%, 0.5-5mm); Intact to fragmented crystals, plagioclase (5-10% 0.5-2 mm) and olivine (5-10% 0.1-1 mm)
	Massive basaltic tuff breccia	CMmBtx			
	Peperitic basaltic intrusions	CMpeBi	Porphyritic, microcrystalline	Fine grain, plagioclase (55%); Ti-augite (25%), olivine (10%), glass (5 %); Fe-Ti oxides (5%)	Subhedral phenocryts containing plagioclase (10-15%, 0.5-3 mm); olivine (10%, 0.1-1 mm); Augite (2-5 %)
	Porphyritic basaltic pillow lava	CMpBp			
	Porphyritic basaltic dykes	CMpBd			

Table 7.1 Petrographic characteristics of volcanic rocks at Cracked Mountain volcano

The rocks show compelling evidence for eruption in the presence of glacial ice. Pervasive palagonitization of tephra, peperitic intrusions, pillow lava, and vitric tuff breccia (i.e., Fig. 7.1) all suggest eruption and deposition within a sustained body of water. Lithofacies variation and disorganisation suggest that this waterbody was dynamic and probably fluctuated in-depth and extent throughout the eruption. The local topography permits the presence of a non-glacial body of water existing in the area at the time of the eruption. Therefore, glacial ice in the form of a thick ice sheet (i.e., Coast Mountain portion of a past CIS) is the only plausible mechanism for damming and maintaining a water body of this size. The Cracked Mountain lithofacies record the presence of an ephemeral englacial lake that was at least 250 m deep during the MIS 12 glaciation. At the time of the eruption (i.e., at 401 ± 38 ka), the local surface of the CIS reached elevations of 1680 m asl or higher (Wilson and Russell 2018; Harris et al. 2022).

7.1. Basement geology

Undivided basement rocks (ub)

Undivided quartz monzonite, hornblende diorite, biotite and muscovite schist and gneiss of the Coastal Plutonic complex and Cadwallader group (Read 1979). The rocks show a steeply-dipping, northwest–southeast striking foliation. The predominant jointing is also steeply dipping and striking northeast to southwest.

7.2. Older volcanic rocks

7.2.1. Undivided volcanic (V) rocks (Non-glaciovolcanic)

Aphyric andesite lava (VaAl)

Dark grey to brown, crudely columnar jointed, sparsely vesicular (<5 %), aphyric, aphanitic andesite forms a small, isolated mound ~100 m east of Cracked Mountain. The contacts with surrounding rocks are not exposed, however, we interpret that the rocks to unconformably overlie undivided basement (ub). Substantial erosion of the deposits suggests that they are considerably older than the adjacent Cracked Mountain phase rocks. Based on previous mapping (Read 1979), these rocks are probably part of the Early Pleistocene Pylon assemblage of the Mount Meager volcanic complex.

7.3. Geology of Cracked Mountain volcano

7.3.1. Cracked Mountain (CM) phase (Glaciovolcanic)

Palagonitised basaltic lapilli tuff (CMpgBlt)

Light tan to orange, matrix-supported, variably sorted lapilli tuff is exposed in the northern, northwestern, and upper central part of Cracked Mountain, as well as in nearly all incised crack exposures at all elevations of the volcano (Harris et al. 2022). The Cracked Mountain lapilli tuffs are intruded by, or overlain by all other volcanic lithofacies, making it the oldest identified phase for the Cracked Mountain volcano. The lapilli tuffs range from incipiently to highly palagonitised. The rocks show a variety of bedding ranging from, massive, crudely stratified, to thinly laminated beds (~0.1 m) (Fig. 7.1A and B). Near the

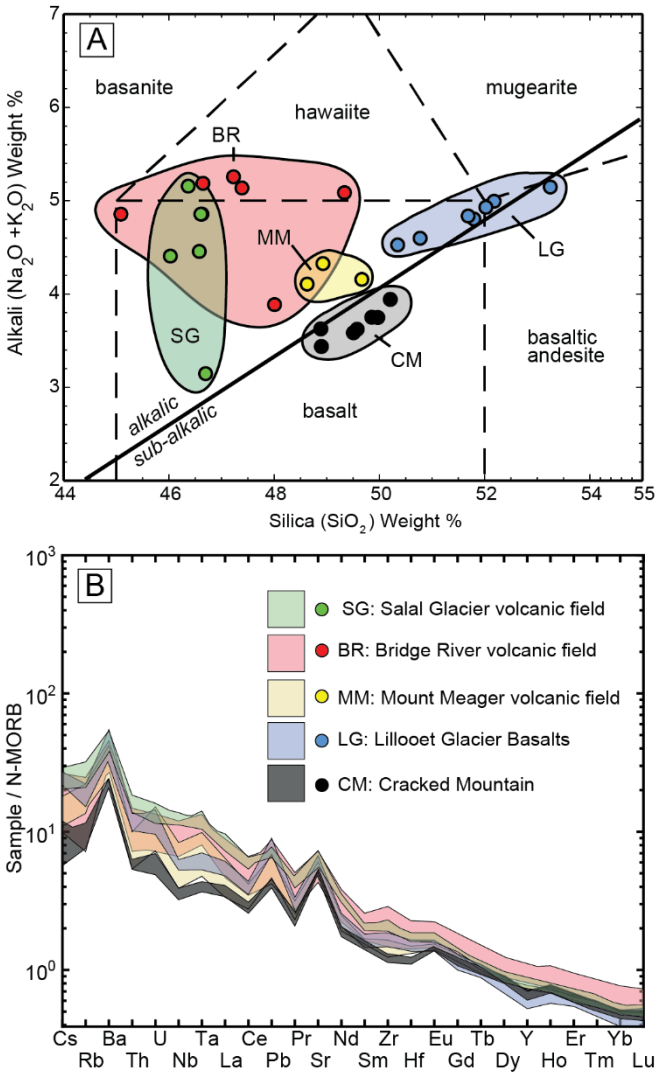

Fig. 7.2. Geochemical characteristics of the Cracked Mountain (CM) lithofacies. (A) Total alkalis vs. silica diagram after Le Bas et al., (1986) showing restricted chemical variation within the suite (closed black circles). Additional analyses of Garibaldi volcanic belt basaltic rocks are shown for comparative purposes (from Mullen and Weis 2015; Wilson and Russell 2017), including the Bridge River Cones (BRC), The Salal Glacier volcanic complex (SG), The Lillooet Glacier basalts (LG) and other rocks from the Mount Meager Mosaic Assemblage (MMA). (B) Trace element compositions of the Cracked Mountain rocks normalised to N-MORB (Sun and McDonough 1989). The rocks are primitive and show very little variation and lack distinctive subduction-related signatures.

summit of Cracked Mountain, incipiently palagonitised basaltic tuff breccia forms a ~250 m-wide accumulation with lensoidal beds dipping outwards at a shallow angle (~20 to 30º). Sorting is variable, ranging from moderately to poorly sorted. Select locations contain spatter-rich lapilli to bomb-sized components supported by the fine ash matrix. Clasts include glassy, angular to rounded, vesicular lapilli and blocks (Fig. 7.1B), subangular to subrounded, vesicular bombs, and quenched lobes fragments of peperitic intrusions (i.e., CMpeBi) (<0.3 m diameter). The rocks have a matrix of vitric ash with both cuspate and blocky margins (~95%) (Figs. 7.3C and D) and liberated and/or partially liberated plagioclase and olivine phenocrysts (~5 %). The matrix

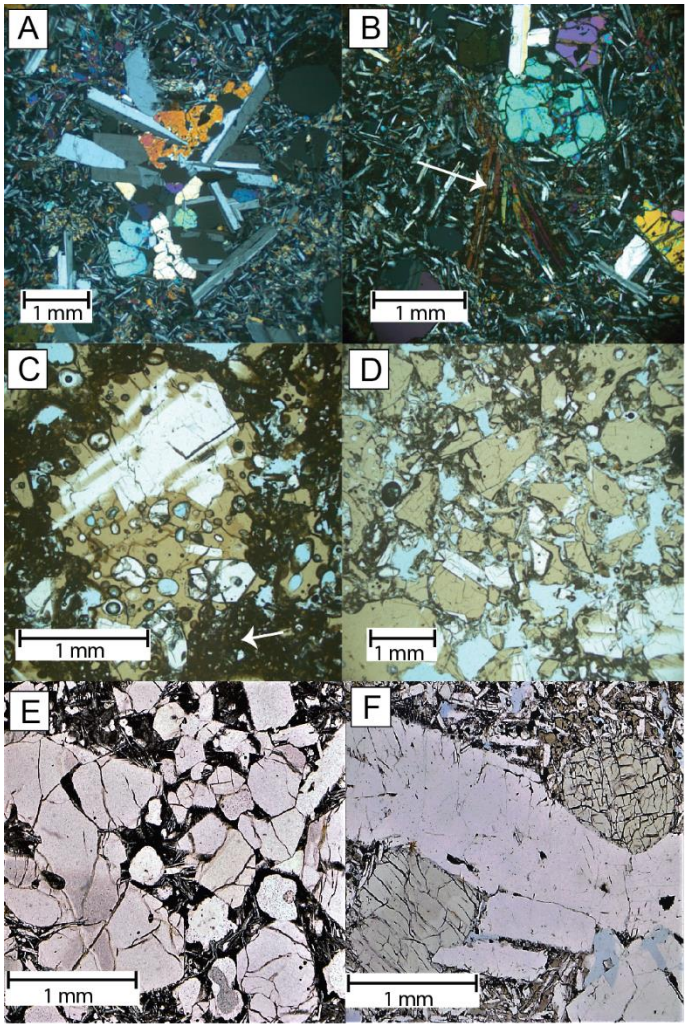

Fig. 7.3. Photomicrographs of coherent and volcaniclastic lithofacies at Cracked Mountain. (A) Glomerophenocryst of plagioclase and olivine set in a holocrystalline groundmass of plagioclase, olivine, Ti-augite and Fe-Ti oxides (unit CMpBd), displayed with cross-polarized light. (B) Groundmass of coherent lithofacies at Cracked Mountain. White arrow indicates a radiating aggregate of acicular Ti-augite (unit CMpBd), displayed with cross-polarized light. (C) Moderately vesicular, porphyritic vitric lapilli set in a dark matrix of moderately palagonitised and microcrystalline ash (unit CMpgBlt), displayed with plain-polarized light. White arrow indicates palagonitised matrix glass. (D) Moderately sorted ash tuff breccia displaying cuspate and blocky ash fragments (unit CMpgBlt), displayed with plain-polarized light. E) Glomerophenocryst of plagioclase and olivine within a hypocrystalline groundmass with microlitic plagioclase and fine grain olivine and clinopyroxene, displayed with plain-polarized light. F) Less common CM petrographic suite containing glomerophenocryst with pale-green augite, displayed with plain-polarized light.

ash is pervasively palagonitised in the palagonitised basaltic tuff breccia unit and is bright orange. High clast vesicularity and blocky and cuspate clast shapes imply explosive magma fragmentation (probably both phreatomagmatic and magmatic). The variable bedforms (i.e., massive, thinly bedded, and spatter-rich stratification) indicate that the explosive style ranged from sustained ash-column derived pyroclastic density currents, pulse-like surge deposits, and fire-fountaining events (Harris et al. 2022). The pervasive matrix palagonitisation and clast rounding in some of the deposits indicate that water was present during the eruption (i.e., an englacial lake) and the tephra was partially reworked before deposition. The incipiently palagonitised tephra variants may indicate deposition involving lesser amounts of water in a "leaky" englacial lake, or eruptions with a lower eruption flux (i.e., resulting in a cooler deposit and a correspondingly lower degree of palagonitisation) (Harder and Russell 2006).

Peperitic basaltic intrusions (CMpeBi)

Basaltic lava bodies that show intrusive relationships to the surrounding lapilli tuffs (CMpgBlt) are exposed in several places on the upper surface of Cracked Mountain and within the incised crack exposures throughout the volcano. The bodies are constructed from pillow lava and display bulbous, semicircular pod shapes with diameters ranging from ~5 to 15 m (Fig. 7.1C). Individual pillows are typically small (i.e., <30 cm-diameter), variably vesicular (~10 to 30 %), and are densely packed together with little to no intra pillow material and or hyaloclastite. Several outcrops indicate that these pods of pillows are probably dike fed and their distribution and morphology are controlled by pre-existing structures within the host tephra (e.g., bedding) (Fig. 7.1H). In some cases, the source dike for each of the pillow pods is easily identified traversing sections of coherent tuff breccia before expanding into a large, pillow accumulation. Their intrusive relationship with the surrounding volcaniclastic rocks suggest that the host tephra was unconsolidated and water-laden during the injections (i.e., a tephra slurry), thus these intrusive bodies are "peperitic" (e.g., White and Houghton 2006). The deposits provide further evidence that the upper portion of Cracked Mountain lithofacies erupted into a sustained body of water.

Porphyritic basaltic pillow lava (CMpBp)

Porphyritic basaltic pillow lava forms a volumetrically predominant component of the lithofacies at Cracked Mountain. The rocks are moderately vesicular (~30 %) and fine-grained (Table 7.1). Pillow lava accumulations occur in two main forms. Around the lower periphery of Cracked Mountain, stacked pillow lava forms steep bluffs that are up to 40 m high (Fig. 7.1E). Along the southeast margin of Cracked Mountain, these peripheral pillow accumulations are observed to rest directly on undivided basement rocks (unit ub) and are overlain by accumulations of massive tuff breccia (CMmBtx). In other areas, partial collapsed zones reveal 1-2 m thick layers of massive, palagonitised lapilli tuff (CMpgBlt) underlying the marginal pillow lava, (e.g., Harris et al. 2022). On the upper surface of Cracked Mountain porphyritic pillows forms irregularly shaped piles of closely packed pillows that are surrounded by a disorganised mixture of the other Cracked Mountain phase volcaniclastic lithofacies (Fig. 7.1D). The pillows range in diameter from ~0.5 m to >3 m and have <2 cm-thick glassy margins. Intra-pillow voids are typically filled with fine, basaltic vitric ash and lapilli.

The abundant pillow lava at Cracked Mountain indicate that the eruption occurred in a subaqueous environment. A sample collected from the interior of a radially jointed pod of holocrystalline pillow lava was analysed using $^{40}Ar/^{39}Ar$ at the

WiscAr laboratory at the University of Wisconsin-Madison. The sample returned an age of 401 ± 38 ka (Harris et al. 2022). Given the lack of stratigraphic indicators for hiatuses in the eruption sequence, as well as overlapping paleomagnetic signatures for all lithofacies, we take this age to be representative of all Cracked Mountain phase volcanics (Harris et al. 2022).

Massive basaltic tuff breccia (CMmBtx)

Dark grey to light orange-brown coloured, massive to crudely bedded hyaloclastite breccia containing large clasts (<30 cm-dimeter) of vesicular pillow lava (~50 %), jointed basaltic blocks (~30 %) and glassy, blocky fragments (~10 %) (Fig. 7.1G). The matrix consists of blocky granules of partially palagonitized glass. The rocks are widely distributed throughout the upper stratigraphy of the map area and commonly mantle accumulations of densely packed, porphyritic basaltic pillow lava (unit CMpBp). We ascribe an autoclastic and hydroclastic origin to these rocks and suggest that they derive from the gravitational collapse of pillow lavas propagating downhill. Finer grained components (i.e., the granular vitric matrix) were probably produced by reworking of explosively derived lapilli tuff units (CMpgBlt) as well as quench fragmentation and spalling of the quenched marginal pillow material (CMpBp and CMpeBi). Near the center of Cracked Mountain, this deposit contains several large (~0.5 m diameter), well-rounded, light tan, indurated accessory tephra clasts (CMpgBlt) (Fig. 7.1F). These tephra bombs were likely entrained within the tuff breccias through later-stage explosive activity within the conduit, ripping up fragments of the lower stratigraphic units (Harris et al. 2022).

Porphyritic basaltic dikes (CMpBd)

The lithofacies at Cracked Mountain are intruded by at least 50 basaltic dikes. The dikes are observed to crosscut all other lithofacies, however, they show syn-emplacement relationships with some peperitic intrusions (Fig. 7.1H). The dikes range in length from ~15 m to ~250 m and mostly strike northeast to southwest. They range in thickness from ~0.5 to 2 m and are subvertical. The dikes show undulating, ~2 cm-thick, glassy selvages. Vesicularity ranges from ~5 % to more than 30 % with vesicles up to 3 mm in diameter that are concentrated within bands along the edges of the dikes. We interpret these dikes to be the source of the lithofacies at Cracked Mountain, whereby the edifice was constructed by a series of subglacial dike injections and fissure eruptions, which built a pile of subaqueous tephra, followed by peperitic intrusions, pillow lava effusions, and tuff breccia derived from pillow pile collapse and explosive tephra fountaining deposits.

7.4. Summary

Cracked Mountain volcano is a small, isolated basaltic tephra pile that is located near Mount Meager in the northern GVB. The edifice erupted in a single phase of glaciovolcanic activity during the Middle Pleistocene (401 ± 38 ka). The lithofacies (i.e., pillow lava, peperite, and palagonitised lapilli tuffs) indicate that the Cracked Mountain eruption occurred within a sustained body of water. Given the eruption site topography (i.e., a topographic high with ample water drainage) these lithofacies strongly indicate a glaciovolcanic eruption event and record the ephemeral presence of an englacial lake (and substantial glacier) during the Middle Pleistocene CIS during the MIS 12 glaciation.

The in situ subaqueous lithofacies at Cracked Mountain cover an elevation range of ~250 m (1350 m to 1600 m). This indicates that the syn-eruptive body of water must have been at least 250 m deep. The lithofacies do not show any mappable discontinuities or breaks in the deposit sequence. These features, combined with the overlapping paleomagnetic signatures for all lithofacies, strongly supports the notion that the Cracked Mountain eruption was monogenetic and short-lived (Harris et al. 2022). To sustain the englacial lake and prevent drainage via ice lifting events (i.e., jökulhlaups) (Wilson and Russell 2017), the CIS thickness must have been ~880 m, with an ice-surface elevation of at least 1680 m a.s.l (Harris et al. 2022).

Volcanism began explosively, driven by magmatic and phreatomagmatic steam explosions, which formed a series of intermittent subaqueous tephra jets that deposited bedded accumulations of lapilli tuff (unit CMpgBlt). The subaqueous pile was then injected with lava and peperitic bodies (unit CMpeBi) formed within the unconsolidated tephra. As dike-fed lavas reached the outer margins of the volcanic pile, effusive pillow lavas formed within the englacial lake (unit CMpBp). During the final stages of the eruption, late-stage dikes continued to cut through the volcanic pile becoming the youngest identified CM phase units.

Following the eruption, post-glacial overriding eroded the deposit producing a rounded edifice morphology and scattered deposits of surficial ablation till, while over-steepening of the edifice above the valleys below has caused the extensional collapse in the form of cracks that dissect the volcano today.

8. Lillooet Glacier volcano (1:10,000)

Lillooet Glacier volcano is situated in the northwestern GVB at the terminus of Lillooet Glacier. The retreat of the glacier over the last ~100 years has exposed a succession of mafic Quaternary volcanic rocks. These rocks form one of several occurrences of Pleistocene alkaline basalt distributed around the periphery of the Mount Meager volcanic complex (Read 1977, 1979; Stasiuk and Russell 1989; Wilson and Russell 2017; Harris et al. 2022). The volcanic rocks unconformably overlie foliated, metavolcanic, and metasedimentary slate and greenschist of the Gambier Group (Cretaceous) and Coastal Plutonic Complex granite and granodiorite (Cretaceous) (Lynch 1992; Monger and Journeay 1994).

The volcanic rocks at Lillooet Glacier were emplaced in a single phase of volcanic activity (Lillooet Glacier (L) phase). The lithofacies include pillow lava, lava flows, lava tubes and subordinate amounts of basaltic breccia and hyaloclastite (Figure. 8.1). The rocks are distributed across the valley floor and occupy an area of 0.95 km^2. The volume of emplaced volcanic material is estimated to be 0.078 km^3 (Wilson and Russell 2017). The deposits are well preserved and cover an elevation range of 580 m (820 to 1400 m asl). The surface of the Lillooet Glacier deposits is covered by scattered glacial debris (ablation till) and other indicators for post-eruptive glacial overriding (e.g., rounded bluffs and striated surfaces). In the

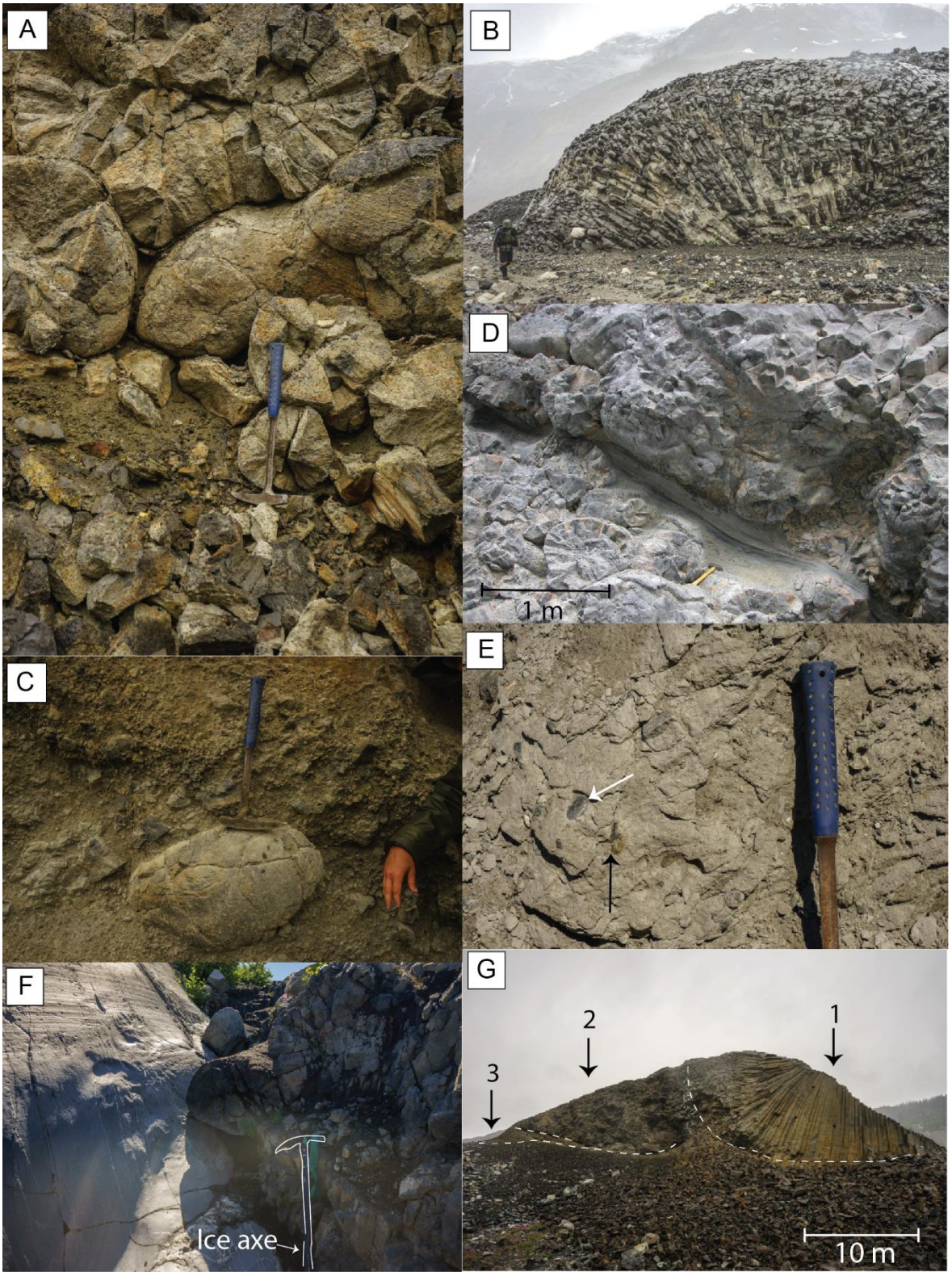

Fig. 8.1. Field photographs showing the Lillooet Glacier volcano lithofacies. (A) Densely packed pillow lava (unit LpBp) exposed near the terminus of Lillooet Glacier. (B) Large, radially jointed lobe of lava (unit LpBl) (person for scale) terminating in abrupt, pervasively jointed toe. (C) Pillow lava clast in a clast-supported, poorly sorted hyaloclastite breccia (unit LpBh). (D) Bedded, well sorted, discontinuous lens of hyaloclastite separating pillow lava accumulations in the northern map area. Photograph courtesy of Dr. John Clague. (E) Massive, sheared diamicton (unit bt) with rounded clasts of basalt (white arrow) and metamorphic clasts (black arrow) set in a matrix of fine silt. (F) Pillow lava (LpBp) overlying smooth, glacially scoured bedrock. (G) Radially jointed basaltic lava tube (1) (unit LpBl) feeding adjacent pillow lava (2). Here the coherent rocks overlie a thin lens of bedded hyaloclastite (3).

northern map area, the Lillooet Glacier phase rocks are unconformably overlain by a southward thickening lens of sheared diamicton (basal till; Fig. 8.1E). This basal till is unconformably overlain by poorly sorted, crudely bedded glacial moraine till which is ~50 m thick and comprises cobbles and boulders of variable lithology. A radiocarbon age on wood fragments from the base of the moraine till deposit yielded an age of 1302 ± 67 BP (Reyes and Clague 2004), providing a minimum age for the Lillooet Glacier phase volcanism. A sample of holocrystalline basalt from the Lillooet glacier phase rocks (unit LpBl) was analysed using $^{40}Ar/^{39}Ar$ geochronology at the University of Fairbanks, Alaska. The sample had a low radiogenic Ar component and was "too young to record an age" (i.e., the plateau and isochron ages approximate a zero-age) (Table 1.1). Given these geochronological data and the well-preserved nature of the deposit, Wilson and Russell (2017) suggest that volcanism at Lillooet Glacier probably took place syn- to post-peak MIS 2 (Fraser) glaciation (i.e., at ~17 to 13 ka).

Petrographically, the volcanic rocks at Lillooet Glacier are alkaline basalt and contain phenocrysts of olivine and plagioclase (Fig. 8.2A; Table 8.1). They have a groundmass of olivine, plagioclase, glass and minor Ti-augite. Chemically, the Lillooet Glacier volcanic rocks are basalt to basaltic andesite and, as a group, represent the highest-silica, mafic alkaline products in the GVB (Fig. 8.4A) (Mullen and Weis 2013, 2015; Wilson and Russell 2017). As observed in other (alkaline) basalts from the northern GVB, they lack the Nb-Ta depletion signature typically associated with subduction-related products (Fig. 8.4B).

The lithofacies and physiographic setting of the deposits at Lillooet Glacier indicate a glaciovolcanic origin. Pillow lava is the dominant lithofacies, requiring a subaqueous eruption environment (i.e., an englacial lake). Pillow lava forms a ~150 m-thick pile in the northern map area (Fig. 8.3). The thickness of this pillow pile indicates that the water body was at least 150 m deep. The pillow pile has no discernable breaks (i.e., passage zones; Jones 1968; Russell et al. 2014), suggesting that the eruption had no significant hiatus and that the body of water was sustained through the duration of the eruption. The physiographic setting of the deposit (i.e., an open, well-drained valley) precludes the possibility that a non-glacier-related body of water existed in the area at the time of the eruption. Thick glacial ice is the only plausible mechanism for damming and maintaining a water body of this depth (Wilson and Russell 2017). Using hydrostatic pressure balance calculations, Wilson and Russell (2017) estimate that the overlying ice was at least 645 m thick, and thus, the Lillooet Glacier deposits record the paleo presence of the last (Fraser) glaciation CIS during MIS 2, with a minimum ice surface elevation of ~1895 m asl.

Volcanic phase	Map unit	Map unit code	Texture	Groundmass	Components
Lillooet Glacier (L) phase	Porphyritic basaltic pillow lava	LpBp1-4	Porphyritic, holocrystalline	Plagioclase (~30 %; 0.01–0.1 mm), Ti-augite (~15 %; 0.01–0.1 mm) and equant Fe-Ti oxides (~10 %; 0.01 mm).	Phenocrysts: Plagioclase (~30 %; 1-3 mm), olivine (~10 %; 0.1–1 mm) ± augite (~1 %).
	Porphyritic basaltic lava	LpBl			
	Bedded basaltic hyaloclastite	LmBh			

Table 8.1 Petrographic characteristics of volcanic rocks at Lillooet Glacier volcano

8.1. Basement geology

Undivided basement rocks (ub)

The basement rocks in the area comprise foliated, metavolcanic, and metasedimentary slate and greenschist of the Gambier group. These rocks are variably intruded by Coastal

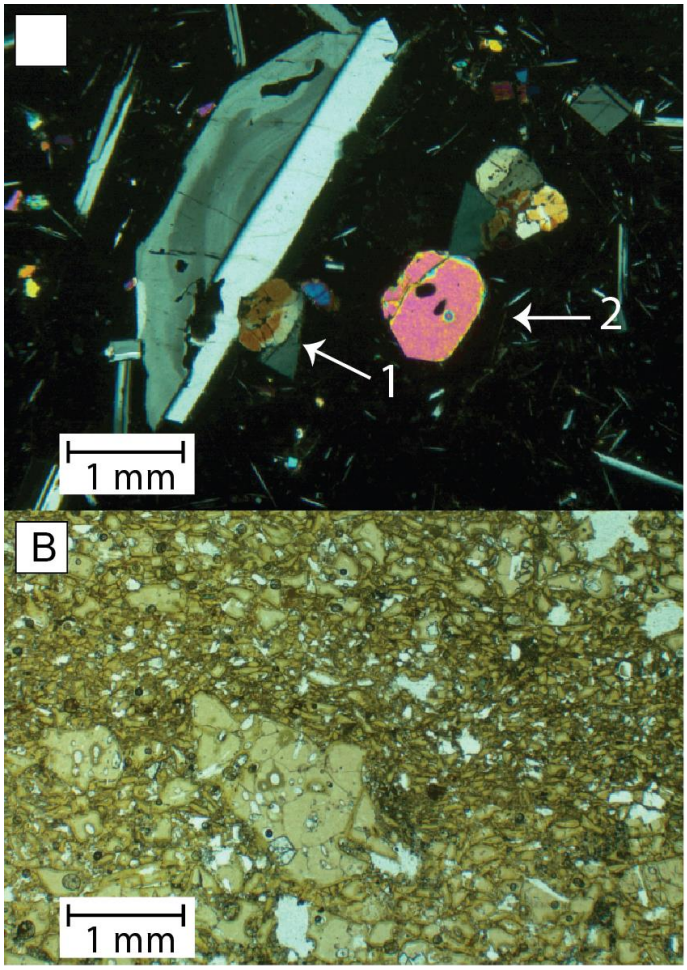

Fig 8.2. Photomicrographs of Lillooet Glacier volcano lithofacies. (A) Glassy, porphyritic pillow lava with small, subhedral augite (arrow 1) ~1mm diameter olivine phenocryst (arrow 2). (B) Well sorted, palagonitised, resedimented, bedded hyaloclastite.

Plutonic complex (Cretaceous) granite and granodiorite (Lynch 1992; Monger and Journeay 1994). The predominant foliation is northeast to southwest, parallel to the direction of the Lillooet River valley. The basement rocks form an irregular, glacially striated topography around the foreground of the Lillooet glacier.

8.2. Lillooet Glacier volcano

8.2.1. Lillooet Glacier (L) phase (Glaciovolcanic)

Porphyritic basaltic pillow lava (LpBp$_{1-4}$)

Pillow lava is the most abundant volcanic lithofacies in the map area (Figs. 8.1A and 8.3). We divide these deposits into four subunits (approximating relative stratigraphic age; 1–oldest and 4–youngest), based on the physical lithofacies distribution and outcrop morphologies. Exposures of porphyritic pillow lava comprise 0.3 to ~1.5 m-diameter pillows that are densely packed. Intra-pillow voids are filled with moderately sorted vitric ash and lapilli. The pillow lavas have 1.5 cm-thick, well-developed glassy rims and have radial fractures. Vesicularity ranges from ~10 to 30 %. Pillow lava subunit LpBp$_1$ comprises an elongate, 1.8 km-long, ~150 m-thick, subvertical pile cropping out along the northern wall of Lillooet River valley (Fig. 8.3). The LpBp$_1$ pillows form a continuous sequence with no mappable stratigraphic horizons. Subunit LpBp$_2$ forms a low elevation, ~20 m-thick sheet infilling the paleo-bedrock topography near the terminus of Lillooet glacier (Fig. 8.1F). The LpBp$_2$ pillow lavas are locally, conformably overlain by 1 to 5 m-thick discontinuous lenses of basaltic hyaloclastite (unit LmBh). Lithofacies subunits LpBp$_3$ and LpBp$_4$ are distributed in 10 to 20 m-thick sheets in the southern map area. The lavas are arranged in two partially overlapping, northwest to southeast striking benches with southwestern margins that terminate in 10 to 15 m-high bluffs. Pillow lava requires a subaqueous deposition environment. Given the physiography of the deposit (i.e., located in a steep-walled glacial valley), the ubiquitous presence of pillow lava at Lillooet Glacier provides strong evidence for a glaciovolcanic eruption. The 150 m-thick, continuous pile of pillows in the northern map area indicates that the body of water (i.e., englacial lake) surrounding these deposits was at least 150 m deep and was sustained throughout the eruption. The arrangement of subunits LpBp$_3$ and LpBp$_4$ as overlapping benches, suggests that the pillow lavas were physically impounded along their southwestern margin during emplacement. We interpret that these lavas propagated downhill as sheets of pillows, confined along their southwestern side by glacial ice.

Porphyritic basaltic lava (LpBl)

Columnar jointed basaltic lava lobes and tubes form a branching network that feeds pillow lava accumulations throughout the map area. The lobes and tubes elongate in the local downhill direction and are typically equidimensional in cross-section. All lobes and tubes display intense radial columnar jointing. In the central part of the map area, the lobes are up to 5 m thick and stratigraphically overly LpBp$_2$ pillow lavas and bedded basaltic hyaloclastite (Fig. 8.1G). Elongate lava tubes are up to 15 m wide and terminate in abrupt, radially jointed toes (Fig. 8.1B). The basaltic lavas are micro-vesicular (<0.1 mm-diameter vesicles) and have a medium to fine-grained groundmass (Table 8.1). A sample of holocrystalline basaltic lava was analysed using $^{40}Ar/^{39}Ar$ geochronology at the University of Fairbanks, Alaska. The sample had a low radiogenic Ar component and was “too young to record an age” (i.e., the plateau and isochron ages approximate a zero-age) (Table 1.1). This result provides an estimate for the timing of volcanism at Lillooet Glacier and indicates that the eruption probably occurred during the last, MIS 2 (Fraser) glaciation (Wilson and Russell 2017). We interpret these lavas to be feeder structures of the pillow and hyaloclastite accumulations in the map area. The radially jointed lava toes probably result from emplacement into subaqueous drainage pathways and local impoundment and cooling against glacial ice.

Massive basaltic hyaloclastite (LmBh)

Volcaniclastic rocks form a volumetrically minor (~5 %) portion of the Lillooet Glacier deposit. The rocks comprise poorly sorted, massive pillow breccia (e.g., Fig 8.1C) and massive to bedded, well-sorted hyaloclastite (Fig. 8.1D). The finer-grained layers contain angular, blocky vitric clasts that are

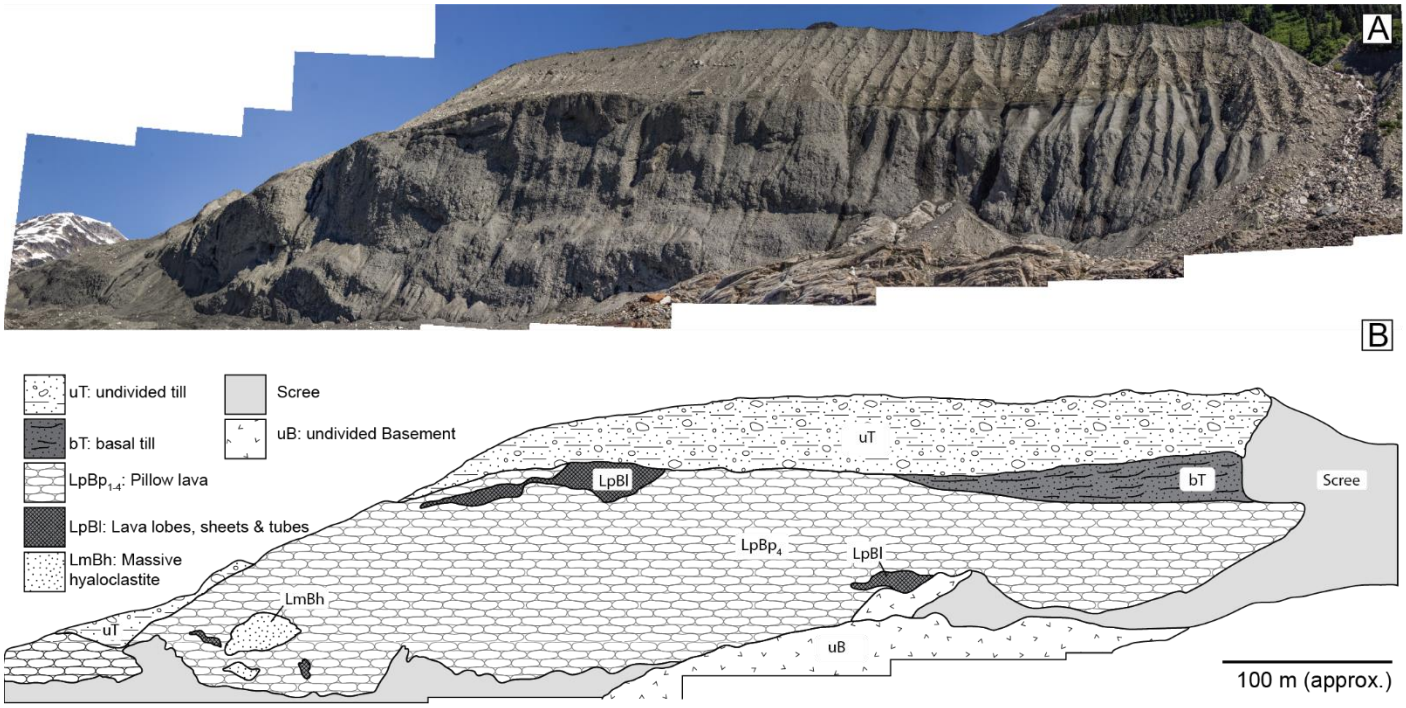

Fig. 8.3. Field photographs and sketch of northern pillow pile at Lillooet Glacier. (A) Panoramic photograph looking north, showing stacked pillow lavas. The light grey material at the top of the image is undifferentiated glacial till (ut). (B) Line diagram reproduction of the panorama showing contact relationships between various lithofacies.

poorly vesicular and densely packed (Fig. 8.2B). These clasts are typically surrounded by thin (<0.1 mm-diameter) rims of dark orange palagonite (Fig. 8.2B). The deposits contain rare, subrounded to rounded accidental metamorphic and plutonic lithic clasts (up to 10 cm diameter). Near the toe of Lillooet Glacier, basaltic hyaloclastite forms poorly sorted, clast supported, <2 m-thick lenses that separate pillow lavas (unit $LpBp_2$), lava lobes and tubes (unit LpBl) and pillow lava unit $LpBp_3$. In other areas, finely bedded, well-sorted hyaloclastite forms thin (<0.5 m-thick) lenses within the pillow lava accumulations (Fig. 8.1D). Blocky, vitric ash, and lapilli clasts probably result from quench fragmentation and spalling of glass from pillow margins during emplacement. Stratification and deposit bedding indicate syn-eruptive transportation and deposit reworking. We interpret that these rocks were deposited by subglacial meltwater that was actively draining from the eruption site. Rare, accidental plutonic, and metamorphic lithic clasts probably originated as glacial cargo melted from the overlying ice during the eruption.

8.3. Glacial sediments

Basal till (bt)

Massive, pervasively sheared, dark grey diamicton (basal till) forms a ~10 to 30 m-thick, southward thickening lens unconformably overlying Lillooet Glacier phase pillow lava (unit $LpBp_1$) in the northern map area. The contact between the volcanic rocks and these glacial deposits is smooth and subhorizontal (Fig. 8.3). The deposit is well sorted and contains clasts of basaltic volcanic, metamorphic and plutonic rocks. The matrix consists of fresh, silt-sized, sub-rounded, vesicular volcanic glass and rounded metamorphic and plutonic fragments and liberated crystals. Reyes and Clague (2004) interpret this unit as basal till, deposited during a phase of late Fraser, CIS expansion.

Undivided till (ut)

Poorly sorted, crudely bedded, clast supported, unconsolidated cobbles and boulders form a ~50 m-thick), sharply crested lateral moraine along the northern side of Lillooet River valley (Fig. 8.3) and a subdued, forested lateral moraine on the southern side of the valley. Clasts comprise rounded, heavily striated basaltic volcanic, plutonic and metamorphic rocks. The unit also contains several organic detritus and woody layers. Reyes and Clague (2004) report a radiocarbon age of 3034 ± 42 ^{14}C years BP from a wood fragment embedded near the base of the deposit. This age provides a minimum age for Lillooet Glacier phase volcanism. These rocks are interpreted to be moraine till emplaced during Holocene Lillooet Glacier advance and retreat fluctuations (Menounos et al. 2009).

Undivided alluvium (ua)

Undivided alluvial deposits comprising lacustrine and alluvial sediments form a wide delta at the northern side of Silt Lake. The deposits comprise poorly sorted, unconsolidated rounded basaltic volcanic and glacial detritus that is supported by fine glacial silt.

8.4. Summary

Lillooet Glacier volcano is a small accumulation of basaltic pillow lava, lava lobes and tubes and bedded hyaloclastite

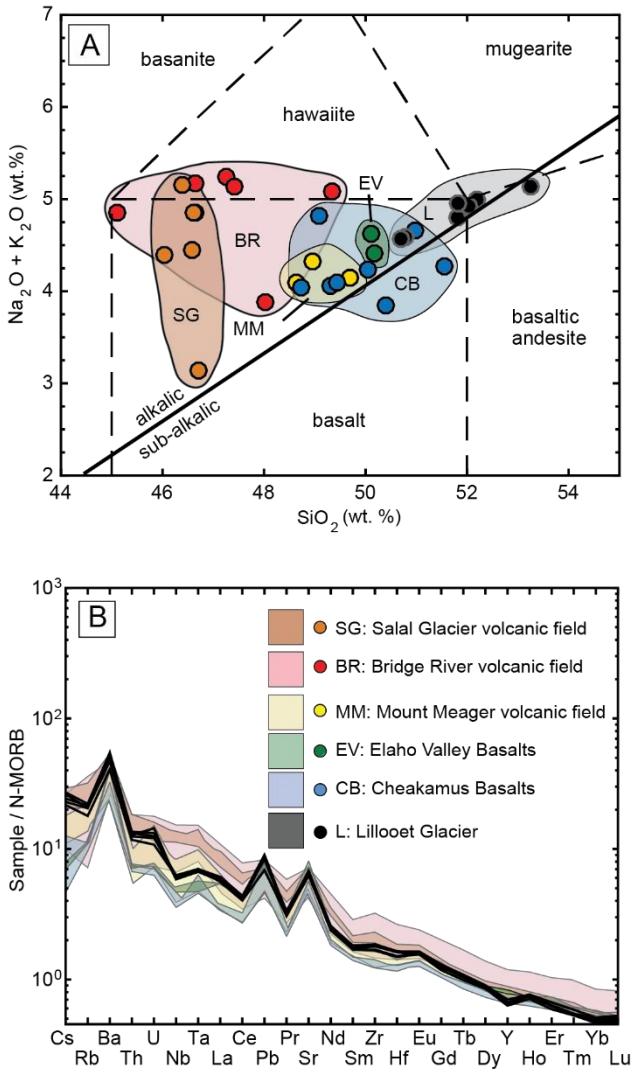

Fig. 8.4. Geochemical characteristics of the Lillooet Glacier volcano rocks. (A) Total alkalis vs. silica diagram (after Le Bas et al. 1986) showing whole rock (closed black circles) analyses for the Lillooet Glacier basalts (modified from Wilson and Russell 2017). Additional analyses of Garibaldi volcanic belt basalts (from Mullen and Weis 2015) are shown for comparison, including; the Bridge River volcanic field (BR), The Salal Glacier volcanic field (SG), the Mount Meager Mosaic Assemblage (MMA), the Elaho Valley Basalts (EV) and the Cheakamus Basalts (CB). Lillooet Glacier volcanic rocks are basalt and basaltic andesite. (B) Trace element compositions showing very little variation within the suite and lack distinctive Nb-Ta subduction-related signatures. N-MORB normalization values are from Sun and McDonough (1989).

located at the terminus of Lillooet Glacier. The edifice erupted in a single phase of glaciovolcanic activity during the Late Pleistocene, probably syn- to post-peak MIS 2 (Fraser) glaciation (i.e., 17 to 13 ka).

The Lillooet Glacier eruption began with effusive activity in the northern map area, where a large pile of basaltic pillow lava was emplaced. These lavas melted a hole in the overlying ice and formed an englacial lake that was at least 150 m deep. Continued eruptions fed lava downslope, where it burrowed beneath the ice, accumulating as thin, benches of pillow lava and lava lobes and tubes. The irregular bedrock topography controlled the distribution of the subglacial lava propagation and corresponding deposit distribution. Spalling and quench fragmentation of glassy, pillow lava margins produced glassy volcaniclastic material, which was mobilised by draining meltwater and deposited as thin, lenses mantling the pillow lava sheets. Following the eruption, the re-advance of Lillooet Glacier eroded the upper surface of the northern pillow pile and deposited a southward thickening lens of sheared, dark grey diamicton (basal till). These deposits were eroded and overlain by successive lateral moraine rocks emplaced during fluctuating Holocene of the Lillooet Glacier to its current extent.

The presence and size of the last MIS 2 (Fraser) CIS in the Lillooet Glacier area can be inferred from the distribution of the glaciovolcanic rocks which provide evidence of an ephemeral englacial lake that existed during the eruption, with a minimum depth of 150 m. The glaciovolcanic rocks at Lillooet Glacier span an elevation range of 580 m (from 820 m to 1400 m above sea level). In order to prevent the draining of the englacial lake through ice lifting events (i.e., jökulhlaups), Wilson and Russell (2017) estimate that the ice covering the area at the time of the eruption must have been at least 645 m thick. The Lillooet Glacier volcano therefore preserves the traces of the last MIS 2 (Fraser) glaciation CIS, with a minimum ice surface elevation of approximately 1895 m asl.

9. The Salal Glacier volcanic field (1:10,000)

The Salal Glacier volcanic field is a collection of six Quaternary volcanoes located in the northern GVB (Fig. 1.1). Five of the volcanoes are alkaline basalt (Lawrence et al., 1984; Mullen and Weis, 2013) and one is calc-alkaline andesite (Salal Mountain phase) (Wilson and Russell 2018) (Fig. 9.1, Table 9.1). The Salal Glacier volcanic field occupies high alpine, rugged Coastal Mountain terrain. The area is currently glaciated with numerous permanent accumulations of snow and ice. Most of the map area is situated at more than 2000 m asl where the vegetation is limited and the ground is covered by felsenmeer, glacial debris, and patchy accumulations of 2360 BP Bridge River tephra (Lawrence et al. 1984; Hickson et al. 1999). The Quaternary volcanic rocks are distributed along ridges and other topographic high points. The volcanic rocks unconformably overlie Salal Pluton quartz monzonite (Late Miocene), one of the youngest plutons in the Coastal plutonic complex (8.0 ± 0.1 Ma) (Roddick and Woodsworth 1975). Although the Salal Glacier map area has been the focus of several studies investigating molybdenum mineral potential (Mustard and Campbell 1971; Lawrence et al. 1984), the Quaternary volcanic rocks have received little attention. A map produced by Lawrence et al. (1984), focused on the petrographic and geochemical character of the rocks and provided two K-Ar ages indicating Pleistocene activity. Subsequently, Salal alkaline basaltic rocks have been included in several regional geochemical studies of the northern GVB (Mullen and Weis 2015; Venugopal et al. 2020).

For this map, we divide the volcanic deposits at Salal Glacier into seven phases of volcanic activity: the Salal Center (SC) phase, the Salal Tindar (ST) phase, the Logan Ridge (LR) phase, the Northwest volcanic remnant (N) phase, the Ochre Mountain (O) phase, the Salal Mountain (SM) phase and the Mud Lake (ML) phase. Broadly, the deposits consist of subaqueous pillow

lava, hyaloclastite, tuff breccia, coherent lavas, and subaerial pyroclastic tephra and lavas. All phases of activity (except for the Salal Center and the Mud Lake phases) show evidence for glaciovolcanism (Wilson and Russell 2018). This evidence mostly includes lithofacies that demonstrate a subaqueous eruption origin (e.g., pillow lava) that are situated in areas that would be incapable of maintaining a standing body of water (i.e., a lake) without the presence of thick glacial ice. Many of the Salal Glacier volcanic field deposits are situated in areas of steep topography and thus they record the paleo-presence of several (now absent) Pleistocene englacial lakes and large ice masses.

Near the center of the volcanic field, the Salal Center (SC) phase rocks comprise an eroded, coarsely jointed hawaiite lava that is unconformably overlain by younger alkaline basalt of the Salal Tindar (ST) phase (Fig. 9.2A). A K-Ar determination from these rocks yielded an age of 970 ± 50 ka, indicating an Early Pleistocene eruption (Lawrence et al. 1984). The Salal Mountain (SM) phase deposits are the only volcanic rocks in the map area that comprise calc-alkaline andesite instead of alkaline basalt (Fig. 9.1). A sample (AW-16-253) of coherent lava from Salal Mountain was analysed at the WiscAr Laboratory, University of Wisconsin-Madison using $^{40}Ar/^{39}Ar$ geochronology. The results indicate an eruption at 831.5 ± 11.43 ka (Fig. 9.3 and Table 1.1). Salal Mountain is located at the southwestern edge of the map area. The southern side of the deposit is well exposed and shows a ~200 m-thick accumulation of coherent lava (Fig. 9.2B) and unconsolidated hyaloclastite (Fig. 9.2C and Fig. 9.2D) that overlies a ~100 m-thick accumulation of glacial basal till. Lava jointing textures and accumulations of poorly consolidated, poorly sorted, glassy andesite hyaloclastite breccia with intrusive pods of coherent andesite suggest rapid quenching and a glaciovolcanic origin. A lack of clast sorting and deposit reworking suggests a dry, well-drained subglacial environment. The Salal Mountain phase rocks record the Early Pleistocene presence of a CIS with a surface elevation of at least 2370 m asl.

The alkaline basalt Salal Tindar phase rocks unconformably overlie Salal Center phase hawaiite in the central map area where they form an elongate, ~65 m-thick accumulation of palagonitised tuff breccia, scoria, and coherent lava (Fig. 9.4). The deposits preserve evidence for a pyroclastic passage zone (i.e., the transition from subaqueous to subaerial deposition environment) at ~2360 m asl (Fig. 9.4A). The passage zone is characterised by underlying palagonitised tuff breccia changing into a ~25 m-thick sequence of unconsolidated, oxidised scoria and lava (Fig. 9.4B). The lavas situated near the southern edge of the deposit are over thickened and shows slender radial and hackly jointing, suggesting physical ice impoundment (Fig. 9.4C). These rocks yielded a K-Ar age of 590 ± 50 ka (Lawrence et al. 1984). We interpret the Salal Tindar phase deposits to be glaciovolcanic, recording the Middle Pleistocene paleo-presence of an englacial lake and surrounding glacier with a surface elevation of at least 2360 m asl.

The Ochre Mountain phase deposits form a <15 m-thick, elongate ridge that trends northeast to southwest along the wall of Athenley Pass valley. The rocks comprise radial columnar jointed alkaline basalt lava, pillow lava, and hyaloclastite (Fig. 9.5A and Table 9.1). The Ochre Mountain phase deposits unconformably overlie patchy accumulations of glacial basal till

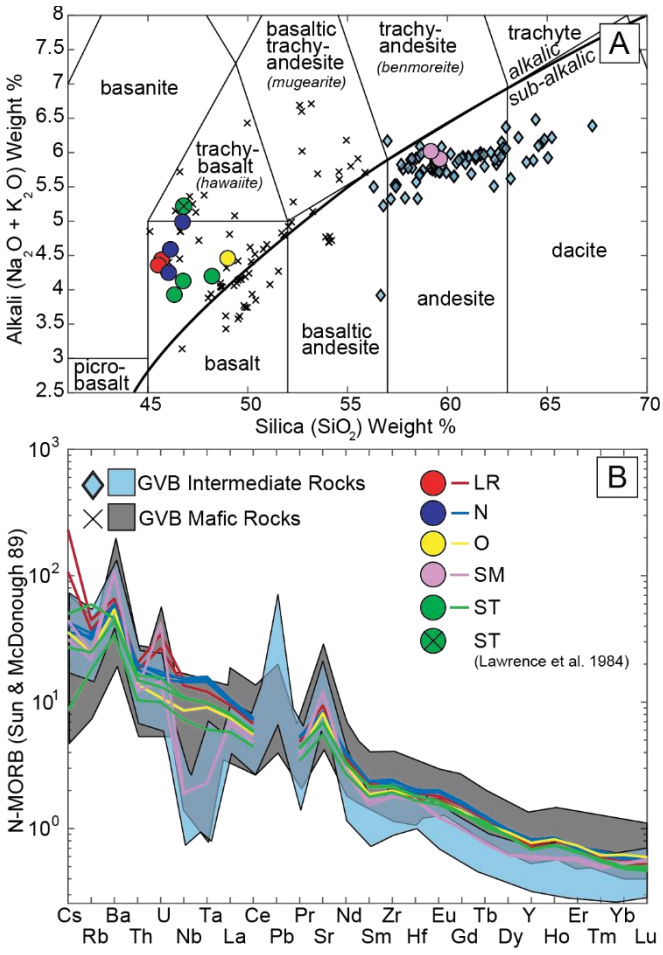

Fig. 9.1. Geochemical characteristics of the Salal Glacier volcanic field lithofacies. (A) Total alkalis vs. silica diagram after Le Bas et al., (1986), showing alkaline basaltic affinity of the Salal Center (SC), Salal Tindar (ST), Ocher Mountain (O), Logan Ridge (LR) and Northwest volcanic remnant (N) phase deposits (circles). The Salal Mountain (SM) phase deposit comprises calc-alkaline andesite. Additional analyses of GVB basalts are from Mullen and Weis (2015) and Wilson and Russell (2017). Additional analyses of GVB intermediate rocks are from Bye et al. (2000); Fillmore and Coulson (2013); Wilson et al. (2016) and other field localities within this study (e.g., the Table, Brohm Ridge area and Monmouth Creek volcano). (B) Trace element compositions of the Salal Glacier volcanic field rocks normalised to N-MORB (Sun and McDonough 1989).

(unit bt) (Fig. 9.5B). A sample (AW-16-259) of coherent lava from Ochre Mountain was analysed at the WiscAr Laboratory, University of Wisconsin-Madison using $^{40}Ar/^{39}Ar$ geochronology. The results indicate eruption during the Middle Pleistocene at 408.7 ± 6.7 ka (Fig. 9.6 and Table 1.1). This age, combined with indicators for glaciovolcanism in the Ochre Mountain phase lithofacies, provides a record of the Middle Pleistocene glacial ice occupation in Athenley Pass. The ice had a minimum surface elevation of 2140 m asl, corresponding with the upper elevation of glaciovolcanic lithofacies.

Logan Ridge is a ~70 m-thick pile of dike-fed basaltic pillow lava, pillow breccia, bedded palagonitised tuff, lapilli tuff, and radially jointed basaltic lava lobes (Fig. 9.5C–G). The deposit is in the northern map area. All Logan Ridge phase lithofacies comprise porphyritic alkaline basalt (Fig. 9.1). The lower portion

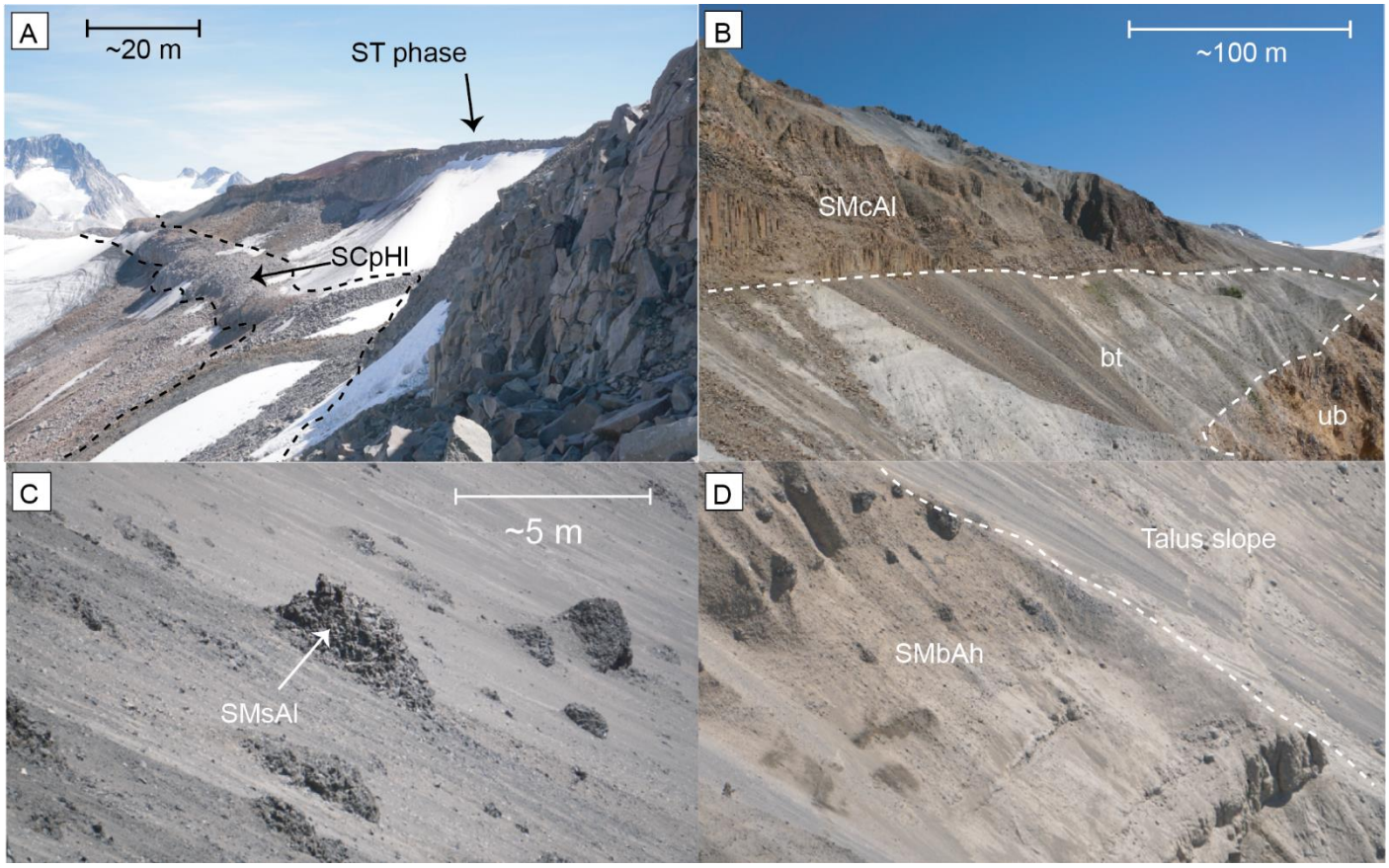

Fig. 9.2. Field photographs showing Salal Center and Salal Mountain phase lithofacies. (A) Image looking southeast showing contact between porphyritic hawaiite lava (unit SCpHl) and overlying Salal Tinder phase rocks. (B) Image looking northeast at the basal sequence at Salal Mountain where coarsely jointed andesite lavas (unit SMcAl) overlie glacial basal till (unit bt). (C) Image looking east at coherent lobes of slender jointed andesite lava (unit SMsAl) surrounded by loose, unconsolidated co-genetic andesite hyaloclastite breccia (unit (SMbAh). (D) Image looking east at accumulation of bedded andesite hyaloclastite breccia (unit SMbAh) in the upper portion of Salal Mountain.

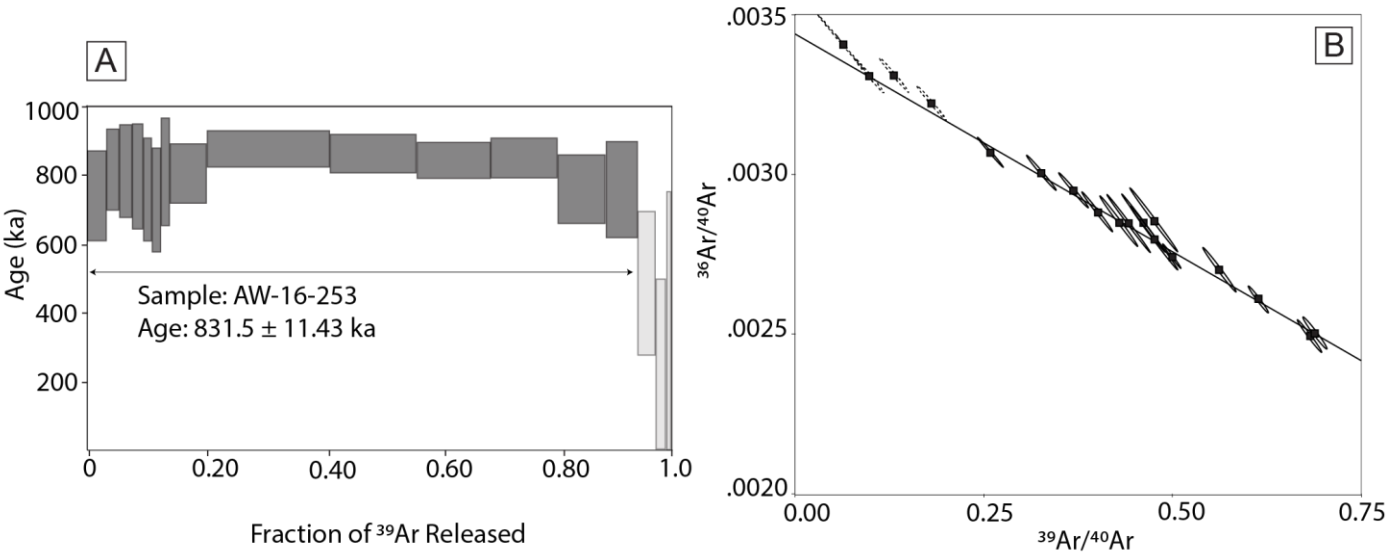

Fig. 9.3. Summary of $^{40}Ar/^{39}Ar$ geochronology results from the Salal Glacier sample AW-16-253 (unit SMcAl). (A) Plateau diagram showing fraction of ^{39}Ar versus age. 14 out of 18 fractions released 94.38 % ^{39}Ar, and the mean squared weighted deviation is equal to 3.09. The sample shows a plateau at 831.5 ka with a calculated 1 uncertainty of 11.4 ka. (B) Inverse isochron plot showing 18 heating steps. Ellipses denote 1 analytical uncertainty.

of the Logan Ridge deposit comprises radially jointed lava lobes and pillow lava. These rocks are overlain by irregular accumulations of hyaloclastite, pillow breccia, and densely packed pillow lava. At the top of the deposit, there is an 8 m-thick, well-bedded pyroclastic surge deposit (bedded palagonitised tuff). The age of volcanism at Logan Ridge is unknown. A sample of basalt from the base of the sequence was sent to the WiscAr Laboratory at the University of Wisconsin-Madison for $^{40}Ar/^{39}Ar$ analysis, however the sample was highly vesicular and contained a large atmospheric gas component, resulting in an inconclusive analysis (Table 1.1). Although Lawrence et al (1984) reported that the lower and upper parts of Logan Ridge were magnetically normal and reversed, respectively (suggesting a minimum age of 0.9 Ma), we observed no physical, chemical, or petrographic discontinuities within the eruption sequence. This suggests that volcanism occurred over a single eruptive cycle, challenging the magnetic polarity measurements made by Lawrence et al (1984). The lithofacies at Logan Ridge are demonstrably glaciovolcanic. Situated on the steep valley wall, the rocks record the paleo-presence of a glacier with a surface elevation of at least 2340 m asl.

The Northwest volcanic remnant (N) phase rocks form a ~1 km-wide and ~1 km-long mound of porphyritic alkaline basalt and hawaiite situated high on an alpine ridge in the northwestern map area. The lithofacies comprise a <100 m-thick, lower unit of dike-fed, massive to weakly bedded, block jointed and palagonitised tuff breccia that is overlain by several thin layers of pillow lava and well-bedded palagonitised tuff (Fig. 9.7A–D). The juvenile tephra clasts at the Northwest volcanic remnant are highly vesicular, glassy, and irregularly shaped. The glassy clasts and matrix show pervasive palagonitisation, giving the units a dull orange colour. Geochemically, the Northwest volcanic remnant phase rocks are alkaline basalt, however, one sample from the upper pillow-lava sequence is hawaiite (Fig. 9.1). Like the Logan Ridge phase rocks, we mapped no discernible breaks or hiatuses within the eruption sequence, suggesting a single eruption event. Situated on the steep valley wall, the rocks record the paleo-presence of a thick ice sheet with a surface elevation of at least 2430 m asl. A sample of lava from a dike at the Northwest volcanic remnant was sent to the WiscAr Laboratory at the University of Wisconsin-Madison for $^{40}Ar/^{39}Ar$ analysis. The sample was vesicular and contained a large atmospheric gas component, resulting in an inconclusive analysis (Table 1.1). Future geochronology studies may provide insight into the age of eruption and the temporal implications of this glaciovolcanic interaction.

Finally, the Mud Lake (ML) phase rocks are the only rocks in the Salal Glacier volcanic field that do not show clear evidence for glaciovolcanism. The rocks consist of a small, isolated basaltic lava that is <30 m-diameter and ~10 m-thick (Fig. 9.7E). The flow overlies a thin basal breccia. The age of the Mud Lake deposit is unknown.

9.1. Basement geology

Undivided basement rocks (ub)

White grey, medium to coarse-grained (2 to 5 mm), Salal Pluton quartz monzonite forms the basement lithology within the map area (Roddick and Woodsworth 1975; Lawrence et al. 1984). Where exposed, the rocks are coarsely jointed and glacially scoured.

9.2. Salal Glacier volcanic field

9.2.1. Salal Center (SC) phase (Non-glaciovolcanic)

Porphyritic hawaiite lava (SCpHl)

Light grey, sparsely vesicular, porphyritic hawaiite lava forms a 10 to 15 m-thick, coarsely columnar jointed lava partially underlying the Salal Tindar phase rocks (Fig. 9.2A). The contact between these lavas and overlying Salal Tindar phase rocks is smooth and glaciated (unconformable). The rocks are porphyritic, medium-grained hawaiite (Fig. 9.1 and Table 9.1). A K-Ar age of 970 ± 50 ka indicates an Early Pleistocene eruption (Lawrence et al. 1984). The lack of evidence for glaciovolcanism may be due to either extensive glacial erosion of the deposits or a subaerial eruption during an ice-free climatic interval.

9.2.2. Salal Mountain (SM) phase (Glaciovolcanic)

Coarsely jointed andesite lava (SMcAl)

Dark grey, sparsely vesicular (<10% vol.) coarsely columnar jointed, porphyritic andesite lava forms a ~100 m-thick pile at the base of Salal Mountain. This map unit comprises at least ten individual lava flows that are distinguished through varying colonnade and entablature joint morphologies. The rocks overlie a thick accumulation of glacial diamicton (unit bt). The contact is sharp and unconformable, and dipping at a shallow angle towards the northeast (Fig. 9.2B). The source of the lavas is exposed as an eroded dike located ~100 m directly south of the deposit. Results of a recent $^{40}Ar/^{39}Ar$ geochronology analysis of these rocks indicate an eruption age of 831.5 ± 11.43 ka (Fig. 9.3A and Table 1.1).

Slender jointed andesite lava (SMsAl)

Dark grey, sparsely vesicular (<10 %), slender and hackly jointed, glassy andesite lava form several coherent lobes and pods at the summit of Salal Mountain. The lava pods are randomly distributed and range in size from ~50 m-diameter, to less than 1 m-diameter. The margins of the pods show gradational (conformable) transitions with poorly consolidated hyaloclastite breccia (Fig. 9.2C). The slender and hackly jointing and glassy texture of these rocks indicate accelerated cooling. We interpret these coherent lavas to be the feeder structures for the accumulations of surrounding hyaloclastite, which formed during an effusive eruption in the presence of glacial ice.

Bedded andesite hyaloclastite (SMbAh)

Dark grey, unconsolidated, monolithologic, poorly sorted, clast supported glassy andesite hyaloclastite forms a ~100 m-thick, crudely bedded accumulation at the top of the Salal Mountain deposit (Fig. 9.2D). The clasts are glassy, angular, conchoidally fractured, and loosely packed. Clast sizes range from <1 cm to >20 cm. The hyaloclastite shows gradational

Volcanic phase	Map unit	Map unit code	Texture	Groundmass	Components
Salal Center (SC) phase	Porphyritic hawaiite lava	SCpHl	Porphyritic, holocrystalline	Dense, with fine plagioclase (~50 %), olivine (~10 %) and Fe-Ti oxide (~10 %)	Phenocrysts: Plagioclase (20%, 0.5 - 1 mm), olivine (20%, 0.2 - 1 mm)
Salal Mountain (SM) phase	Coarsely jointed andesite lava Slender jointed andesite lava Bedded andesite hyaloclastite	SMcAl SMsAl SMbAh	Porphyritic, hypocrystalline	Plagioclase (15 %), orthopyroxene (5 %), Fe-Ti oxide (5 %) and glass (60 %)	Phenocrysts: Plagioclase (10%, 0.1 - 0.5 mm), orthopyroxene (5%, 0.2 mm)
Salal Tinder (ST) phase	Palagonitised basaltic pillow breccia Palagonitised basaltic tuff breccia Porphyritic basaltic lava Massive basaltic tephra Agglutinated basaltic lava	STpgBpx STpgtBtx STpBl STmBt STagBl	Porphyritic, holocrystalline to hypocrystalline	Plagioclase (~50 %), augite (~1 %), olivine (<10 %), glass (~10 %)	Phenocrysts: Olivine (20%, 0.1-3 mm), plagioclase (10%, 0.1-4 mm), augite (~1 %, <1 mm). Megacrysts: rare, < 10% olivine and plagioclase
Ochre Mountain (O) phase	Massive basaltic hyaloclastite Slender columnar jointed basaltic lava	OmBh OsBl	Porphyritic, holocrystalline	Moderately vesicular with plagioclase (30%); Fe-Ti oxides (15%), augite (10%) and olivine (<1%)	Phenocrysts: Olivine (20%, 0.1 - 2 mm), augite (15%, 0.2 - 2 mm), plagioclase (10%, 0.1 - 1 mm)
Logan Ridge (LR) phase	Porphyritic basaltic lava Massive basaltic hyaloclastite Porphyritic basaltic pillow lava Bedded basaltic tuff	LRpBl LRmBh LRpBp LRbBtu	Porphyritic, hypocrystalline	Plagioclase (~10 %), augite (~5 %), olivine (~5 %), and glass (~50 %)	Phenocrysts: Olivine (15%, 0.1-2 mm), plagioclase (10%, 0.1-1 mm), augite (5%, 0.2-2 mm)
Northwest volcanic remnant (N) phase	Coarsely jointed basaltic tuff breccia Massive basaltic tuff breccia Porphyritic basaltic pillow lava Bedded basaltic tuff breccia Porphyritic basaltic dikes	NcBtx NmBtx NpBp NbBtx NpBd	Porphyritic, holocrystalline to hypocrystalline	Plagioclase (10 %), olivine (1 %), Fe-Ti oxides (1 %) and glass (30 %)	Phenocrysts: Plagioclase (30%, 0.2-2 mm), olivine (30%, 0.1-0.5 mm). Megacrysts: rare, plagioclase and augite (~1%, < 1 cm)
Mud Lake (ML) phase	Porphyritic basaltic lava Massive basaltic breccia	MLpBl MLmBbx	Porphyritic, hypocrystalline	Plagioclase (15 %), olivine (10 %), Fe-Ti oxide (5 %) and glass (50 %)	Phenocrysts: Plagioclase (10%, 0.1 - 0.5 mm), olivine (5%, 0.2 mm)

Table 9.1 Petrographic characteristics of volcanic rocks in the Salal Glacier volcanic field

contact relationships with hackly-jointed lava pods, suggesting a common origin. The monolithologic nature of these rocks and their intimate affiliation with the slender jointed glassy andesite lavas (unit SMsAl) suggests that they were produced through hydroclastic fragmentation of the andesite lava (i.e., quenching).

9.2.3. Salal Tindar (ST) phase (Glaciovolcanic)

Palagonitised basaltic pillow breccia (STpgBpx)

Orange-brown, matrix to clast supported, weakly indurated, palagonitised basaltic pillow breccia and dikes form the basal part of the Salal Tindar deposit. The rocks overlie undivided basement rocks (ub) and Salal Center phase hawaiite lava (unit SCpHl) on a smooth, glacially scoured, unconformable surface. The palagonitised basaltic pillow breccia is up to 30 m thick and includes several lithofacies variations, including clast-supported pillow breccia, basaltic dikes (<0.5 m-diameter) with irregular, pillowed (i.e., undulating) margins, partially intact vesicular pillows, and fine, matrix-supported, bedded vitric tephra (Fig. 9.4D). Angular, accessory quartz monzonite lithics (1 to 20 cm-diameter) make up ~10 % of the deposit. Moderate palagonitisation of finer clasts gives the rocks a deep brown-orange colour. Palagonitisation of the vitric clasts and pillow lava fragments indicate that the deposits were water-saturated during the eruption.

Palagonitised basaltic tuff breccia (STpgBtx)

Yellow-orange, matrix-supported, basaltic tuff breccia forms a ~40 m-thick sequence conformably overlying palagonitised basaltic pillow breccia (unit STpgBpx) and unconformably overlying Salal Centre phase rocks. The rocks cover an elevation range of ~2320 to 2360 m. The tuff breccia comprises vesicular (~60 %), irregular, glassy, porphyritic, palagonitised basalt clasts (0.5 to 20 cm-diameter). The matrix comprises light-yellow, indurated, palagonitised ash. In several places, the rocks contain up to 20 % accessory lithic clasts of angular, quartz monzonite (unit ub) (1 to 30 cm-diameter) (Fig. 9.4E). The unit is coarsely block jointed (1 to 3 m-diameter) and is crudely, normal, and reverse graded. The large ash component and presence of angular accessory basement lithics indicate an explosive eruption with significant wall-rock quarrying. Pervasive matrix palagonitisation suggests subaqueous deposition, consistent with eruption into an englacial lake.

Porphyritic basaltic lava (STpBl)

Dark grey, sparsely vesicular, porphyritic, columnar jointed basaltic lava forms a ~10 to 20 m-wide, ~1 km-long central ridge and several large lobes along the southeastern and southwestern margins of Salal Tindar. Near the summit of the edifice, the lavas crosscut underlying palagonitised tuff breccia and are overlain by massive basaltic tephra (unit STmBt). Further south, these lavas form a thick flow, overlying the palagonitised tuff breccia lithofacies (unit STpgBtx). Columnar joint size and orientation are variable throughout the deposit. Along the top of the ridge, the columnar joint spacing is coarse (~0.5 to 1 m) and the joints are subhorizontal. Along the northern side of the ridge, the joints are slender and have irregular, radial orientations (Fig. 9.4F). On the southern side of Salal Tindar, a ~10 m-thick lava flow extends from the summit of the edifice to the southern margin, where it becomes more than 60 m thick (Fig. 9.4C). South-facing subvertical exposures along the southern margin are coated in fine, hackly, and slender jointed glassy lava (Fig. 9.4G). A sample collected from this lava yielded a K-Ar age of 590 ± 50 ka (Lawrence et al. 1984). Given the geochemical and petrographic similarity of these rocks to other Salal Tindar phase lithofacies (Table 9.1), we take this age to be representative of all Salal Tindar phase volcanism. Radially oriented, fine scale, subhorizontal columnar joints suggest formation against a subvertical cooling surface. The thickness of the lava in the southern area (to more than 60 m-thick) is unusual for a basaltic composition, suggesting lava pooling and impoundment against a physical barrier. Taken together, these features are consistent with ice confinement during the eruption.

Massive basaltic tephra (STmBt)

Red, oxidised, poorly sorted, massive, unconsolidated scoria and agglutinated spindle bombs form a broad cone at the summit of Salal Tindar (Figs. 9.4A and 9.4B). These rocks overlie palagonitised tuff breccia (unit STpgBtx) via a contact at ~2360 m asl. The deposit is unconsolidated, and a clear contact is not directly exposed, however, petrographic and geochemical equivalency suggest that these lithofacies are closely related to the other Salal Tindar phase rocks (Table 9.1). The presence of oxidised scoria and spindle bombs indicate a subaerial eruption and deposition environment (Fig. 9.4H). We interpret that this unit overlies the palagonitised tuff breccia (unit STpgBtx) via a pyroclastic passage zone (e.g., Russell et al. 2013). The passage zone was constructed during either: i) emergence of the volcanic pile from an englacial lake with a water surface at ~2360 m asl, or, ii) englacial lake breaching and lake level drainage.

Agglutinated basaltic lava (STagBl)

Dark red–grey, vesicular, porphyritic basalt forms several thin (<5 m-thick), discontinuous layers interspersed within the massive basaltic tephra (unit STmBt) at the summit of Salal Tindar. The lavas are agglutinated and show lensoidal-shaped, fluidal clasts of variable vesicularity and size (Fig. 9.4I). This agglutinated texture suggests clastogenic aggregation, likely formed during a subaerial strombolian basaltic spatter eruption and mobilisation of the deposit (i.e., the aggregated lava started to flow).

9.2.4. Ochre Mountain (O) phase (Glaciovolcanic)

Massive basaltic hyaloclastite (OmBh)

Dark grey to orange-brown, massive to crudely bedded, poorly sorted hyaloclastite breccia containing pillow lava fragments comprises a 1 to 3 m-thick layer underlying coherent Ochre Mountain phase basaltic lava (unit OsBl) (Fig. 9.5A). The matrix comprises ash to lapilli-sized, glass fragments that are palagonitised. The rocks are observed to unconformably overlie patchy accumulations of glacial basal till (unit bt), via an

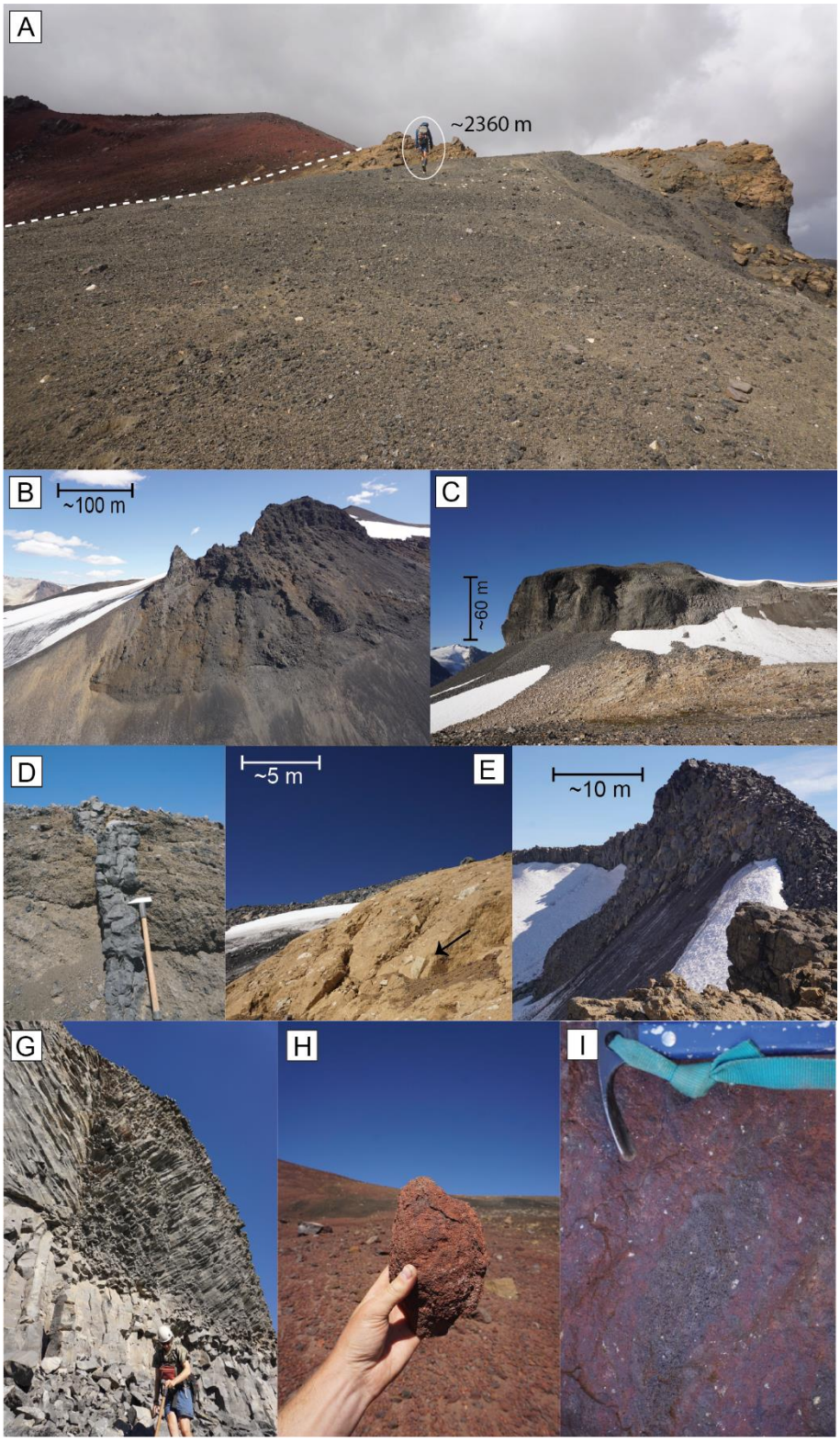

Fig. 9.4. Field photographs showing Salal Tindar phase lithofacies. (A) photograph looking west of passage zone contact (dashed white line) between subaerial and subaqueous pyroclastic volcanic deposits at ~2360 m (person circled for scale). (B) Image looking north showing oxidised tephra cone at the summit of Salal Tindar (unit STmBt). (C) Image looking south at an over thickened porphyritic basaltic lava (unit STpBl) (the "Elephant"). (D) Image looking west showing irregular-margined basaltic dike injected into palagonitised basaltic pillow breccia (unit STpgBpx). (E) Image showing indurated, massive palagonitised basaltic tuff breccia (STpgBtx). A large monzonite accessory clast is indicated with a black arrow. (F) Irregular, radially oriented columnar jointing exposed along the northern side of Salal Tindar (unit STpBl). (G) Image showing hackly fractured porphyritic basaltic lava (unit STpBl) at Salal Tindar. (H) Oxidised spindle bomb collected from near the summit of Sala Tinder (unit STmBt). (I) Agglutinated, clastogenetic lava exposed on the northern upper side of Salal Tindar (unit STagBl).

undulating, irregular lower margin (Fig. 9.5B) and surround lobes of coherent lava. Rounded, striated accessory cobbles originating from the till are common near the base of the unit. We interpret that these rocks were produced by hydroclastic fragmentation of coherent basaltic lava while in contact with ice and/or water.

Slender columnar jointed basaltic lava (OsBl)

Dark grey, moderately vesicular (~30 %), slender columnar jointed, porphyritic basalt forms a 2 to 5 m-thick veneer at ~2140 m elevation along the northern side of Athenley valley. The lavas have irregular, glassy, pillowed (i.e., undulating) margins and form large lobes of basaltic lava that are surrounded by, and overlie, mounds of pillow lava and hyaloclastite breccia (unit OmBh) (Fig. 9.5A). Irregular, slender columnar jointing is fanning and radially oriented. The jointing features and glassy, undulating chill margins along with co-genetic hyaloclastite and pillow lavas indicate a dynamic, subaqueous cooling environment. The location of these deposits (i.e., situated on the steep valley wall above Athenley Pass valley), suggests that they erupted beneath glacial ice. The age of the Ochre Mountain phase event is constrained by a sample of coherent lava that was analysed at the WiscAr Laboratory, University of Wisconsin-Madison using $^{40}Ar/^{39}Ar$ geochronology. The results indicate an eruption during the Middle Pleistocene at 408.7 ± 6.7 ka (Fig. 9.6 and Table 1.1).

9.2.5. Logan Ridge (LR) phase (Glaciovolcanic)

Porphyritic basaltic lava (LRpBl)

Columnar jointed, porphyritic basaltic lava forms several 15 to 20 m-thick lava lobes in the lower part of the Logan Ridge deposit (Fig. 9.5D). The rocks are moderately vesicular and medium-grained (Table 9.1). Columnar jointing is slender and oriented in large-scale fan structures. The smooth, glacially scoured (unconformable) lower contact with underlying plutonic bedrock is exposed in several places on the northern side of the deposit, however, the lower southern contact is obscured by talus. The individual lava lobes are laterally discontinuous and are interspersed within thick accumulations of massive basaltic hyaloclastite (unit LRmBh) pillow lava (unit LRpBp) and bedded basaltic tuff (unit LRbBtu). The rapidly changing columnar jointing orientations (i.e., radial) and close association of the lavas to other Logan Ridge phase lithofacies that are demonstrably subaqueous (e.g., pillow lava and hyaloclastite) suggest that these lavas were also emplaced in a wet environment. Given the location of the Logan Ridge deposit (i.e., situated astride a steep, alpine ridge), we interpret that the rocks erupted beneath glacial ice.

Massive basaltic hyaloclastite (LRmBh)

Dark brown-orange, massive to crudely bedded, poorly sorted hyaloclastite breccia forms several discontinuous layers and lenses surrounding coherent lava pods at Logan Ridge. The rocks have clasts of angular, glassy lapilli (~10 to 50 %), basaltic blocks (~20 %), and a fine matrix of palagonitised ash (~30–70%) (Fig. 9.5E). The hyaloclastite is mostly massive. However, some exposures show minor clast sorting, grading, and subtle, shallow southward dipping beds. We ascribe an autoclastic to hydroclastic origin fragmentation to these rocks and suggest that they derive from gravitational collapse and quench fragmentation of lava lobes in the presence of ice.

Porphyritic basaltic pillow lava (LRpBp)

Dark grey to black, dense to moderately vesicular, porphyritic basaltic pillow lava comprise a ~20 m-thick layer in the central part of Logan Ridge and several ~1 m-diameter pods surrounding coherent lava lobes at the base of the volcanic pile. The pillows are densely packed, 0.3 to 0.5 m-diameter, and have intra-pillow voids that are filled with vitric volcaniclastic sediment (i.e., hyaloclastite) (Fig. 9.5F). Pillow lava is a strong indicator of a subaqueous eruption environment. Given the location of the Logan Ridge deposit (i.e., situated on a steep, alpine ridge), the pillow lava lithofacies provide strong evidence for a glaciovolcanic eruption.

Bedded basaltic tuff (LRbBtu)

Dark brown-orange, well-bedded, matrix-supported basaltic tuff forms an ~8 m-thick layer near the upper part of the Logan Ridge deposit. The beds are ~1–20 cm-thick, are subhorizontal to gently southward dipping, and show subtle normal grading. Bed forms include crossbedding, and drape and sag structures around volcanic bombs. The matrix consists of fine, palagonitised ash and lapilli and sporadic vesicular, juvenile pyroclastic bombs (1 to 20 cm-diameter), and angular, accessory quartz monzonite clasts (Fig. 9.5G). Fine bed laminations and cross bed structures along with the abundance of palagonitised vitric ash are strong indicators for phreatomagmatic fragmentation. The presence of large, angular accessory monzonite lithics indicates significant explosivity and quarrying of the vent wall material. We interpret these rocks as surge-modified fallout, likely emplaced in response to the subaqueous emergence of the volcanic pile from an enclosing englacial lake.

9.2.6. Northwest (N) volcanic remnant phase (Glaciovolcanic)

Coarsely jointed basaltic tuff breccia (NcBtx)

Dark, yellow brown, crudely bedded, matrix-supported, well-sorted, indurated basaltic tuff breccia forms a ~50 m-thick basal unit at the Northwest volcanic remnant. A sharp unconformable lower contact with underlying quartz monzonite (unit ub) is exposed in the southern part of the deposit. These rocks are coarsely jointed into 2 to 5 m-diameter blocks and show crude, shallow westward dipping beds that are defined by subtle clast sorting. Vesicular tephra clasts are typically subrounded and lapilli to block sized. The rocks also contain rare, angular accessory quartz monzonite lithic clasts (<1 %). Pervasive palagonitisation of the vitric matrix gives the unit a deep orange colour and suggests subaqueous deposition and cooling of the deposit (Fig. 9.7A).

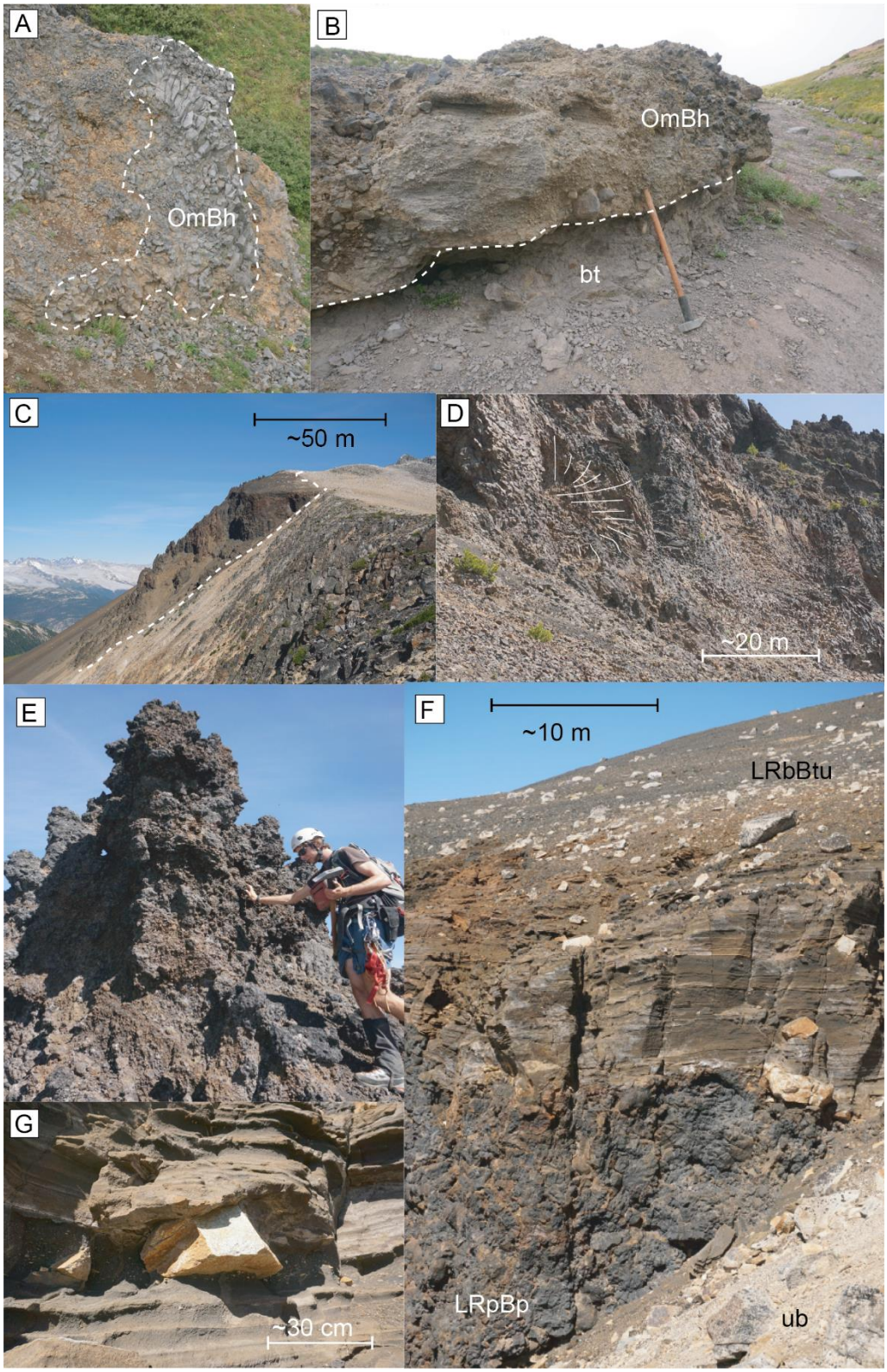

Fig. 9.5. Field photographs showing Ochre Mountain and Logan Ridge phase lithofacies. (A) Image looking north showing Ochre Mountain phase massive basaltic hyaloclastite (unit OmBh) and a large lobe of jointed lava (outlined with dashed line). (B) Photograph showing glacial basal till (unit bt), underlying Ochre Mountain lithofacies. Dashed line shows contact with basal till. C) Image looking northwest showing the Logan Ridge phase deposit situated on the side Salal Glacier valley. (D) Image looking east showing columnar-jointed porphyritic basaltic lava lobes (unit LRpBl) exposed near the base of the Logan Ridge deposit. The orientations of columnar joints are outlined with white lines. (E) Image looking north showing massive basaltic hyaloclastite (unit LRmBh) at the summit of Logan Ridge (person shown for scale). (F) Photograph showing massive, porphyritic basaltic pillow lava underlying bedded tephra on the eastern margin of the Logan Ridge deposit (unit LRpBp). (G) Image showing angular quartz monzonite accessory lithic incorporated into bedded basaltic tuff (unit LRbBtu).

Massive basaltic tuff breccia (NmBtx)

Dark grey to orange, matrix-supported, indurated massive basaltic tuff breccia comprise several 10 to 15 m-thick layers throughout the Northwest volcanic remnant deposit. In the west, the rocks unconformably overlie bedrock and conformably underlie a small accumulation of basaltic pillow lava. In the central deposit area, the rocks form an eastward thinning lens between coarsely jointed basaltic tuff breccia (unit NcBtx) and porphyritic basaltic pillow lava (NpBp) (Fig. 9.7B). The rocks comprise vesicular (up to 60 %), subrounded, glassy porphyritic basaltic lapilli and blocks, many of which are altered to palagonite. The matrix consists of dark orange, indurated, palagonitised ash. Minor clast rounding and pervasive deposit palagonitisation indicate subaqueous reworking and deposition. The physiographic setting of the Northwest volcanic remnant (situated on a steep-sided alpine ridge) indicate that this water was glacial in origin.

Porphyritic basaltic pillow lava (NpBp)

Dark grey, moderately vesicular (~30 %), porphyritic pillow lava forms two accumulations at the Northwest volcanic remnant (Table 9.1). In the northern part of the deposit, pillow lava partially overlies massive basaltic tuff breccia (unit NmBtx). This contact is well exposed and shows an irregular conformable surface with no indication of glacial reworking or erosion (Fig. 9.7C). Near the summit of the Northwest volcanic remnant, a 20 to 30 m-thick layer of dike-fed pillows overlie and partially intrude the massive basaltic tuff breccia (unit NmBtx). The pillow lavas are 0.3 to 0.5 m-diameter and have intra-pillow voids that are filled with fine, glassy hyaloclastite. These pillow lavas, situated along the steep-sided Northwest volcanic remnant ridge, are strong indicators of a subaqueous (glaciovolcanic) eruption environment.

Bedded basaltic tuff breccia (NbBtx)

Dark yellow-orange, massive, matrix-supported, well-bedded tuff breccia forms a ~20 m-thick layer that is draped over the upper part of the Northwest volcanic remnant deposit. The clasts comprise highly vesicular (up to 60 %), irregular, basaltic lapilli and blocks, and rare agglutinated basaltic cauliflower bombs. The deposit comprises ~1 % angular accessory monzonite lithic clasts. The matrix is strongly palagonitised (Fig. 9.7D). Bedding is well developed and arranged in a series of shallow, outward dipping fine laminations with minor crossbedding. Pervasive palagonitisation of the glassy clasts indicates interaction with water during the eruption. Fine, laminated bedding and accessory bedrock lithic clasts indicate high-energy, phreatomagmatic surge deposition in response to an eruption in a subaqueous environment. Like the other deposits in the Salal Glacier volcanic field, the local physiography of the Northwest volcanic remnant indicates that this water was probably sourced and dammed by a glacier.

Porphyritic basaltic dikes (NpBd)

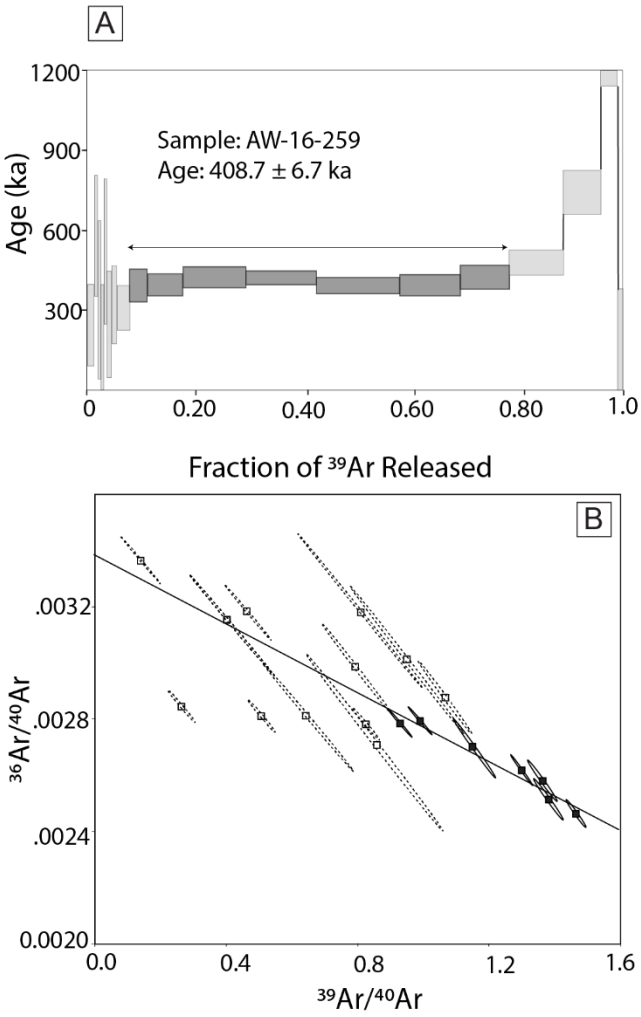

Fig. 9.6. Summary of $^{40}Ar/^{39}Ar$ geochronology results from the Salal Glacier sample AW-16-259 (unit OsBl). (A) Plateau diagram showing fraction of ^{39}Ar versus age. 7 out of 19 fractions released 70.87 % ^{39}Ar, and the mean squared weighted deviation is equal to 11.12. The sample shows a plateau at 408.7 ka with a calculated 1 uncertainty of 6.7 ka. (B) Inverse isochron plot showing 19 heating steps. Ellipses denote 1 analytical uncertainty.

The Northwest volcanic remnant deposit is intruded by at least 10 porphyritic basaltic dikes. The dikes crosscut all volcanic lithologies are up to 200 m-long, typically 0.5 to 1 m thick, and have subvertical orientations. Erosion of the surrounding volcaniclastic lithofacies at the Northwest volcanic remnant has sculptured many of these coherent intrusive bodies into narrow spires and spines. The rocks are moderately vesicular and show irregular, undulating margins that have ~2 cm-thick glassy margins. These margins indicate injection into an unconsolidated, water-saturated sediment.

9.2.7. Mud Lake (ML) phase (Non-glaciovolcanic)

Porphyritic basaltic lava and massive basaltic breccia (MLpBl and MLmBbx)

Dark grey, sparsely vesicular basalt forms an isolated mound at the northeastern edge of Windy Glacier. The rocks comprise a

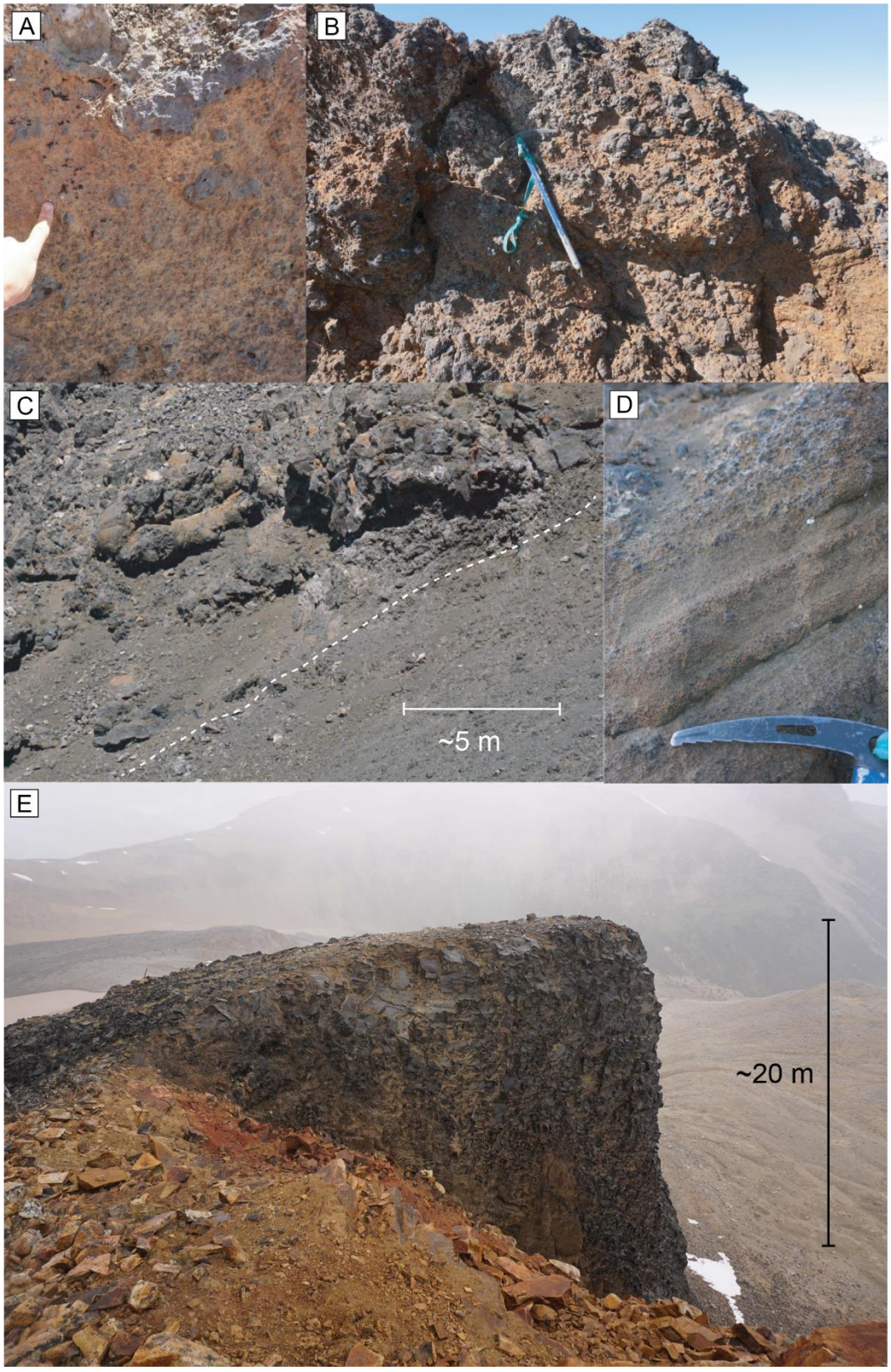

Fig. 9.7. Field photographs showing Northwest volcanic remnant and Mud Lake phase lithofacies. (A) Basaltic tuff breccia near the base of the Northwest volcanic remnant phase deposit (unit NcBtx). (B) Photograph showing palagonitised, indurated massive basaltic tuff breccia exposed in western portion of Northwest volcanic remnant. (C) Image looking northwest showing porphyritic basaltic pillow lava (unit NpBp) overlying coarsely jointed basaltic tuff breccia (unit NcBtx). Contact delineated with a white dashed line. (D) Photograph showing bedded, indurated lapilli tuff and tuff breccia in the upper part of the Northwest volcanic remnant deposit. (E) Photograph looking northeast showing porphyritic basaltic lava and massive basaltic breccia in the lower portion of the Mud Lake phase deposit (units MLpBl and MLmBbx).

coarsely columnar jointed, ~15 m-thick lava that is underlain by a 1 to 3 m-thick, co-genetic unconsolidated basal breccia. Columnar jointing in the lava dips moderately towards the southeast (perpendicular to the underlying basement surface). These rocks show no indication of glaciovolcanic emplacement.

9.3. Glacial sediments

Basal till (bt)

Consolidated, massive, matrix-supported diamicton partially underlies the Salal Mountain and Ochre Mountain phase deposits. The sediments range in thickness from ~30 cm to more than 50 m. The rocks have a fine matrix of grey-brown, silt, and sand and show cobbles and boulder-sized clasts of rounded, striated, vesicular porphyritic basalt, white-grey quartz monzonite, and other plutonic and metamorphic lithologies. At Salal Mountain, the unconformable contact with overlying volcanic rocks (unit SMcAl) is sharp and dips at ~20° towards the northeast. At the Ochre Mountain phase deposit, the glacial sediments are thin and patchy and have no discernible structure or dip. The inclusion of rounded, locally derived porphyritic basaltic clasts suggests that these glacial sediments post-date at least one of the volcanic deposits in the area. Detailed geochemical analysis of the volcanic clasts would be required to fingerprint the volcanic source(s) and determine local glacial history (i.e., minimum age of the deposits and paleo-glacial flow direction).

9.4. Summary

The Salal Glacier volcanic field contains six Quaternary volcanoes that are situated in the northern GVB (Fig. 1.1). Five of the volcanoes are constructed from alkaline basalt and one is constructed from calc-alkaline andesite. All phases of volcanic activity in the area (except for the Salal Center (SC) and Mud Lake (ML) phases) show compelling evidence for glaciovolcanic emplacement. This evidence includes subaqueous volcanic lithofacies (e.g., pillow lava, palagonitised tephra, glassy and hackly-jointed lava) that are in topographic areas with limited capacity to support sustained bodies of water (e.g., along alpine ridges). Given that the main topographical features of the area are unlikely to have changed extensively since the onset of local volcanic activity (i.e., in the last ~1 Ma), glacial ice is the most plausible mechanism for creating the impounded bodies of water required to form the lithofacies (e.g., pillow lava and hyaloclastite). The ages of each of the volcanoes in the Salal Glacier volcanic field provide insight into the extent and thickness of local ice at the time of the eruptions. Taken together, these data provide a detailed record of waxing and waning of the Coast Mountain sectors of the CIS in southern British Columbia throughout the Pleistocene.

Quaternary volcanic activity in the Salal Glacier area began in the Early Pleistocene (970 ± 50 ka; Lawrence et al. 1984) with a small, effusive eruption of hawaiite lava at Salal Center (SC). The lava was emplaced in a subaerial environment that probably hosted a similar amount of glacial ice as today. The next eruptions (Salal Mountain (SM) phase) occurred in the western map at 831.5 ± 11.43 ka. Initially, the Salal Mountain phase eruption emplaced a ~100 m-thick mound of calc-alkaline andesite lava. Erratic, fanning and radial columnar joint configurations and a conformable relationship with underlying fresh, un-weathered basal till (unit bt) indicate that these lavas were emplaced in a subglacial environment. As the eruption progressed, the lava emplacement transitioned from thin flows and sheets to steep-sided domes. Lava quenching on the dome margins during contact with ice produced large quantities of unconsolidated hyaloclastite breccia. The deposits at Salal Mountain record the paleo presence of a thick Early Pleistocene glacier that had a surface elevation of at least 2370 m asl.

Volcanic activity began at Salal Tindar (ST) in the Middle Pleistocene at 590 ± 50 ka (Lawrence et al. 1984). The initial eruptions were phreatomagmatic and constructed a broad, ~90 m-thick mound of palagonitised tephra that contained abundant conduit wall rock lithic fragments. Volcanism melted a hole in the overlying ice and formed an englacial lake with a water surface elevation of ~2360 m asl (inferred from the presence of a passage zone). As the volcanic pile grew, it eventually breached the lake surface, and the drying of the vent permitted a small strombolian cinder cone and associated subaerial lavas to be constructed. Near the end of the Salal Tindar phase event, subaerial lava emplaced near the summit of the cinder cone flowed south and became impounded against the surrounding glacial ice. The deposits at Salal Tindar record the paleo-presence of an englacial lake with a depth of ~90 m. Accordingly, the surrounding glacial ice had a surface elevation of at least 2360 m asl.

The Ochre Mountain (O) phase eruption occurred during the Middle Pleistocene at 408.7 ± 6.7 ka (Fig. 9.6A). Effusive eruption of alkaline basalt began at a vent located near the southwestern edge of the Ochre Mountain deposit in a water-rich, subglacial environment. As lavas were emplaced, they propagated along the Athenley Pass valley wall towards the northeast, forming thin sheets of pillow lava, radially jointed lava lobes, and hyaloclastite breccia. The Ochre Mountain phase lithofacies record the paleo-presence of glacial ice occupying Athenley Pass with a minimum ice surface elevation of 2140 m asl.

The Logan Ridge (LR) phase eruption began with effusive emplacement of alkaline basaltic lava beneath a glacier. Volcanism melted a hole in the ice and produced an englacial lake that was maintained throughout the entire eruption (i.e., the lake was not drained). Continued lava effusions constructed a ~100 m-thick pile of pillow lava and hyaloclastite situated on the steep Logan Ridge valley wall. As the growing volcanic pile reached the surface of the englacial lake, the volcanism transitioned to shallow water phreatomagmatism. These explosive events produced an 8 m-thick layer of surge-bedded tuff breccia that is draped over the summit of the Logan Ridge deposit. The deposits at Logan Ridge record the paleo-presence of an extensive Pleistocene glacier (probably the CIS) that had a surface elevation of at least 2340 m asl. The age of volcanism at Logan Ridge is unknown and further geochronology is required to fully evaluate the paleoenvironmental implications of the glaciovolcanic event.

The Northwest volcanic remnant (N) phase eruption began with explosive emplacement of a ~50 m-thick layer of alkaline

basaltic tuff breccia. The breccia is palagonitised and shows evidence for minor deposit reworking, indicating a glaciovolcanic, subaqueous eruption environment. Continued eruptions constructed a pile of tuff breccia with minor effusive events creating several layers of basaltic pillow lava. Near the end of the eruption, the volcanism transitioned to explosive phreatomagmatism. These events produced a ~20 m-thick veneer of well-bedded surge deposits that are draped over the upper portion of the Northwest volcanic remnant deposit. The final volcanism is represented by several subvertical basalt dikes that crosscut all other volcanic lithofacies. The age of the glaciovolcanic Northwest volcanic remnant (N) phase eruption is also unknown.

10. The Bridge River volcanic field (1:20,000)

The Bridge River volcanic field (formerly referred to as the Bridge River Cones; Roddick and Souther 1987; Green et al. 1988) is an area of predominantly alkaline mafic volcanic rocks that are located near the northern end of the Garibaldi volcanic belt (Fig. 1B). The Bridge River volcanic field hosts basalt, hawaiite and mugearite lava domes and lava flows, tephra cones, and a large, polygenetic tuya. The volcanic deposits are distributed at high elevation (>1720 m) in the rugged, alpine terrain of the Coast Mountains. The area is presently glaciated with several portions covered in permanent accumulations of ice and snow. The ground surface is covered by sparse vegetation, loose felsenmeer and scattered glacial debris. All volcanic deposits are covered by variable accumulations of glacial erratic material (i.e., ablation till). The first geological map to consider the volcanic deposits was produced by Roddick and Souther (1987). This map provided eruption ages for three of the deposit areas (Sham Hill, Tuber Hill and Nichols Valley) and interpreted the deposits to reflect interactions between volcanic eruptions and Late Pleistocene glacial ice. Here, we present a complete lithofacies map that delineates the volcanic stratigraphy of the Bridge River area at high resolution. Our maps correlate several important stratigraphic markers that extend across the geologically recent Arrowhead and Thunder Creek valleys. These cross-valley lithofacies associations are the foundation to a new stratigraphic framework that is used to organize the local volcanic deposits and interpret their geologic history.

At the western edge of the map, the oldest volcanic rocks are exposed at Sham Ridge (SR). The deposits comprise an isolated, highly eroded package of alkaline basalt located on the ridge above the Arrowhead Creek valley. They are deeply eroded and there is no clear evidence for either glaciovolcanic or subaerial emplacement. We interpret these rocks to be the oldest volcanic rocks in the region.

The Sham Hill (SH) phase rocks comprise a small, isolated subglacially erupted dome of mugearite lava with an irregular, glassy lower margin and a fine-scale, columnar jointed southern exterior (Fig. 10.1A). There is a single K-Ar age estimate for Sham Hill phase rocks of 752 ± 9 ka (Roddick and Souther 1987).

In the centre of the map, Tuber Hill is a large, polygenetic basaltic tuya (Roddick and Souther 1987; Wilson and Russell 2018). The deposits are distributed in a wide, north-to-south trending paleo valley (Fig. 10.1B). The Tuber Hill group has an

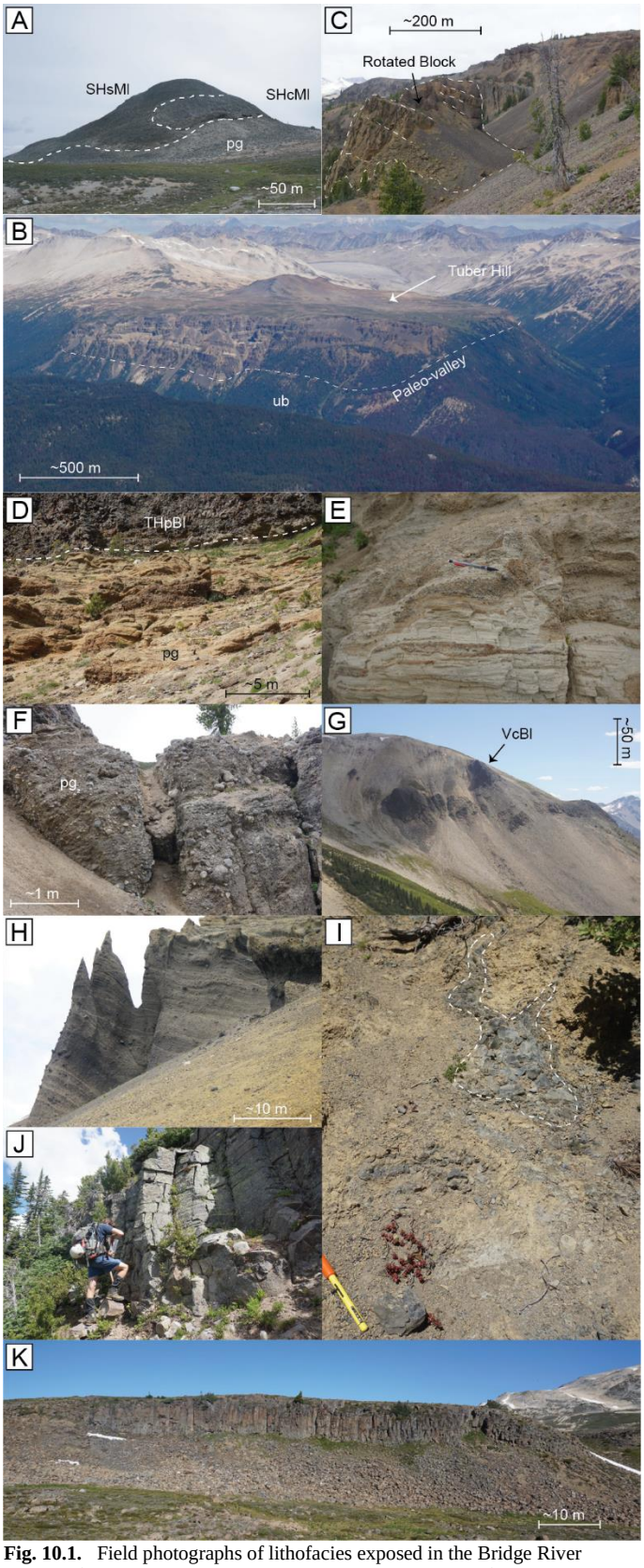

Fig. 10.1. Field photographs of lithofacies exposed in the Bridge River volcanic field. (A) Photograph looking west at coarsely and finely jointed columnar-jointed rocks of Sham Hill. (B) Looking north at Tuber Hill, a complex, polygenetic tuya. The Tuber Hill lithofacies fill a paleo-valley. (C) Photograph looking west at large, partially rotated block in the upper Tuber Hill sequence. The stratigraphic layers are indicated with fine, dashed white lines…

Fig. 10.1 cont… (D) Looking west at bedded sedimentary fluvial conglomerate, sandstone and mudstone (unit pg) underlying finely jointed basalt. (E) Cross-bedded, polymictic sandstone with up to 20 % volcanic clasts. (F) Photograph looking east at crudely bedded variant of coarse, polymictic conglomerate. Rounded mafic volcanic boulders comprise up to 15% of the unit. (G) Looking southeast at undivided, finely jointed coherent mafic lavas exposed on a ridge in the Bridge River volcanic field. (H) Looking north at dipping, bedded tuff breccia at Thunder Creek. (I) Photograph looking north at intensely jointed apophyses of glassy coherent lava intruding cogenetic hyaloclastite breccia. Pen launcher shown for scale. (J) Photograph looking northeast at the coarsely-columnar-jointed Nichols Valley porphyritic basalt. (K) Photograph looking east at Glacier View phase, coarsely jointed basalts exposed on the Plateau east of Tuber Hill.

older central core (herein called the Bridge Glacier (BG) phase) comprising palagonitised hawaiite volcaniclastic rocks, finely jointed, stacked basalt lava and coarsely jointed basaltic lava. The coarsely jointed lava unit (that was presumably subaerially erupted) yielded a K-Ar age of 731 ± 13.5 ka (Roddick and Souther 1987).

Overlying these deposits, separated by horizons of glacial sediments (basal till and paraglacial sediment), the Tuber Hill (TH) phase deposits consist of hawaiite and alkaline basaltic pillow lava, pillow breccia, and hyaloclastite that are overlain - via a passage zone (e.g. Russell et al. 2014) - by chemically and petrographically equivalent basaltic lava flows. This group of rocks yielded a K-Ar age determination of 598 ± 7.5 ka (Roddick and Souther 1987). In the western map area, the massive hyaloclastite deposits are crossed by several layers of bedded and massive basaltic tuff, lapilli tuff, and tuff breccia. These rocks provide evidence of at least one period of explosive subaqueous eruptions, suggesting that the Tuber Hill phase volcanic activity was not solely effusive.

The Tuber Hill group rocks are intercalated with several sedimentary layers consisting of volcaniclastic mudstone, sandstone, gravel, and conglomerate. Wilson and Russell (2018) suggest that given the present-day local physiography (i.e., high alpine, mountainous terrain with ample water drainage) these alluvial plain style deposits are probably syn volcanic and have a glaciofluvial origin (i.e., they were formed in the presence of ice-dammed temporal lakes and drainage channels). Tuber Hill is faulted along the steep, eastern, and southern margins. In these areas, partially rotated blocks cause several apparent repetitions in the stratigraphic succession (Fig. 10.1C).

The Sham Plateau (SP) phase forms a ~1 km-long and ~20 m-thick mugearite lava flow situated in the center of the Sham highland area. Although the contact is not directly exposed, the rocks appear to stratigraphically overly Tuber Hill phase pyroclastic deposits (unit THbBtu). The lava has a fine-scale, hackly jointed exterior (e.g. Lodge and Lescinsky, 2009) and pillow lava exposed at several places around the perimeter. A new $^{40}Ar/^{39}Ar$ geochronology determination (sample AW-16-182, unit SPsBl) yielded an age of 746.9 ± 15 (Fig. 10.2, Table 1.1), which is inconclusive when compared with the expected age of the (stratigraphically older) Tuber Hill deposits (expected to be ~598 ± 7.5 ka, see above).

The eastern part of Tuber Hill is partially overlain by coherent alkaline basalt, hawaiite, mugearite and volcaniclastic rocks, herein called the Glacier View (GV) phase. A distinctive stratigraphic marker layer within the Glacier View phase lava

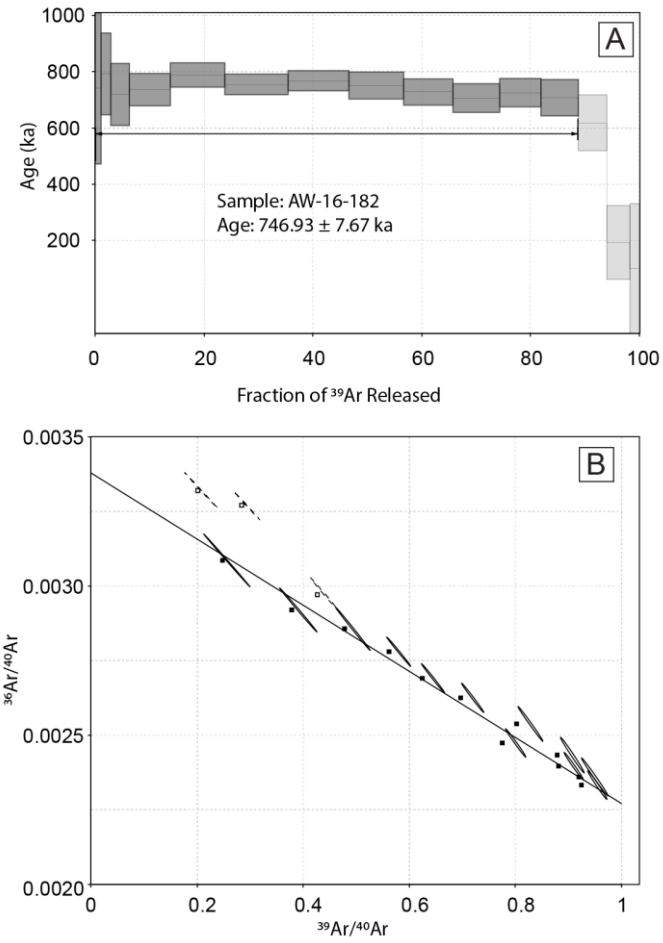

Fig. 10.2. Summary of $^{40}Ar/^{39}Ar$ geochronology results for sample AW-16-182 (unit SPsBl). (A) Plateau diagram showing fraction of ^{39}Ar versus age for the sample. (B) Inverse isochron plot. Ellipses denote 1 analytical uncertainty.

stack (unit GVmBc, a massive basaltic conglomerate) provides evidence that the deposits extend eastward across the adjacent plateau and pre-date the age of excavation of the Thunder Creek valley. The Glacier View phase succession is up to 60 m-thick and comprises at least 5 individual lava flow units. $^{40}Ar/^{39}Ar$ geochronology was attempted on a sample of holocrystalline basalt collected from one of the Glacier View phase lavas (sample AW-16-122, unit GVcMl, Fig. 10.3 Table 1.1). The results returned a plateau age of 806.9 ± 8.5 ka, which is inconclusive when compared with expected age of the (older) Tuber Hill (TH) and Bridge Glacier (BG) phase rocks (dated by the K-Ar method to be 598 ± 7.5 ka and 731 ± 13.5 ka, respectively).

The Nichols valley area is a collection of coarsely jointed alkaline basalt lava that occupies the Nichols valley in the eastern map area, overly an exposure of undifferentiated paraglacial sediment (unit pg). The rocks yielded K-Ar ages of 374 ± 11.5 and 405 ± 11.5 ka (Roddick and Souther 1987).

The recently exposed Arrowhead Glacier (AG) phase deposits comprise mugearite hyaloclastite, pillow lava and columnar jointed basalt lava located at the terminus of the Arrowhead Glacier. The age of the Arrowhead Glacier deposits is unknown, however, the lithofacies suggest that the eruption

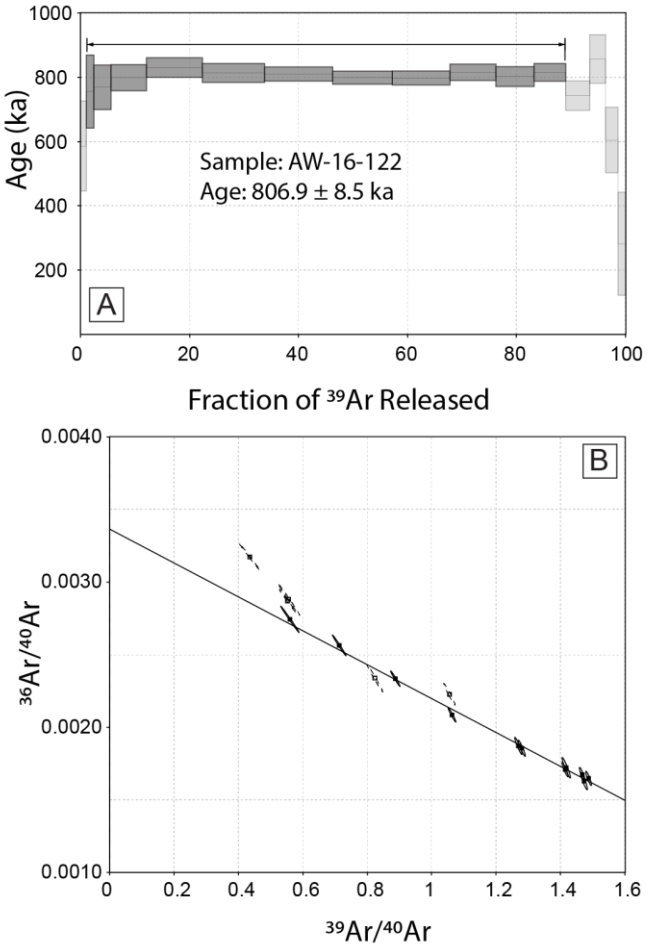

Fig. 10.3. Summary of $^{40}Ar/^{39}Ar$ geochronology results for sample AW-16-122 (unit GVcMl). (A) Plateau diagram showing fraction of ^{39}Ar versus age for the sample. (B) Inverse isochron plot. Ellipses denote 1 analytical uncertainty.

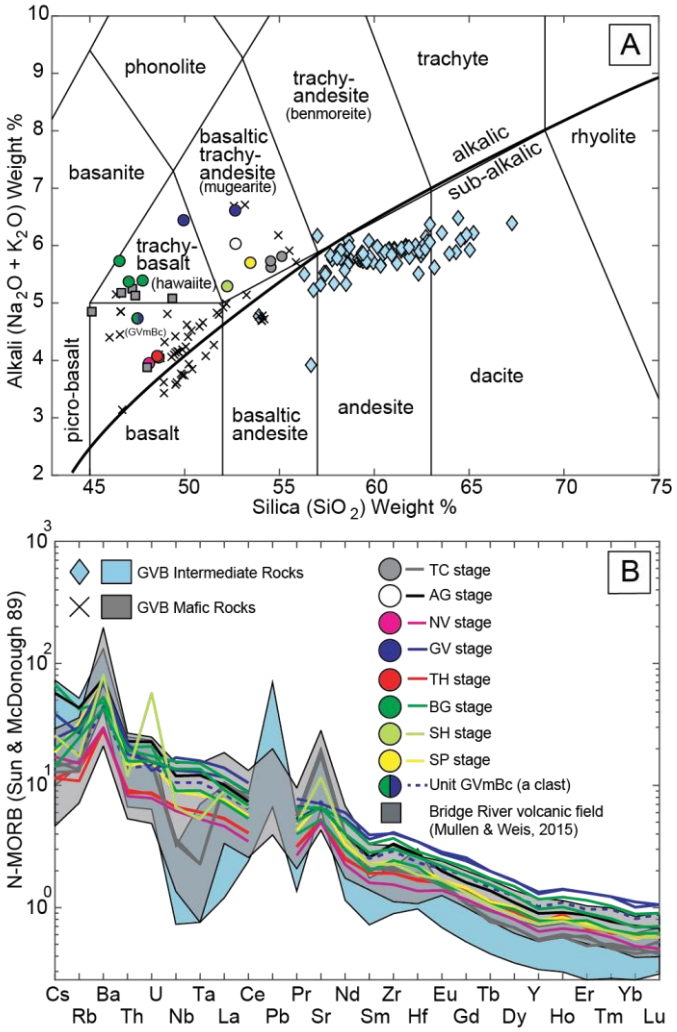

Fig. 10.4. Geochemical characteristics of the Bridge River volcanic field lithofacies. (A) Total alkalis vs. silica diagram after Le Bas et al., (1986), showing predominant alkaline basaltic affinity of the Nichols Valley, Glacier View, Tuber Hill, Bridge Glacier and Sham Hill phases of volcanic activity. The Thunder Creek phase deposit comprises calc-alkaline basaltic trachyandesite. Additional analyses of Garibaldi volcanic belt mafic rocks are from Mullen and Weis (2015) and Wilson and Russell (2017). Analyses of mafic rocks from the Bridge River volcanic field from Mullen and Weis (2015) are shown using grey squares. Additional analyses of intermediate rocks are from Bye et al. (2000); Fillmore and Coulson (2013); Wilson et al. (2016) and other field localities within this study (i.e. the Table volcanic complex, Brohm Ridge and Monmouth Creek volcanic complex) (B) Trace element compositions of the Bridge River volcanic field lavas normalised to N-MORB (Sun and McDonough 1989).

probably occurred in the presence of a small alpine glacier (Wilson and Russell 2018).

Finally, the Thunder Creek (TC) phase rocks comprise a ~350 m-thick package of mugearite lobes that are surrounded by matrix-supported hyaloclastite. The upper parts of the deposit form a crude cone of bedded, indurated tuff breccia. These deposits are the only rocks in the Bridge River volcanic field that have a calc-alkaline affinity (Fig. 10.4B). A sample of one of the basaltic trachyandesite lobes (sample AW-16-201) was sent to the WiscAr Laboratory at the University of Wisconsin-Madison for $^{40}Ar/^{39}Ar$ analysis. The contained a large atmospheric gas component, resulting in an inconclusive analysis (Table 1.1). As these rocks appear to have been erupted in a valley that was not present during the Tuber Hill and Bridge Glacier phase events (see above), future geochronology studies may be useful in providing a bracketed age on the formation of the Thunder Creek valley.

10.1. Basement geology

Undivided basement rocks (ub)

White-grey, medium to coarse-grained (2 to 5 mm), block jointed, phaneritic quartz diorite, and granodiorite of the Coast Plutonic Complex. Adjacent areas of similar lithology have yielded K-Ar ages ranging from 47 to 76 Ma (Roddick and Woodsworth 1975). The adjacent Salal Pluton is one of the youngest exposed plutons in the Coastal Plutonic Complex with a K-Ar age of 8.0 ± 0.1 Ma (Roddick and Woodsworth 1975).

10.2. The Bridge River volcanic field

10.2.1. Sham Ridge (SR) phase (Non-Glaciovolcanic)

Coarsely jointed basaltic lava (SRcBl)

Volcanic phase	Map unit	Map unit code	Texture	Groundmass	Components
Sham Hill (SH) phase	Slender jointed mugearite lava Coarsely jointed mugearite lava	SHsMl SHcMl	Porphyritic	Hypocrystalline, groundmass of plagioclase (~10 %; 0.01-0.1 mm), Fe-Ti oxides (~10 %; 0.01 mm), olivine (~10 %; 0.01-0.1 mm) and Ti-augite (~10 %; 0.01-0.1 mm) and minor interstitial glass (~5 %)	Plagioclase (~35 %; 1-3mm) and olivine (~20 %; 0.1-1 mm)
Bridge Glacier (BG) phase	Slender jointed hawaiite lava Massive hawaiite tuff breccia Bedded hawaiite tuff breccia Coarsely jointed hawaiite lava	BGsHl BGmHtx BGbHtx BGcHl	Porphyritic, holocrystalline	Plagioclase (20 %; 0.01-0.1 mm), Fe-Ti oxides (~10 to 20 %; 0.01 mm) and augite (~5 %; 0.01-0.1 mm).	Phenocrysts: Plagioclase (~40%; 1-3 mm), olivine (~15 %; 0.1-1 mm) and augite (<1 %; 0.1-1 mm). Megacrysts: rare, large (up to 3 cm-diameter) plagioclase
Tuber Hill (TH) phase	Bedded basaltic tuff Massive basaltic lapilli tuff Bedded basaltic hyaloclastite Porphyritic basaltic lava	THbBtu THmBlt THbBh THpBl	Porphyritic, hypo-to holocrystalline	Plagioclase (~30 %; 0.01-0.1 mm), glass (~5%), olivine (~5 %; 0.01-0.1 mm) and Fe-Ti oxides (~1%; 0.01 mm)	Phenocrysts: Plagioclase (~40%; 1-3mm), olivine (~20 %; 0.1-1 mm) and Augite (~1 %; 0.1-1 mm). Megacrysts: plagioclase and pyroxene (up to 3 cm-dimeter)
Glacier View (GV) phase	Massive basaltic conglomerate Coarsely jointed mugearite lava Massive mugearite breccia	GVmBc (clasts) GVcMl GVmMbx	Porphyritic, holocrystalline	Interlocking, acicular Ti-Augite (~20 %; 0.01-0.1 mm), plagioclase microlites (~20 %; 0.01-0.1 mm) and minor glass	Phenocrysts: Plagioclase (~30 to 40 %; 1-3mm), olivine, (~1 to 5 %; 0.1-1 mm) and Ti-augite (~1 %; 0.1-1mm)
Sham Plateau (SP) phase	Slender jointed basaltic lava Slender jointed basaltic pillow lava	SPsBl SPsBp	Porphyritic, holocrystalline to hypocrystalline	Plagioclase (~65 %; 0.01-0.1 mm), Fe-Ti oxides (~20 %; 0.01 mm), and olivine (~5 %; 0.01-0.1 mm)	Phenocrysts: Olivine (~5 %; 0.1-1mm) and plagioclase (~2 %; 1-3mm)
Nichols Valley (NV) phase	Coarsely Jointed basaltic lava Massive basaltic breccia	NVcBl NVmBbx	Porphyritic, holocrystalline	Interlocking crystals of plagioclase (~40 %; 0.1 to 0.5 mm), augite (~15 %; 0.1 mm) and equant Fe-Ti oxides (~15 %).	Phenocrysts: Olivine (~30 %; 0.5 to 2 mm) and augite (~5 %; 0.5 to 1 mm), Xenolithic material: ~5 % (1 to 10 cm-diameter clasts of granite, sandstone, and conglomerate), and megacrysts: rare, plagioclase, olivine, and pyroxene (1 to 2 cm-diameter)
Arrowhead Glacier (AG) phase	Slender jointed mugearite lava Massive mugearite hyaloclastite	AGsMl AGmMh	Porphyritic, hypocrystalline	Plagioclase (~30 %; 0.01-0.1 mm), augite (~15 %; 0.01-0.1 mm), olivine (~10 %; 0.01-0.1 mm) and glass (~40%)	Phenocrysts: Olivine (~10 %; 0.2-1mm) and plagioclase (~5 %; 1-3mm). Megacrysts: rare olivine, augite and plagioclase (1 to 2 cm-diameter)
Sham Ridge (SR) phase	Coarsely Jointed basaltic lava	SRcBl	Porphyritic, holocrystalline	Interlocking plagioclase (~50 %; 0.01-1 mm), Fe-Ti oxides (~20 %; 0.01 mm), and augite (~10 %; 0.01-1 mm)	Phenocrysts: plagioclase (~20 %; 0.1-3 mm) and olivine (~10 %; 0.1-1 mm)
Thunder Creek (TC) phase	Slender jointed mugearite lava Massive mugearite hyaloclastite Bedded mugearite tuff breccia	TCsMl TCmMh TCbMtx	Sparsely porphyritic to aphyric, holocrystalline	Fine plagioclase (50 %, 0.01 mm) and augite (~10 %, 0.01 mm)	Phenocrysts: rare plagioclase (<5 %; 0.1-3 mm) and olivine (< 1 %; 0.1-1 mm)

Table 10.1 Petrographic characteristics of volcanic rocks in the Bridge River volcanic field

Dark red to grey, dense to moderately vesicular, porphyritic basalt forms a ~500 m-wide, ~100 m-high, ridge of lava at the northern side of the Sham Plateau (Fig. 10.5E). The rocks are coarsely columnar jointed (0.5 to 1 m-diameter); the columns dip moderately towards the southwest (perpendicular to the valley wall). The rocks are holocrystalline and plagioclase, olivine phyric (Table 10.1). All samples show moderate oxidation and minor weathering. The basal contact (with plutonic rocks) is sharp and follows the steep, northeastern Arrowhead Valley wall. No pillows, glass, or associated volcaniclastic sediments or till were observed along the contact. The Sham Ridge rocks are highly eroded and have no original surface textures preserved, prohibiting accurate diagnosis of the emplacement environment. The rocks are observed to unconformably overlie undivided basement (ub) however the exact age of the Sham Ridge deposit is unknown.

10.2.2. Sham Hill (SH) phase (Glaciovolcanic)

Slender and coarsely jointed mugearite lava (SHsMl and SHcMl)

Dark grey to black, dense, porphyritic mugearite comprises a ~60 m-high, dome-shaped mound called Sham Hill (Table 10.1, Figs. 10.1A, 10.5D). At the northern edge of the deposit, the columnar joints have a shallow, southward dip. The rocks overlie a thin accumulation of glacial sediments via an irregular and glassy basal contact. The southern margin is draped over the wall of the Bridge River valley. Here, the deposit overlies the plutonic basement and shows fine-scale (10 to 20 cm-diameter) columnar joints that point outwards in the open air above the valley (Fig. 10.5D). Subvertical, coarsely jointed (20 to 50 cm-diameter) rocks are exposed in the core of Sham Hill (unit SHcMl). A sample from Sham Hill yielded an age of 752 ± 9 ka (Roddick and Souther 1987). The dome-shaped, finely jointed marginal characteristics of Sham Hill indicate that the edifice was emplaced beneath the ice, and the recumbent columnar jointing along the southern edifice margin suggests that at the time of the eruption, the adjacent Bridge Valley was also filled with ice (Wilson and Russell 2018).

10.2.3. Bridge Glacier (BG) phase (Glaciovolcanic)

Slender jointed hawaiite lava (BGsHl)

Dark grey, dense, medium-grained, aphyric to sparsely olivine and augite phyric, finely columnar jointed hawaiite form the basal part of the Tuber Hill sequence. These rocks have a maximum observed thickness of ~50 m. At Tuber Hill, they underlie unit BGmHtx volcaniclastic rocks and pg sedimentary deposits. Eastern Tuber Hill exposures are geochemically and petrographically like BGcHl, however they are distinguished by their finer jointing character and low groundmass crystallinity. The very base of the southern Tuber Hill sequence is inaccessible, however the unconformably overlying relationship with basement rocks is visible. The columnar joints in these basal exposures are ~10 to 20 cm in diameter and form radiating, fanning, and irregular joint sets (Fig. 10.5A). These irregular cooling fractures suggest that the lavas probably interacted with ice or water during emplacement. We interpret these rocks to be the first, subglacial stage of eruption at Tuber Hill. Their age most likely coincides with emplacement of the central Tuber Hill cone (i.e. units BGcHl probably circa 760 ± 16.5 ka; Roddick and Souther 1987).

Massive hawaiite tuff breccia (BGmHtx)

Dark orange-brown, massive to bedded, matrix-supported, moderate to well-sorted, consolidated, tuff breccia is a major component of the Bridge Glacier phase sequence. At the southern margin of Tuber Hill, unit BGmHtx deposits are coarsely jointed (2 to 5 m-diameter), massive to bedded and normally graded, and up to 100 m-thick. Where bedding exists, it is typically subhorizontal to gently south and westward dipping. The tuffs and tuff breccias show subrounded, vesicular basaltic blocks and bombs, bomb sag structures, and minor growth faults (Fig. 10.6K). Towards the summit of Tuber Hill, the deposits become increasingly enriched in angular plutonic lithic clasts which are 1 to 20 cm-diameter clasts and form up to 20 % of the deposit. The matrix to the deposits is weakly palagonitised, giving the rocks a dull orange-brown color. Like other deposits in the Bridge Glacier phase, these rocks show evidence for subaqueous volcanic interaction (palagonitised matrix clasts, subrounded grains, bomb sags, graded beds, etc.) The large-scale joint features indicate emplacement and in situ cooling (Fig. 10.6L). Like unit BGbHtx, these deposits are probably the product of a subaqueous, explosive eruption. We interpret that the core of Tuber Hill comprises a ~300 m-thick sequence of BGbHtx and BGmHtx rock. Given these geometric parameters, it is likely that the BG phase eruption occurred when the local area was covered by ice that had a surface elevation of > 2400 m (Wilson and Russell 2018).

Bedded hawaiite tuff breccia (BGbHtx)

Dark, yellow orange, bedded, matrix-supported, moderate to well-sorted tuff breccia forms a broad cone in the northern Tuber Hill region. Along the western side of Tuber Hill, the deposits form bluffs up to 20 m high. Across the valley, along the southeastern margin of Sham Plateau these rocks form a ~30 m thick layer that is observed to directly overlie pg sedimentary deposits (Fig. 10.6J) and unconformably underlie a thin layer of basal till (unit bt). The beds are normally graded and comprise vesicular, irregular, porphyritic basaltic lapilli and blocks, agglutinated basaltic cauliflower bombs, and a consolidated, palagonitised ash-lapilli matrix (Fig. 10.6I). Pervasive palagonitization of the glassy clasts indicate interaction with water during eruption and emplacement and we interpret that they result from a subaqueous, explosive eruption forming pyroclastic density currents.

Coarsely jointed hawaiite lava (BGcHl)

Dark grey, dense, aphyric to sparsely olivine phyric, coarsely columnar jointed hawaiite occurs in a 10 to 30 m-thick lava ridge and 10 to 15 m-thick flow in the northern part of Tuber Hill. The lava ridge exhibits crude, glassy and brecciated margins with the surrounding BGbHtx and BGmHtx tephra (Fig. 10.6G). A sample collected from this lava yielded an age of 760 ± 16. 5 ka

(Roddick and Souther 1987). Further north, a 1 to 2 m-diameter exposed dike is connected to a 100 to 200 m-wide, 10 to 15 m-thick, coarse, subvertically jointed hawaiite lava flow (Fig. 6H). The lava has a thin, brecciated base and overlies unit BGmHtx. A sample from this lava produced an age of 731 ± 13.5 ka (Roddick and Souther 1987). These two ages are within the 1-sigma level of uncertainty, suggesting coeval emplacement. We interpret that the lava ridge (unit BGcHl) is probably a feeder structure for the surrounding Bridge Glacier phase deposits.

10.2.4. Tuber Hill (TH) phase (Glaciovolcanic)

Bedded basaltic hyaloclastite (THbBh)

Dark orange and black, crudely bedded, poorly sorted, matrix and clast supported basaltic pillow breccia, pillow lava, lobes and hyaloclastite are a volumetrically predominant component of the Tuber Hill phase deposits. Their upper contact is clearly defined by a passage zone, separating basaltic pahoehoe lava (unit THpBl), distributed throughout the western, eastern, and southern parts of Tuber Hill. In the east, Tuber Hill (stratigraphic section 5), the deposits are up to 80 m-thick and form crude, southward dipping (20-30º) foreset beds. Further south (stratigraphic section 3) the cumulative thickness is up to 180 m. Layers (40 to 50 m-thick in some places) are separated by bands of paraglacial sediment (unit pg) and at least one horizon of tephra (see units THmBlt, THbBtv and THmBlt). Clastic parts of the deposit comprise pillow lava fragments and jointed basaltic blocks with a matrix of angular, palagonitised ash, and lapilli (Fig. 10.6D). Coherent parts of the deposit comprise stacked pillow piles and large, irregularly shaped lobes and sheets. The presence of pillow lava, crude bedding, and pervasive palagonitisation suggests that these rocks were emplaced subaqueously (i.e., within a sustained body of water).

Bedded basaltic tuff (THbBtu)

Well sorted, vesicular, matrix-supported, palagonitised ash tuff forms a 15 to 20 m-thick accumulation at the eastern margin of Sham Plateau and a 5 to 10 m-thick deposit at the western margin of Tuber Hill (Fig. 10.6F). At the Sham Plateau exposure, the rocks are observed to unconformably overlie a thick accumulation of basal till (bt), and locally represent the base of the Tuber Hill phase sequence. Further east, these rocks form a thin band within the massive to crudely bedded hyaloclastite rocks (unit THbBh). The deposits are well bedded, orange in colour and have a pervasively-palagonitised matrix. The clasts are indurated and fine, angular and vesicular cuspate-shaped ash with minor lapilli. Minor (<1 %) 10 to 20 cm-diameter basaltic bombs and smaller (5 to 10 cm-diameter) angular accessory plutonic lithic clasts are randomly distributed throughout the deposit. The unit is fractured by a tight network of carbonate-filled cracks. Petrographic and textural similarity to a massive basaltic lapilli tuff (unit THmBlt) exposed on the opposite side of the Arrowhead valley (towards Tuber Hill), suggest that the deposits may be closely related and contiguous; although, the finer grain size of this unit suggests a more distal proximity.

Massive basaltic lapilli tuff (THmBlt)

Well sorted, highly vesicular, clast (supported vitric lapilli tuff occurs in a 1 to 3 m-thick layer in along the southern margin of Tuber Hill (Fig. 10.6E). The unit extends ~1 km laterally. The clasts are highly vesicular (pumice), glassy and augite and olivine phyric. Some clasts margins show incipient palagonitisation. The indurated matrix comprises fine, angular, glassy ash. In thin section, the rocks are fractured by a tight network of carbonate-filled cracks. Moderate sorting and vitric, vesicular, and basaltic clasts suggest that this tephra was deposited during a brief explosive Tuber Hill phase eruption, and we interpret these deposits to be a product of subaqueous pyroclastic density currents and fallout. Along with unit THbBtu, these rocks provide evidence for at least one period of explosive subaqueous eruptions within the Tuber Hill phase.

Porphyritic basaltic lava (THpBl)

Dark grey, dense to moderately vesicular, porphyritic, alkaline basalt forms a ~20 m-thick capping sequence at Tuber Hill. The deposits comprise numerous individual flow units that are each 1 to 5 m-thick (Fig. 10.6C). The rocks contain phenocrysts and megacrysts (up to 2 cm-diameter) of plagioclase, olivine and augite. These rocks overlie, via a passage zone, a sequence of geochemically and petrographically identical basaltic pillow lava, bedded pillow breccia, and hyaloclastite (unit THbBh; Fig. 10.4). This “passage zone” occupies a semi-consistent elevation at ~1990–2010 m asl around the margins of Tuber Hill. No overlapping stepped, or repeating passage zone sequences were observed (Russell et al. 2013, 2014). Columnar jointing is typically fine-scale (i.e. <30 cm diameter columnar joints) and oriented subvertical. Sectional exposures show an internal structure of overlapping pahoehoe toes with ropey, glassy surfaces.

The presence of a well-developed passage zone defining the base of these subaerial lavas, supports a glaciovolcanic emplacement of the Tuber Hill phase. Along with the underlying hyaloclastite rocks (unit THbBh), the deposits form a lava-delta sequence that extends across the southern portion of Tuber Hill. Intersecting layers of paraglacial sediment (pg) suggest that the Tuber Hill eruption phase was long-lived and intermittent. The age of the rocks is constrained by a exposed K-Ar age of 598 ± 7.5 ka (Roddick and Souther 1987).

10.2.5. Sham Plateau (SP) phase (Glaciovolcanic)

Slender jointed basaltic lava and pillow lava (SPsBl and SPsBp)

Dark grey to black, dense to moderately vesicular, porphyritic basalt comprises a 10 to 15 m-thick, fine-scale radially jointed, lobe that is ~1 km long and ~400 m wide on Sham plateau (Fig. 10.5C). The lava is observed to overlie ThbBtu (tephra) in the south and the plutonic basement rocks in the north. The southeastern base of the flow has glassy pillow lava (mapped as unit SPsBp). Like Bridge River volcanic field rocks, the fine marginal jointing character and the presence of pillows suggest that these lavas erupted subglacially. A new $^{40}Ar/^{39}Ar$ geochronology determination on these rocks (sample AW-16-182, unit SPsBl) yielded an age of 746.9 ± 15 (Fig. 10.2, Table

1.1). This age determination is inconclusive, given the stratigraphic position of the rocks, which are overlying tephra of the Tuber Hill phase (unit ThbBtu). These rocks are laterally connected to across the Arrowhead Valley to rocks dated by the K-Ar method at ~598 ± 7.5 ka (Roddick and Souther 1987). The K-Ar determination may be anomalously young, or the new $^{40}Ar/^{39}Ar$ age is erroneous. Further, comprehensive geochronological analysis would be required to resolve these issues.

10.2.6. Glacier View (GV) phase (Non-Glaciovolcanic)

Coarsely jointed mugearite lava and massive mugearite breccia (GVcMl and GVmMbx)

Light grey, dense to sparsely vesicular, coarsely jointed, plagioclase, olivine, and augite phyric mugearite form at least five stacked flows that are distributed across the eastern part of Tuber Hill and cover the adjacent plateau to the east (stratigraphic sections 5, 6 and 7) (Fig. 10.1K). In the eastern part of Tuber Hill, these rocks comprise two individual layers that are 5 to 10 m-thick, are highly porphyritic, flow banded and coarsely jointed. Here, the relative stratigraphic relationship with underlying Tuber Hill phase rocks is delineated clearly with a thin band of paraglacial sediment (unit pg). The two Glacier View phase lava layers are themselves separated by a thin band (2 to 5 m-thick) of massive, poorly sorted volcaniclastic sandstone with basaltic clasts (unit GVmBc). To the east, across the Thunder Creek valley, the rocks form a wide plateau at ~2000 to 1980 m-elevation. Here, up to five individual flows are up to 60 m-thick and dip gently towards the east. At the western margin of the plateau (stratigraphic section 6), the lowermost flows are separated by a ~10 m-thick accumulation of distinctive volcaniclastic sandstone with basaltic clasts (i.e., a conglomerate, unit GVmBc). All Glacier View phase lavas support discontinuous accumulations of poorly sorted, clast-supported basal breccia (unit GVmMbx). The stacked lavas terminate at the eastern margin of the plateau in a steep, stepped bluff that is ~50 m high.

A sample of holocrystalline basalt collected from a coarsely jointed lava layer (unit GVcMl) was analysed using $^{40}Ar/^{39}Ar$ at the WiscAr laboratory at the University of Wisconsin-Madison. The sample returned an age of 807 ± 8.5 ka (Table 1.1, Figure 10.3). This age determination is also inconclusive, given the stratigraphic position of these rocks, overlying Tuber Hill and Bridge Glacier phase rocks, which are dated by K-Ar method to be between ~598 to 760 ka (Roddick and Souther, 1987). The K-Ar determinations may be anomalously young; however these rocks are also stratigraphically younger than rocks of the Sham Plateau (SP) phase (dated in this report to be 746.9 ± 15 ka). Further geochronological analysis is required to resolve these discrepancies.

Massive basaltic conglomerate (GVmBc)

Massive, poorly sorted, matrix-supported, volcaniclastic sandstone with basaltic clasts (a conglomerate) occurs between the lowermost Glacier View phase lavas on both the eastern and western sides of Thunder Creek valley. In the west (stratigraphic

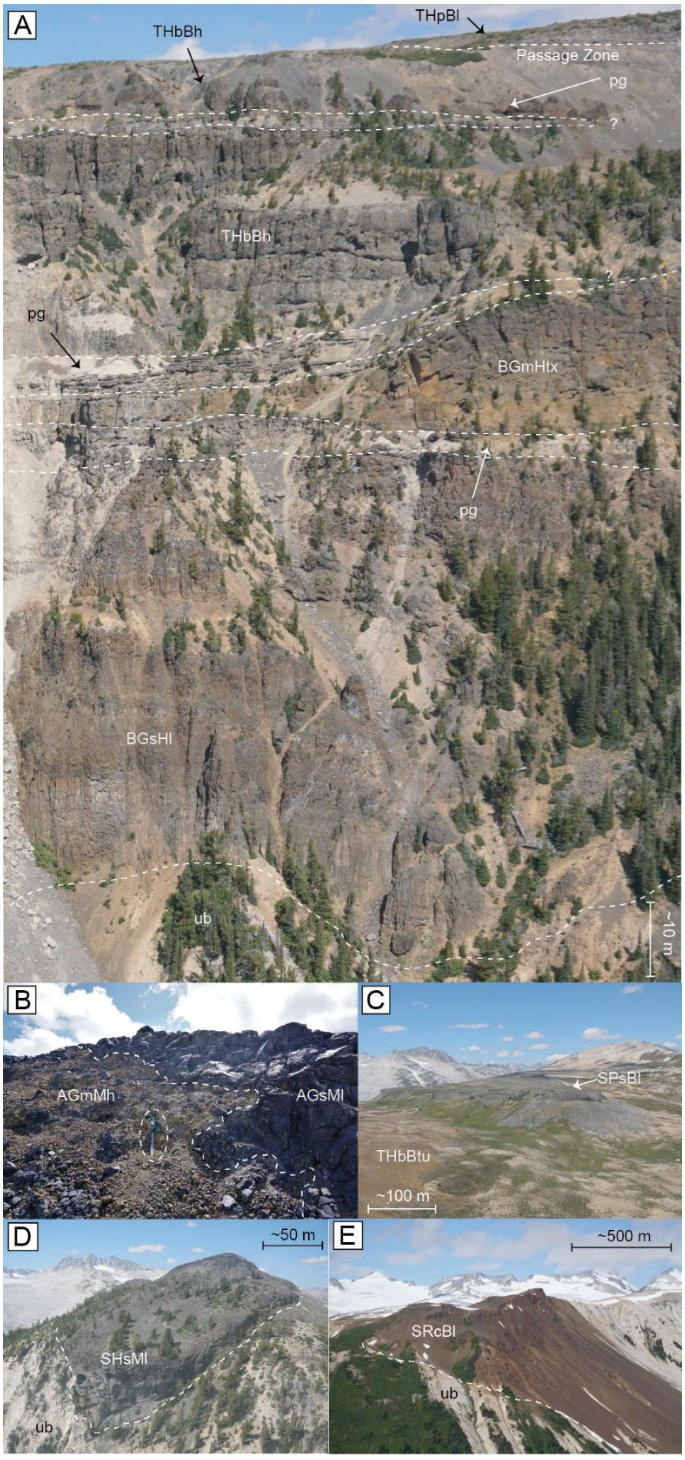

Fig. 10.5 Field photographs of lithofacies exposed in the Bridge River volcanic field. (A) Aerial image looking north outlining stratigraphy exposed along the southern margin of Tuber Hill. The cliff exposure is ~150 m high. (B) Photograph looking southwest showing irregular contact between finely jointed lobe of porphyritic mugearite lava and massive palagonitised hyaloclastite breccia at the Arrowhead Glacier deposit. (C) Aerial image looking north showing Sham Plateau subglacial lava flow (SPsBl). (D) Aerial photograph looking north showing finely jointed Sham Hill lavas (unit SHsMl) draped over the wall of the Bridge River valley. (E) Photograph looking northwest showing highly eroded Sham Ridge rocks exposed on the ridge above the Arrowhead valley.

section 5), the layer is ~5 m-thick (Fig. 10.6A). In the east, (stratigraphic section 6) the layer is slightly thicker (5 to 10 m) and is exposed at a slightly lower elevation (~1970 m versus 2020 m). The deposits are bimodal and comprise a fine, sandy matrix with up to 80 % large (1 to 30 cm diameter), fluidal, oxidised, vesicular, glassy, porphyritic basaltic tephra clasts. The clasts are angular to subrounded, irregularly shaped, and resemble fresh basaltic spatter. The matrix is well-sorted, fine sandstone with sub-rounded grains of quartz (~80 %), feldspar (~10 %), and fresh volcanic glass (~10 %). Fine bedding in the matrix wraps around the individual tephra clasts (Fig. 10.6B). The matrix surrounding individual clasts is not baked or discoloured. The basaltic tephra clasts have amygdules that are filled with fine, carbonate precipitant.

The matrix support and fine, bedding structures around clasts indicate that the basalt clasts were deposited alongside the unconsolidated sandstone matrix (i.e., the sandstone did not infiltrate later) and the lack of significant clast rounding implies a proximal volcanic source. A lack of matrix baking or discoloration suggests that the clasts were not at a high temperature during the deposition. The deposits show undulating, conformable upper and lower contacts with bounding GVcMl coherent rocks. A whole-rock analysis of a clast from the deposit (Fig. 10.4) weakly suggests a geochemical affinity to the older Bridge Glacier phase deposits (i.e., they are not geochemically like the bracketing Glacier View phase lavas). Taken together, these features suggest that this unit is a conglomerate representing a short period of Glacier View phase volcanic quiescence and remobilisation of older, proximal Bridge Glacier phase tephra deposits. The source of this oxidised (i.e., presumably a subaerially erupted) Bridge Glacier phase tephra was not located. The distinctive, recognisable nature of this unit facilitates extrapolation of the surrounding Glacier View phase lava stack across the Thunder Creek valley. The deposit layer dips towards the east, suggesting that the source of the rocks lay uphill towards the west. At the time of deposition, the Thunder Creek valley did not exist, meaning that its age must be younger than the age of the Glacier View phase deposits.

10.2.7. Nichols Valley (NV) phase (Non-Glaciovolcanic)

Coarsely jointed basaltic lava and massive basaltic breccia (NVcBl and NVmBbx)

Light grey, dense to sparsely vesicular, coarsely columnar jointed, olivine and augite phyric alkaline basalt forms a ~7 km-long, <80 m-thick packages of at least 3 individual stacked flows in the eastern map area (Fig. 10.1J). The individual flows are distinguished by discontinuous layers (1 to 5 m-thick) of poorly sorted basal breccia (unit NVmBbx). The rocks contain phenocrysts of olivine and augite, xenolithic material (granite, sandstone, and conglomerate), and rare megacrysts of plagioclase, olivine, and pyroxene (Table 10.1). The surface is glacially scoured and coated in scattered glacial debris. In the northern part of the Nichols valley, the rocks overlie a ~60 m-thick layer of sedimentary conglomerate (pg) and minor undifferentiated glacial deposits (bt). The contact with the sediments is discrete and hosts numerous large, irregularly shaped boulders of glacial detritus. We interpret this contact to be unconformable. Roddick and Souther (1987) provide two K-Ar ages for the Nichols valley group (374 ± 11.5 and 405 ± 11.5 ka). These ages indicate eruption coinciding with MIS 11, a relatively warm climatic period during the Middle Pleistocene (Raymo et al. 2006; Wilson and Russell 2018). The age of these deposits suggests that over 60 m of sediment (unit pg) has been eroded from the adjacent valleys since this time.

10.2.8. Arrowhead Glacier (AG) phase (Glaciovolcanic)

Slender jointed mugearite lava (AGsMl)

Dark grey to black, dense to moderately vesicular, porphyritic mugearite forms a 15 to 20 m-thick, jointed lobe, and a ~500 m long flow at the terminus of the Arrowhead Glacier. The rocks have phenocrysts and megacrysts of plagioclase, olivine and augite. The lobes are finely columnar and radial columnar jointed and overlie cogenetic accumulations of pillow lava and hyaloclastite (unit AGmMh). The lobate, elongate profiles of these deposits, along with their fine-marginal fracture characteristics suggest that these lavas were subglacially confined during the eruption.

Massive mugearite hyaloclastite (AGmMh)

Dark orange and black, massive, poorly sorted, matrix and clast supported basaltic pillow lava and hyaloclastite form a shallow mound underlying AGsMl at the terminus of the Arrowhead Glacier. The maximum exposed thickness is ~10 m. The clasts consist of lapilli and blocks of pillow lava and glassy, moderately vesicular basaltic blocks. The matrix comprises angular, blocky fragments of sparsely vesicular ash and lapilli that are palagonitised (Fig.10.5B). The Arrowhead Glacier deposit has been exposed by the retreat of the adjacent Arrowhead Glacier. Although the lithofacies (fine-scale jointing, pillow lava, hyaloclastite, etc.) may indicate that the rocks erupted subglacially, their alpine location and low deposit profile do not necessitate significant quantities of overlying ice (Wilson and Russell 2018). The age of the deposit is unknown.

10.2.9. Thunder Creek (TC) phase (Glaciovolcanic)

Slender jointed mugearite lava (TCsMl)

Dark grey, sparsely vesicular (<10 %), massive, sparsely plagioclase (<5 %), and olivine (< 1 %) phyric to aphyric, hackly and radially jointed, lobes and flows are surrounded by accumulations of matrix-supported, jig-saw-fit hyaloclastite (unit TCmMh) at the base of the Thunder Creek succession. Several lobes (~10 to 20 m-diameter) also occur in the upper Thunder Creek sequence where they show apparent intrusive relationships with the surrounding bedded tephra (unit TCbMtx). The fine-scale hackly jointing, glassy nature of the rocks and surrounding abundant quench fragmented material require an accelerated cooling environment to form. Because the local topography would have caused surface water to drain, these lithofacies are consistent with emplacement under and/or against glacial ice and record a climatic interval when the Thunder Creek valley was filled with a glacier. A sample of one of the mugearite lobes (sample AW-16-201) was sent to the WiscAr Laboratory

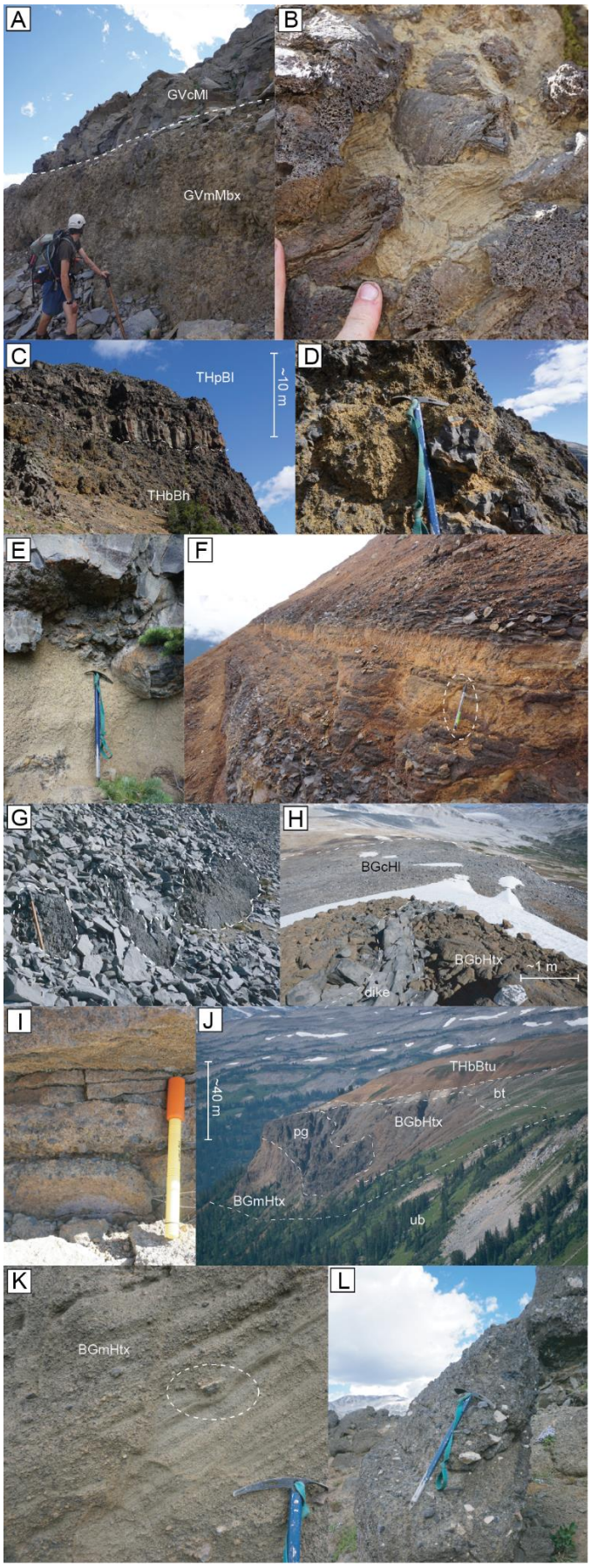

Fig. 10.6. Field photographs of lithofacies exposed at Bridge River. (A) Photograph looking southwest at exposed contact between coarsely jointed Glacier View phase basalts and massive, volcaniclastic sediments. (B) Vesicular basaltic spatter hosted in finely bedded quartz sandstone, a proximal conglomerate (unit GVmBc). (C) Photograph looking north at passage-zone transition (dashed white line) from massive to coarsely bedded pillow breccia and hyaloclastite to finely jointed subaerial basalt. (D) Basaltic pillow lava fragment within palagonitised hyaloclastite breccia (unit THbBh). (E) Photograph looking north at massive, indurated vitric tephra layer (unit THmBlt) within the upper Tuber Hill sequence. (F) Photograph looking southwest at bedded, palagonitised basaltic vitric tephra (unit THbBtu) exposed on the eastern side of the Sham Plateau. Pencil circled for scale. (G) Photograph looking north at glassy margins (dashed white line) of Bridge Glacier phase intrusive dike (unit BGcHl). A hammer is shown for scale in the left of the picture. (H) Photograph looking north from near the summit of Tuber Hill showing coarsely-jointed dike intruding bedded tephra and feeding a small, subaerial flow (unit BGcHl). (I) Bedded, palagonitised tuff breccia with vesicular, palagonitised basaltic clasts exposed at the western margin of Tuber Hill (unit BGbHtx). (J) Photograph looking southwest showing stratigraphy and contact relationships along the eastern side of Sham Plateau. Unit BGbHtx deposits overlie an irregular, ~30 m thick accumulation of volcaniclastic sandstone and conglomerate (pg) and underlie a layer of glacial basal till (unit bt). (K) Dipping, fine beds showing fine, bomb sag structure (circled). A subtle growth fault cross cuts the center of the image. (L) Photograph looking north at massive tuff breccia (unit BGmHtx) with abundant, angular, plutonic granite accessory lithic clasts.

at the University of Wisconsin-Madison for $^{40}Ar/^{39}Ar$ analysis. The contained a large atmospheric gas component, resulting in an inconclusive analysis (Table 1.1). While the age of these deposits remains unknown, as a group, the Thunder Creek phase deposits record a period of subglacial volcanic activity that postdates the formation of Thunder Creek valley.

Massive mugearite hyaloclastite (TCmMh)

Dark grey to orange, unconsolidated, massive, monolithic, poorly sorted, clast to matrix-supported, glassy, porphyritic mugearite hyaloclastite breccia forms a thick carapace surrounding lobes and flows of unit TCsMl. The breccias contain clasts that are angular, conchoidally fractured, and show crude jig-saw-fit textures. The matrix consists of orange yellow palagonitised vitric ash. The margins of individual TCsMl lobes commonly transition into loosely packed TCmMh breccia over several centimeters (Fig. 10.1I). Unit TCmMh has a gradational contact with overlying TCbMtx volcaniclastic rocks. The restricted componentry of these breccias and their intimate affiliation with the glassy lobes of unit TCsMl suggests a hydroclastic origin (i.e., they are hyaloclastites). Likely, the water required during the formation of these deposits was glacially sourced, recording a climatic interval when the Thunder Creek valley was filled with ice.

Bedded mugearite tuff breccia (TCbMtx)

Dark grey, moderately sorted, clast supported, bedded, unconsolidated tuff breccia forms an ~150 m-thick accumulation at the top of the Thunder Creek deposit (Fig. 10.1H). The lower contact with unit TCmMh hyaloclastite is gradational and indiscrete. Unit TCbMtx tephra hosts numerous bulbous intrusions of finely jointed porphyritic mugearite. The tephra consists of vesicular (up to 70%), sub-rounded, glassy, plagioclase-phyric mugearite lapilli, blocks, and bombs. The

matrix comprises grey, incipiently palagonitised blocky ash and fractured crystal clasts. Near the core of the deposit, the beds dip moderately towards the east and show weak normal grading. The blocky, incipiently palagonitised matrix clasts are indicators for phreatomagmatic activity; however, the bedding structures do not necessitate subaqueous deposition. Given the gradational contact relationship with underlying subaqueously erupted material, these deposits probably record an effusive to explosive eruption transition in conjunction with subaqueous edifice emergence.

10.2.10. Undivided Volcanic (V) rocks

Coarsely jointed basaltic lava (VcBl)

At least 8, undivided, a small volume (i.e. <100 m^2), isolated exposures of mafic volcanic rocks occur around the periphery of the map area, cropping out as steep-sided, highly eroded, alpine exposures (Fig. 10.1G). The rocks are black to grey, olivine, and plagioclase phyric basalts, suggesting a close affiliation with the other local mafic deposits. The deposits exhibit a range of fracture morphologies including coarse columnar, fine-scale columnar, radial columnar, and hackly joints, however, individually, they do not provide sufficient field evidence to be classified as glaciovolcanic or subaerial.

10.3. Glacial sediments

Basal till (bt)

Consolidated, massive to crudely bedded, undivided glacial deposits occur in thin (1 to 10 m-thick) accumulations throughout the map area. Accumulations that are <1 m-thick are not mapped, however their presence is recorded in the supplied stratigraphic logs (see stratigraphic sections 1, 2 and 3). The deposits have a fine matrix (~70 to 80 %) of grey-brown silt and sand and have interspersed larger clasts (<20 to 30 %; <1 m-diameter) of rounded, striated, vesicular porphyritic basalt (<10 %) and other Coastal plutonic and metamorphic lithologies. These rocks are important indicators for temporal readvance of local glaciers and indicate that the area has been covered several times by advancing ice. One layer exposed on the eastern side of Sham Plateau defines an unconformity between the younger Tuber Hill phase rocks and the older Bridge Glacier phase rocks. The presence of till along this boundary indicates that the two phases of volcanic activity may have been separated by a considerable period.

Paraglacial sediments (pg)

Bedded, variably sorted, massive to bedded, clast and matrix-supported, undivided polymictic mudstone, sandstone, gravel, and conglomerate form numerous layered, <30 m-thick accumulations throughout the map area (Fig. 10.1D). The rocks contain clasts of plutonic and metamorphic rocks (~up to 30 %), bedded sedimentary material (e.g., mudstone and sandstone) and basaltic clasts reminiscent of the local volcanic lithofacies. The clasts are mostly rounded and range in size from <1 cm to >30 cm in diameter. The deposits are well bedded and normally graded, with frequent crossbedding and weak clast imbrication structures observed (Fig. 10.1E).

In the southern Tuber Hill and eastern Sham Plateau areas (stratigraphic sections 1 and 4), these sedimentary rocks lie between Bridge Glacier phase bedded tuff breccia and Bridge Glacier phase lavas (inaccessible). Another horizon is traceable and continuous almost across the entire map area, undulating in thickness from ~5 m to ~30 m and defines a separation boundary between the Bridge Glacier phase rocks and the younger Tuber Hill phase rocks (Fig. 10.1F). Additional sedimentary layers also occur up sequence: i) as a discontinuous layer within the Tuber Hill phase pillow breccia, pillow lava, and hyaloclastite (stratigraphic sections 2, 3, and 4), ii) as a thin (<5 m-thick) and discontinuous layer that separates the Glacier View and Tuber Hill phase deposits, and, iii) as a thin band occurring between the two lowermost flows of the Glacier View phase basalts (stratigraphic sections 5 and 6).

The spatial and intercalated stratigraphic relationship of these numerous sedimentary layers with the local volcanic rocks suggest that they have a close affinity with repeated glaciovolcanic activity in the Bridge River area. The horizons are semi-continuous across the volcanic area, and contain clast and depositional structures consistent with fluvial reworking and mobilization of the local volcanic deposits. We interpret them as paraglacial sediments that were deposited during periods of meltwater movement during large-scale ice melting from volcanic heating (Wilson and Russell 2018).

10.4. Summary

Here, we provide a summary delineating the sequence of volcanic events at Bridge River and their respective paleoenvironmental implications. Effusive basaltic volcanism began in the Sham Ridge area during the Early-Mid Pleistocene (before ~800 ka). These deposits are significantly eroded, prohibiting recovery of any potential glacial ice interaction.

At ~ 752 ± 9 ka (Roddick and Souther 1987) an isolated, effusive glaciovolcanic eruption occurred at Sham Hill. The local physiography suggests that substantial accumulations of overlying ice were present, and the adjacent Bridge River valley was occupied by a large glacier.

The Hawaiite composition Bridge Glacier (BG) phase volcanism occurred before ~731 ± 13.5 ka (Roddick and Souther 1987). The eruption began effusively, depositing slender-columnar joined lavas in local, subglacial paleochannels that cooled and interacted with the local glacial environment. The eruption transitioned to explosive, building a broad pyroclastic cone comprising massive and locally bedded units. This pyroclastic cone is the older core of a large polygenetic tuya (e.g., Russell et al., 2013, Russell et al., 2014). Local layers of paraglacial sediment (unit pg) suggest that the eruptions were long-lived and interspersed by periods of quiescence and glaciofluvial reworking of the volcanic deposits.

Following another sustained period of volcanic quiescence and local glacial readvance (indicated by the presence of basal till along the eastern side of Sham Plateau), renewed glaciovolcanic activity near Tuber Hill formed the upper part of the Tuber Hill polygenetic tuya. The onset of this volcanic activity is delineated by a layer of paraglacial sediment that partially segregates the

Bridge Glacier and Tuber Hill phase deposits. The rocks mostly comprise a lava-delta sequence; a lower portion of basaltic hyaloclastite and pillow lava that is overlain by stack of geochemically and petrographically similar subaerial lavas, however there are several layers of volcaniclastic lithologies that suggest localized, explosive eruption events. The transition surface or passage zone (i.e., from a subaqueous to subaerial deposition environment) resided at ~2000 m-elevation and is laterally continuous around most of the margin of the Tuber Hill area. The passage zone is significant as it marks the paleosurface of an ephemeral glacial lake that existed in the Tuber Hill area at the time of the eruption (dated at ~598 ± 7.5 ka) record a lava-delta sequence that extends across the southern portion of Tuber Hill and a period of ice confinement and an ephemeral glacial lake during MIS 15.

Following another period of quiescence, subaerial Glacier View (GV) phase effusive mugearite eruptions occurred on the eastern flank of the Tuber Hill tuya. The lava propagated downhill towards the east, stretching across the (then absent) Thunder Creek valley. Minor reworking of older volcanic rocks during this time formed a distinctive layer of basaltic conglomerate that separates the lower Glacier View flows and suggests that the area still contained significant mobile water (i.e., likely meltwater draining from the central volcanic edifice towards the east). The Glacier View phase events were succeeded by an extended period of glaciation and glacial erosion. This period developed the U-shaped Arrowhead Creek and Thunder Creek valleys and was likely responsible for a significant quantity of volcanic material being removed for the southern margin of Tuber Hill (which lies along the established Bridge Glacier valley).

Late stage, monogenetic effusive volcanism occurred in several areas surrounding the periphery of the Bridge River volcanic field, including:

i) A mugearite deposit on Sham Plateau forming a small, elongated mound with fine-scale, hackly jointing textures and basal pillow lavas indicating enhanced cooling in the presence of water. These textures suggest that the area may have been covered with ice (age unknown).
ii) The Nichols Valley lava sequence, which erupted from a vent located at the head of the Nichols Valley between 374 ± 11.5 and 405 ± 11.5 ka. The lava erupted subaerially, onto a substrate of older, paraglacial sediment and propagated downhill (i.e., down the Nichols Valley) for ~7 km.
iii) The Arrowhead Glacier phase deposits, which consists of mugearite hyaloclastite, pillow lava, and columnar jointed basalt located at the terminus of the Arrowhead Glacier. The lithofacies are consistent with an eruption in the presence of a small alpine glacier (Wilson and Russell 2018).
iv) The Thunder Creek volcano, comprising finely jointed mugearite lava and hyaloclastite along the side of Thunder Creek valley. The rocks suggest eruption into a glacial environment that postdates formation of the Thunder Creek valley. The absolute age of this volcanic event is unknown however the age is constrained by the older Glacier View lavas and Tuber Hill phase deposits (i.e., less than ~598 ± 7.5 ka).

11. Conclusion

We present nine geologic maps showcasing glaciovolcanic interactions in the Quaternary Garibaldi volcanic belt (GVB) of southwestern British Columbia, Canada. The mapped areas include: (1) Monmouth Creek volcano, (2) Brohm Ridge of the Mount Garibaldi volcanic complex, (3) the Table, (4) the Black Tusk, (5) the Cinder Cone, (6) Cracked Mountain volcano, (7) Lillooet Glacier volcano, (8) the Salal Glacier volcanic field, and (9) the Bridge River volcanic field.

These maps are a result of extensive fieldwork and offer a substantial database of new field observations, empirical data and associated geological interpretations. Each map is supported by detailed lithostratigraphic analysis involving field sampling and accompanying geochemical, geochronological, and petrographic analysis. The maps provide detailed information on several previously unmapped areas (e.g., Cracked Mountain and the Bridge River volcanic field) and investigate a few well-known volcanic deposits at a high spatial resolution (e.g., the Table and the Black Tusk). Our maps identify 23 volcanic eruption events that interacted with ice (i.e., are classified as glaciovolcanic) alongside a further 11 events that demonstrate an ice-free depositional environment. For each event we subdivide and describe the deposit lithofacies, offering interpretations of the eruption environment, eruption style, and paleoenvironment. We reveal the ages of the events by collating existing geochronological information and providing 7 new successful $^{40}Ar/^{39}Ar$ age determinations and the results from an additional 5 unsuccessful age estimation attempts.

This new information fills significant gaps in the geological record while establishing the GVB as a key terrestrial archive for studying the interactions between volcanic and glacial systems. The integration of high-resolution geochronological data that is directly supported by detailed field analysis, provides a robust framework for unravelling this relationship, enabling a more accurate correlation with global paleoclimate records. By developing these empirical data as a paleoenvironmental proxy, the glaciovolcanic rocks delineated by these maps serve as a valuable resource for tracking the fluctuations of the Coast Mountain sector of the Cordilleran ice sheet beyond the last glacial stage.

Acknowledgements

This research was supported by the Natural Sciences and Engineering Research Council of Canada (NSERC) Discovery and Discovery Accelerator Supplements program and Engage grants held by JKR. AMW was supported by an NSERC Canada Graduate Scholarship–Doctorate (CGS-D) grant at The University of British Columbia. The authors would like to thank Nikolas Matysek, Nathan Willett, Steve Quane, Mila Huebsch and Lucy Porritt for their assistance in the field. Annie Borch for sharing Cinder Cone geochronology, Dale Douglas, Murry Sovereign, Tony Cailes, Black Tusk aviation, Blackcomb aviation and Kootenay Valley Helicopters for the logistical support. BC Parks for their on-going support of the project. Brian Jicha at the WiscAr laboratory, University of Alaska-Fairbanks,

and Jeff Beonwitz at the Geochronology laboratory, University of Wisconsin-Madison, for the geochronology determinations. We also thank Blake Brodland, Peter Read, Karen Hincks, Drum Cavers and Paul Adam, Brent Ward and Glyn Williams Jones for their insightful and helpful conversations and the British Columbia Geological Survey (BCGS), specifically Bram van Straaten, Yao Cui and Lawrence Aspler for the detailed reviews of the maps and supporting information.

References

ALS. 2020. Mineral trace- element chemistry for exploration.

Andrews, G.D.M., Porritt, L., and Russell, J.K. 2014. Quaternary subglacial and explosive volcanism in the Canadian Cascade arc (Sea-to-Sky Corridor), British Columbia. In Trials and Tribulations of Life on an Active Subduction Zone: Field Trips in and around Vancouver, Canada. Geological Society of America. pp. 125–167. doi:10.1130/2014.0038(07).

Le Bas, M.J., Le Maitre, R.W., Streckeisen, a., and Zanettin, B. 1986. A Chemical Classificatron of Volcanic Rocks Based on the Total Alkali-Silica Diagram. Journal of Petrology, 27: 745–750. doi:10.1093/petrology/27.3.745.

Benowitz, J.A., Layer, P.W., and Vanlaningham, S. 2014. Persistent long-term (c. 24 Ma) exhumation in the Eastern Alaska Range constrained by stacked thermochronology. Advances in 40Ar/39Ar Dating: from Archaeology to Planetary Sciences, 378: 225–243. doi:10.1144/SP378.12.

Booth, D.B., Troost, K.G., Clague, J.J., and Waitt, R.B. 2003. The Cordilleran Ice Sheet. In Developments in Quaternary Science. Elsevier. pp. 17–43. doi:10.1016/S1571-0866(03)01002-9.

Bostock, H.H. 1963. Geology, Squamish, Vancouver, West Half, British Columbia. doi:10.4095/108691.

Bustin, A.M.M., Clowes, R.M., Monger, J.W.H., Journeay, J.M., and Spence, G. 2013. The southern Coast Mountains, British Columbia: New interpretations from geological, seismic reflection, and gravity data. Canadian Journal of Earth Sciences, 50: 1033–1050. doi:10.1139/cjes-2012-0122.

Bye, A., Edwards, B.R., and Hickson, C.J. 2000. Preliminary field, petrographic, and geochemical analysis of possible subglacial, dacitic volcanism at the Watts Point volcanic centre, southwestern British Columbia. Current Research, A20: 9.

Clague, J.J., Friele, P.A., and Hutchinson, I. 2003. Chronology and hazards of large debris flows in the Cheekye River basin, British Columbia, Canada. Environmental and Engineering Geoscience, 9: 99–115. doi:10.2113/9.2.99.

Clague, J.J., and Ward, B. 2011. Pleistocene Glaciation of British Columbia. In Quaternary Glaciations - Extent and Chronology, 1st edition. Elsevier Inc. doi:10.1016/B978-0-444-53447-7.00044-1.

Cui, Y., and Russell, J.K. 1995. Nd-Sr-Pb isotopic studies of the southern Coast Plutonic Complex, southwestern British Columbia. Geological Society of America Bulletin, 107: 127–138. doi:10.1130/0016-7606(1995)107<0127:NSPISO>2.3.CO;2.

Fillmore, J., and Coulson, I.M. 2013. Petrological and geochemical constraints on the origin of adakites in the Garibaldi Volcanic Complex, southwestern British Columbia, Canada. Bulletin of Volcanology, 75: 1–23. doi:10.1007/s00445-013-0730-5.

Forbes, A.E.S., Blake, S., and Tuffen, H. 2014. Entablature: Fracture types and mechanisms. Bulletin of Volcanology, 76. doi:10.1007/s00445-014-0820-z.

Friele, P. a., and Clague, J.J. 2009. Paraglacial geomorphology of Quaternary volcanic landscapes in the southern Coast Mountains, British Columbia. Geological Society, London, Special Publications, 320: 219–233. doi:10.1144/SP320.14.

Friele, P.A., and Clague, J.J. 2002. Readvance of glaciers in the British Columbia Coast Mountains at the end of the last glaciation. Quaternary International, 87: 45–58. doi:10.1016/S1040-6182(01)00061-1.

Fulton, R.J. 1991. A Conceptual Model for Growth and Decay of the Cordilleran Ice Sheet. Géographie physique et Quaternaire, 45: 281. doi:10.7202/032875ar.

Green, N.L. 1977. Multistage andesite genesis in the Garibaldi Lake area, southwestern British Columbia. The University of British Columbia.

Green, N.L. 1981. Geology and petrology of Quaternary volcanic rocks, Garibaldi Lake area, southwestern British Columbia. Part II. Geological Society of America Bulletin, 92: 1359–1470. doi:10.1130/0016-7606(1981)92<697:GAPOQV>2.0.CO;2.

Green, N.L. 1990. Late Cenozoic Volcanism in the Mount Garibaldi and Garibaldi Lake Volcanic Fields, Garibaldi Volcanic Belt, Southwestern British Columbia. Journal of the Geological Association of Canada, 17: 171–175. Geoscience Cana. doi:10.12789/gs.v17i3.3673.

Green, N.L. 1994. Mechanism for middle to upper crustal contamination: Evidence from continental-margin magmas. Geology, 22: 231. doi:10.1130/0091-7613(1994)022<0231:MFMTUC>2.3.CO;2.

Green, N.L., Armstrong, R.L., Harakal, J.E., Souther, J.G., and Read, P.B. 1988. Eruptive history and K-Ar geochronology of the late Cenozoic Garibaldi volcanic belt, southwestern British Columbia. Geological Society of America Bulletin, 100: 563–579. doi:10.1130/0016-7606(1988)100<0563:EHAKAG>2.3.CO;2.

Green, N.L., and Harry, D.L. 1999. On the relationship between subducted slab age and arc basalt petrogenesis, Cascadia subduction system, North America. Earth and Planetary Science Letters, 171: 367–381. doi:10.1016/S0012-821X(99)00159-4.

Harder, M., and Russell, J.K. 2006. Basanite glaciovolcanism at Llangorse mountain, northern British Columbia, Canada. Bulletin of Volcanology, 69: 329–340. doi:10.1007/s00445-006-0078-1.

Harris, M.A., and Russell, J.K. 2022. Polymagmatic Glaciovolcanism : Cracked Mountain Tuya , Canadian Cascades. 10: 1–19. doi:10.3389/feart.2022.859794.

Harris, M.A., Russell, J.K., Barendregt, R., Porritt, L.A., and Wilson, A. 2022. Explosive glaciovolcanism at cracked Mountain Volcano, Garibaldi Volcanic Belt, Canada. Journal of Volcanology and Geothermal Research, 423: 107477. Elsevier B.V. doi:10.1016/j.jvolgeores.2022.107477.

Hebda, R.J., Lian, O.B., Hicock, S.R., and Fisher, T.G. 2016. Olympia Interstadial: vegetation, landscape history, and paleoclimatic implications of a mid-Wisconsinan (MIS3) nonglacial sequence from southwest British Columbia, Canada. Canadian Journal of Earth Sciences, 53: 304–320. doi:10.1139/cjes-2015-0122.

Hickson, C.J. 1994. Character of volcanism, volcanic hazards, and risk, northern end of the Cascade magmatic arc, British Columbia and Washington State. In Geology and Geological Hazards of the Vancouver Region, Southwestern British Columbia. Edited by J.W.H. Monger. Geological Survey of Canada Bulletin 481. pp. 231–250. doi:10.4095/203253.

Hickson, C.J., Russell, J.K., Stasiuk, M. V, and Swanson, D.A. 1999. Volcanology of the 2350 B.P. Eruption of Mount Meager volcanic complex, British Columbia, Canada: implications for hazards from eruptions in topographically complex terrain 1. Bulletin of Volcanology, 60: 489–507. Springer-Verlag.

Hildreth, W. 2007. Quaternary magmatism in the Cascades; geologic perspectives. U.S. Geological Survey Professional Paper 1744,: 125. doi:http://pubs.usgs.gov/pp/pp1744/.

Jicha, B.R., Singer, B.S., and Sobol, P. 2016. Re-evaluation of the ages of 40Ar/39Ar sanidine standards and supereruptions in the western U.S. using a Noblesse multi-collector mass spectrometer. Chemical Geology, 431: 54–66. doi:10.1016/j.chemgeo.2016.03.024.

Johnson, D.M., Hooper, P.R., and Conrey, R.M. 1999. XRF analysis of rocks and minerals for major and trace elements on a single low dilution Li-tetraborate fused bead. In International Centre for Diffraction Data. International Centre for Diffraction Data. pp. 843–867.

Jones, J.G. 1968. Intraglacial volcanoes of the Laugarvatn region, south-west Iceland--I. Quarterly Journal of the Geological Society, 124: 197–211. doi:10.1144/gsjgs.124.1.0197.

Kelman, M.C. 2005. Glaciovolcanism at the Mount Cayley Volcanic Field, Garibaldi Volcanic Belt, Southwestern British Columbia. University of British Columbia.

Kelman, M.C., Russell, J.K., and Hickson, C.J. 2002a. Effusive intermediate glaciovolcanism in the Garibaldi Volcanic Belt, southwestern British Columbia, Canada. Geological Society, London, Special Publications, 202: 195–211. doi:10.1144/GSL.SP.2002.202.01.10.

Kelman, M.C., Russell, J.K., and Hickson, C.J. 2002b. Glaciovolcanism at Ember Ridge, Mount Cayley volcanic field, southwestern British Columbia. Geological Survey of Canada, Current Research, A15: 7. doi:10.4095/213082.

Kuiper, K.F., Deino, A., Hilgen, F.J., Krijgsman, W., Renne, P.R., and Wijbrans, J.R. 2008. Synchronizing Rock Clocks of Earth History. Science, 320: 500–504. doi:10.1126/science.1154339.

Lawrence, R.B., Armstrong, R.L., and Berman, R.G. 1984. Garibaldi group volcanic rocks of the Salal Creek area, southwestern British Columbia: alkaline lavas on the fringe of the predominantly calc-alkaline Garibaldi (Cascade) volcanic arc. Journal of Volcanology and Geothermal Research, 21: 255–276.

Layer, P.W., Hall, C.M., and York, D. 1987. The derivation of 40Ar/39Ar age spectra of single grains of hornblende and biotite by laser step-heating. Geophysical Research Letters, 14: 757–760. doi:10.1029/GL014i007p00757.

Lee, J.Y., Marti, K., Severinghaus, J.P., Kawamura, K., Yoo, H.S., Lee, J.B., and Kim, J.S. 2006. A redetermination of the isotopic abundances of atmospheric Ar. Geochimica et Cosmochimica Acta, 70: 4507–4512. doi:10.1016/j.gca.2006.06.1563.

Lescinsky, D.T., and Fink, J.H. 2000. Lava and ice interaction at stratovolcanoes: Use of characteristic features to determine past glacial extents and future volcanic hazards. Journal of Geophysical Research: Solid Earth, 105: 23711–23726. doi:10.1029/2000jb900214.

Lescinsky, D.T., and Sisson, T.W. 1998. Ridge-forming, ice-bounded lava flows at Mount Rainier, Washington. Geology, 26: 351. doi:10.1130/0091-7613(1998)026<0351:RFIBLF>2.3.CO;2.

Lisiecki, L.E., and Raymo, M.E. 2005. A Pliocene-Pleistocene stack of 57 globally distributed benthic D 18 O records. Paleoceanography, 20: 1–17. doi:10.1029/2004PA001071.

Lodge, R.W.D., and Lescinsky, D.T. 2009. Fracture patterns at lava–ice contacts on Kokostick Butte, OR, and Mazama Ridge, Mount Rainier, WA: Implications for flow emplacement and cooling histories. Journal of Volcanology and Geothermal Research, 185: 298–310. Elsevier B.V. doi:10.1016/j.jvolgeores.2008.10.010.

Lynch, G. 1992. Deformation of Early Cretaceous volcanic-arc assemblages, southern Coast Belt, British Columbia. Canadian Journal of Earth Sciences, 29: 2706–2721. doi:10.1139/e92-214.

Mathews, W.H. 1948. Geology of the Mount Garibaldi Map-area, Southwestern British Columbia. University of California.

Mathews, W.H. 1951. The Table, a flat-topped volcano in southern British Columbia. American Journal of Science, 249: 830–841. doi:10.2475/ajs.249.11.830.

Mathews, W.H. 1952a. Mount Garibaldi, A Supraglacial Pleistocene Volcano in Southwestern British Columbia. American Journal of Science, 250: 81–103.

Mathews, W.H. 1952b. Ice-dammed lavas from Clinker Mountain, southwestern British Columbia. American Journal of Science, 250: 553–565. doi:10.2475/ajs.250.8.553.

Mathews, W.H. 1958. Geology of the Mount Garibaldi Map-Area, Southwestern British Columbia. Part II: Geomorphology and Quaternary Volcanic Rocks. Geological Society of America Bulletin, 69: 179–198. doi:10.1130/0016-7606(1958)69[179:GOTMGM]2.0.CO;2.

Menounos, B., Osborn, G., Clague, J.J., and Luckman, B.H. 2009. Latest Pleistocene and Holocene glacier fluctuations in western Canada. Quaternary Science Reviews, 28: 2049–2074. Elsevier Ltd. doi:10.1016/j.quascirev.2008.10.018.

Min, K., Mundil, R., Renne, P.R., and Ludwig, K.R. 2000. A test for systematic errors in 40Ar/39Ar geochronology through comparison with U/Pb analysis of a 1.1-Ga rhyolite. Geochimica et Cosmochimica Acta, 64: 73–98. doi:10.1016/S0016-7037(99)00204-5.

Monger, J.W.H., and Journeay, J.M. 1994. Guide to the geology and tectonic evolution of the southern Coast Mountains.

Mullen, E.K., and Weis, D. 2013. Sr-Nd-Hf-Pb isotope and trace element evidence for the origin of alkalic basalts in the Garibaldi Belt, northern Cascade arc. Geochemistry, Geophysics, Geosystems, 14: 3126–3155. doi:10.1002/ggge.20191.

Mullen, E.K., and Weis, D. 2015. Evidence for trench-parallel mantle flow in the northern Cascade Arc from basalt geochemistry. Earth and Planetary Science Letters, 414: 100–107. Elsevier. doi:10.1016/j.epsl.2015.01.010.

Mustard, D.K., and Campbell, C.B. 1971. Salal Creek Molybdenum Property.

Raymo, M.E., Lisiecki, L.E., and Nisancioglu, K.H. 2006. Plio-Pleistocene Ice Volume, Antarctic Climate, and the Global 18O Record. Science, 313: 492–495. doi:10.1126/science.1123296.

Read, P.B. 1977. Meager Creek Volcanic Complex, southwestern British Columbia. Geological Survey of Canada Paper, 1A: 277–281. doi:10.4095/102701.

Read, P.B. 1979. Geology, Meager Creek geothermal area, British Columbia. Geological Survey of Canada Open File,: 1 sheet. doi:10.4095/129507.

Read, P.B. 1990. Mount Meager Complex, Garibaldi Belt, southwestern British Columbia.

Reyes, A. V, and Clague, J.J. 2004. Stratigraphic evidence for multiple Holocene advances of Lillooet Glacier, southern Coast Mountains, British Columbia. Canadian Journal of Earth Sciences, 41: 903–918. doi:10.1139/e04-039.

Roddick, J.A., and Woodsworth, G.J. 1975. Coast Mountains Project: Pemberton (092J West Half) Map-Area, British Columbia. Geological Survey of Canada, 75–1A: 37–40.

Roddick, J.C., and Souther, J.G. 1987. Geochronology of Neogene volcanic rocks in the northern Garibaldi Belt, British Columbia. Geological Survey of Canada, 87–2: 21–24.

Rogers, G.C. 1985. Variation in Cascade volcanism with margin orientation. Geology, 13: 495. doi:10.1130/0091-7613(1985)13<495:VICVWM>2.0.CO;2.

Russell, J.K., Edwards, B.R., Porritt, L., and Ryane, C. 2014. Tuyas: A descriptive genetic classification. Quaternary Science Reviews, 87: 70–81. doi:10.1016/j.quascirev.2014.01.001.

Russell, J.K., Edwards, B.R., and Porritt, L.A. 2013. Pyroclastic passage zones in glaciovolcanic sequences. Nature Communications, 4. Nature Publishing Group. doi:10.1038/ncomms2829.

Ryder, J.M., Fulton, R.J., and Clague, J.J. 1991. The Cordilleran Ice Sheet and the Glacial Geomorphology of Southern and Central British Colombia. Géographie physique et Quaternaire, 45: 365. doi:10.7202/032882ar.

Sherrod, D.R., and Smith, J.G. 1990. Quaternary extrusion rates of the Cascade Range, northwestern United States and southern British Columbia. Journal of Geophysical Research, 95: 19465. doi:10.1029/JB095iB12p19465.

Smellie, J.L. 2013. GLACIAL LANDFORMS | Quaternary Vulcanism: Subglacial Landforms. In Encyclopedia of Quaternary Science. Elsevier. pp. 780–802. doi:10.1016/B978-0-444-53643-3.00074-1.

Smellie, J.L. 2018. Glaciovolcanism: A 21st Century Proxy for Palaeo-Ice. In Past Glacial Environments: Second Edition. Elsevier Ltd. doi:10.1016/B978-0-08-100524-8.00010-5.

Smellie, J.L., and Edwards, B.R. 2016. Glaciovolcanism on Earth and Mars: Products, Processes, and Palaeoenvironmental Significance. Cambridge University Press, Cambridge.

Smellie, J.L., Johnson, J.S., McIntosh, W.C., Esser, R., Gudmundsson, M.T., Hambrey, M.J., and van Wyk de Vries, B. 2008. Six million years of glacial history recorded in volcanic lithofacies of the James Ross Island Volcanic Group, Antarctic Peninsula. Palaeogeography, Palaeoclimatology, Palaeoecology, 260: 122–148. doi:10.1016/j.palaeo.2007.08.011.

Souther, J.G. 1980. Geothermal Reconnaissance in the Central Garibaldi Belt, British Columbia. Geological Survey of Canada Paper, 80–1A: 1–11. doi:10.4095/106174.

Souther, J.G. 1991. Volcanic Regimes. In Geology of the Cordilleran Orogen in Canada. Edited by H. Gabrielse and C.J. Yorath. Geological Survey of Canada. pp. 457–490. doi:10.4095/134103.

Stasiuk, M. V., and Russell, J.K. 1990. The Bridge River Assemblage in the Meager Mountain volcanic complex , southwestern British Columbia. Geological Survey of Canada Paper, 90–1E: 227–233.

Stasiuk, M. V, and Russell, J.K. 1989. Petrography and Chemistry of the Meager Mountain Volcanic Complex, southwestern British Columbia. Current Research, Part E: 189–196. doi:10.4095/127482.

Stewart, M.L., Russell, J.K., and Hickson, C.J. 2003. Discrimination of hot versus cold avalanche deposits: Implications for hazard assessment at Mount Meager, B.C. Natural Hazards and Earth System Science, 3: 713–724. doi:10.5194/nhess-3-713-2003.

Stroncik, N.A., and Schmincke, H.U. 2002. Palagonite - A review. International Journal of Earth Sciences, 91: 680–697. doi:10.1007/s00531-001-0238-7.

Sun, S., and McDonough, W.F. 1989. Chemical and isotopic systematics of oceanic basalts: implications for mantle composition and processes. Geological Society, London, Special Publications, 42: 313–345. doi:10.1144/GSL.SP.1989.042.01.19.

Venugopal, S., Moune, S., Williams-Jones, G., Druitt, T., Vigouroux, N., Wilson, A., and Russell, J.K. 2020. Two distinct mantle sources beneath the Garibaldi Volcanic Belt: Insight from olivine-hosted melt inclusions. Chemical Geology, 532: 119346. Elsevier. doi:10.1016/j.chemgeo.2019.119346.

White, J.D.L., and Houghton, B.F. 2006. Primary volcaniclastic rocks. Geology, 34: 677–680. doi:10.1130/G22346.1.

Wilson, A.M. 2019. Glaciovolcanism in the Garibaldi volcanic belt. University of British Columbia.

Wilson, A.M., and Russell, J.K. 2017. Lillooet Glacier basalts, southwestern British Columbia, Canada: products of Quaternary glaciovolcanism. Canadian Journal of Earth Sciences, 54: 639–653. doi:10.1139/cjes-2016-0201.

Wilson, A.M., and Russell, J.K. 2018. Quaternary glaciovolcanism in the Canadian Cascade volcanic arc – paleoenvironmental implications. Geological Society of America Special Papers, 2538: 133–157. doi:10.1130/2018.2538(06).

Wilson, A.M., Russell, J.K., Kelman, M.C., and Hickson, C.J. 2016. Geology of the Monmouth Creek volcanic complex, Garibaldi volcanic belt, British Columbia. Geological Survey of Canada Current Research, 2: 13. Natural Resources Canada. doi:10.4095/298798.

Wilson, A.M., Russell, J.K., and Quane, S.L. 2019. The Table, a flat-topped volcano in southern British Columbia: Revisited. American Journal of Science, 319: 44–73. doi:10.2475/01.2019.02.

Wilson, A.M., Russell, J.K., and Ward, B.C. 2020. Paleo-glacier reconstruction in southwestern British Columbia , Canada : A glaciovolcanic model. Quaternary Science Reviews, 218: 178–188. Elsevier Ltd. doi:10.1016/j.quascirev.2019.06.024.

York, D., Hall, C.M., Yanase, Y., Hanes, J.A., and Kenyon, W.J. 1981. 40Ar/39Ar dating of terrestrial minerals with a continuous laser. Geophysical Research Letters, 8: 1136–1138. doi:10.1029/GL008i011p01136.